Studies on Characterization and Gas Sensing Mechanism of Electroconducting Thin Solid Films

Hiroyasu Nagase

Faculty of Pharmaceutical Sciences
Osaka University
1994

Preface

The present dissertation is a collection of author's studies which have been carried out under the direction of Professor Toshinobu Imanaka in his laboratory at Department of Chemical Engineering, Faculty of Engineering Science, Osaka University during the years 1988–1993.

A great number of sensors are now used in the world. However, most of them are the physical sensors to measure physical quantities, such as temperature, light, sound, pressure and magnetic force. The chemical sensors have been developed in recent years. Since then, chemical sensors for measuring gaseous materials have been studied actively. Making up odor–sensing systems is one of the purposes of these studies. The development of gas–sensing materials for sensing pollutants is also required to protect the environment of the earth.

This dissertation is concerned with two types of the conducting thin films; conducting polymer and metal oxide semiconductor. They are both important materials for gas–sensing systems. It is expected that the electrochemically deposited conducting polymers have possibilities for the development of 'intelligent' gas sensors. The resulting devices would find applications in areas such as the monitoring of complex gas mixtures and flavors. The thin film metal oxide semiconductor, SnO_X, can be used to detect NO_X. In recent years, the simple method for sensing NO_X in exhaust gas, which is one of the source materials of acid rain, is required seriously. This sensor can be applied to the instruments for combustion. The author hopes that the findings obtained in this work would give some suggestions for development of chemical sensors, which are beneficial to comfortable living and environmental protection.

Acknowledgements

The author wishes to express his sincere gratitude to Professor Toshinobu Imanaka for his guidance, discussions, and encouragement given to the author during the course of this work. Without his kind support, the present studies would have never been accomplished. The author is deeply grateful to Professor Michio Matsumura for his helpful and stimulating discussions and suggestions, to Dr. Kiyosuke Wakabayashi for his helpful suggestions and cooperation for measurement of gas response, to Messrs. Takaaki Kuroiwa and Tetsuya Miyagishi for their continuous encouragement and for providing substrates for sensors, and to Professor Kazuhisa Miyamoto and Associate Professor Kazumasa Hirata for their kindness to allow him to finish writing this dissertation. Grateful acknowledgement is made to Professor Yoshihiro Nakato and Associate Professor Hikaru Kobayashi for measurements of XPS, FT-IR and UV-vis, to Dr. Hiroshi Hori for measurement of EPR, and to Dr. Kimiya Takeshita for measurement of EQCM.

The author thanks to Drs. Yasuaki Okamoto, Kiyotomi Kaneda and Yuriko Nitta for their continuous encouragement. He also thanks to Messrs. Tetsuo Hirono, Susumu Kato, Hiroyuki Abe, Norikazu Nishiyama, Masahiko Muramoto, Junnosuke Nakatani, and Tadashi Nohata for their active collaboration and hot discussions, and to Messrs. Masashi Yamamura, Takahiro Honda, and many other members of the Imanaka Laboratory for their continual encouragement.

Finally, the author is grateful to his parents, Keiichi and Junko Nagase, his grandmother, Tamako Nagase, his sisters, Tomoko Nagase and Noriko Nagase, and his fiancée, Junko Minemoto, for their heartful encouragement and all kinds of support to everything he faced during the course of his studies.

Hiroyasu Nagase

January, 1994.

Contents

General Introduction

For environmental and personal protection together with widespread requirements for more accurate process control, new and improved sensors for measuring both physical and chemical parameters have increasingly been required. This need for better sensors is strongly influenced by the increasing use of intelligent microelectronics for monitoring and control.

It is required for sensors to detect a wide range of gases, from organic and inorganic pollutants, which must be measured at the level of parts per million or lower, to inflammable gases such as methane and hydrogen, or gases such as water vapor and CO_2, which must be measured at the level of 1% or higher.

While many methods of gas sensing have been developed in laboratories, and some have found commercial application, higher specificity and sensitivity, and better durability and stability of response are required for variety of applications. They are gas sensors in life-support systems, food processing, industrial drying and monitoring of chemical plant, vehicle exhaust pollution control, etc..

The semiconducting gas sensors, where the resistance of a porous pellet or thin film of metal oxides such as SnO_2 or ZnO is sensitive to inflammable or toxic gases in air, have been developed in recent years as a particularly economical solution to monitoring certain gases. While their applications to sensing toxic gases have been proposed, their principal applications at present are in the detection of flammable gases such as H_2, CO and CH_4, at relatively high concentrations. They are used to prevent fire or explosion. A large market has been developed particularly in Japan, where many kinds of gas sensors are required for the industrial and personal use to protect the life and environment and to improve the comfortable living.

Although the sensors made of metal-oxides are cheap and simple in the

structure, which are mainly based on porous pellets of SnO_2, have some shortcomings. Prominent among these are their relative lack of sensitivity to toxic gases at low concentrations, their sensitivity to ambient moisture, and their inherent lack of specificity to organic gases; these disadvantages can be overcome to some extent by use of SnO_2 thin films instead of pellets, and by incorporating catalysts, such as Pt and Pd. Finally, a serious disadvantage is the instability at low temperatures; in most applications, operation at 300° C or above is required. In the majority of applications, therefore, it is necessary to power devices for heaters continuously from the mains. A wide range of applications including portable personal monitors and all uses where mains power is not available are therefore inaccessible with present technology.

The development of semiconducting gas-sensing materials which could be sensitive to a wider range of gases and vapors would permit construction of new type of sensors for much wider range of applications than is covered at present. For example, these materials can be used to form arrays of gas-sensing elements in an 'intelligent' gas sensor system. In such a system a number of different gas sensors are connected to a pattern recognition system, which analyzes the data from the various sensors.

In this study, we have been interested in two types of sensors. One is a sensor for an 'intelligent' gas-sensing system, and the other is a NO_x sensor for environmental protection. This dissertation consists of two parts as follows:

1. Conducting polymer thin films for sensing organic vapor.
2. SnO_x thin films for sensing NO_x prepared by microwave plasma CVD.

In the first part, much attention is devoted to the thin films of polypyrrole and substituted polypyrroles, because doped polypyrrole is one of the most stable conducting polymers in ambient environments. These conducting polymers can detect various kinds of organic vapors through the change of electric resistance at around room temperature, and have the potential

application to an odor sensing system. The gas sensing properties and characterization of these polymer films are studied, and gas sensing mechanism for methanol vapor is elucidated. This first part is composed of following 5 chapters.

Chapter 1 describes a method for preparation of gas sensors made of polypyrrole by using electrochemical polymerization technique from various kinds of solutions of supporting electrolytes and the response of these sensors to organic vapors.

Chapter 2 shows the effects of anions doped in polypyrrole films on their structures and response to methanol, and the reason for their difference in the gas response is pursued.

In Chapter 3, the influences of dopant anions and methyl groups of substituted polypyrroles on the response of these films to methanol vapor are discussed on the basis of resistivity and XPS measurements. A gas response mechanism is also proposed.

In Chapter 4, the chemical states of polymers doped with anions and the interaction between the polymer backbone and dopant anions are investigated by measuring the FT-IR and EPR spectra of polypyrrole, poly(3-methylpyrrole) and poly(N-methylpyrrole) doped with various anions.

In Chapter 5, the adsorption and absorption processes of methanol on and in polypyrrole films are presented on the basis of the results obtained by a QCM method, and the relationship between the sorption of methanol and the change in the resistance of polypyrrole films is discussed.

In the second part, a thin film of SnO_X is prepared by a microwave plasma CVD method, and is used to detect NO_X. From the results, possibility of constructing a sensor for NO_X included in the exhaust gas is suggested. This part consists of 2 chapters.

In Chapter 6, the relationship between the preparation conditions of the SnO_X thin films and the thickness, surface condition, electrical and optical

properties of these films is described.

In Chapter 7, the gas response properties of the SnO_X thin films against NO_X (NO and NO_2) and inflammable gases included in the exhaust gas, such as carbon monoxide, hydrogen and hydrocarbons, are investigated, and the conditions for the operation of the sensor is optimized. The gas response mechanism and the possibility of its application to NO_X sensor are discussed.

Part 1

Conducting Polymer Thin Films for Sensing Organic Vapor

Chapter 1

Preparation of Polypyrrole Films and Their Gas-sensing Properties against Organic Vapors

Conductive polypyrrole films can be used to detect various organic vapors through changes in their film resistance. These sensors are sensitive to polar molecules, such as methanol, ethanol, acetone and water. Sensitivity to methanol is especially high, and the response patterns of polymer films against methanol changes with the anions doped in polypyrrole. These sensors are suggested to have potentials to be applied to an intelligent gas sensing system.

1.1 Introduction

A number of studies have revealed that the conductivity of π-conjugated polymer films varies when they are exposed to gases or vapors such as ammonia [1–4], nitrogen dioxide [1, 4–8], halogens [7, 9] and organic vapors [10–12]. Although the detailed mechanism of the response has not yet been elucidated, preliminary studies on these materials have shown that these polymers exhibit fast and reversible responses to a wide concentration range of gases and vapors at room temperature [1, 10]. These polymers have a number of distinct advantages for gas sensing applications. First, a wide variety of polymers are available, including polypyrrole [1, 2, 4, 6, 7, 9–12], polythiophene [8], polyaniline [3] and substituted polyindole [12]. Secondly, they are easily grown by electrochemical polymerization of the monomer under controlled conditions. Thirdly, they are sensitive to gases and vapors at room temperature.

A disadvantage of these materials is their lack of specificity. This disadvantage can be turned to an advantage, if these materials are used in form of arrays of gas-sensing elements in an 'intelligent' gas sensor system. In general, they show responses to a wide range of gases and vapors with different response patterns [12]. In such a system, a number of different gas sensing-elements are connected to a pattern recognition system. From the analysis of responses of various sensors, kinds and concentrations of gases will be determined. Only a few examples of such a approach have been described in literature [13], but the reported results are encouraging. A number of different types of sensors have been employed, including electrochemical sensors [14], FET devices [15], piezoelectric sensors [16, 17] and a combination type sensors [18].

We have been carrying out research on the possibility of using electrochemically deposited conducting polymers for the development of

such 'intelligent' gas sensors. The resulting devices should find application in areas such as monitoring of gas mixtures and flavors. In these applications the entire device, consisting of an array of sensors, a detection system and the associated pattern recognition programs, mimics the mammalian nose [19].

In this chapter we describe a simple, controlled method for the electrochemical fabrication of polypyrrole films for gas sensors from the solutions of various kinds of supporting electrolytes and their responses to organic vapors.

1.2 Experimental

1.2.1 Solutions and chemicals

All chemicals used in this study were reagent grade. Electrochemical polymerization was carried out from solutions of 0.1 moldm^{-3} pyrrole (Wako) containing 0.1 moldm^{-3} electrolyte. Deionized and then distilled water was used as the solvent. The pyrrole was distilled twice and stored under nitrogen. The electrolytes, such as $NaBF_4$, Na_2SO_4 $NaClO_4$, CF_3SO_3Na, $C_2H_5SO_3Na$, $CH_3(CH_2)_5SO_3Na$, sodium p-toluenesulfonate (NaTOS) and sodium poly(4-styrenesulfonate) (NaPSS), were used as received from commercial sources. All solutions were deoxygenated by bubbling nitrogen for more than 20 min before addition of the pyrrole monomer.

1.2.2 Film formation

The substrates used in the gas response measurements were Corning 7059 glass plates (10 mm × 20 mm). On one side of the glass, a platinum film (40 nm) was evaporated on Niobium underlayer (10 nm) to form electrodes. The electrodes consist of two sets of platinum stripes (10 μm × 3 mm) about 10 μm apart, as shown in Fig. 1.1. The platinum stripes work as electrodes for

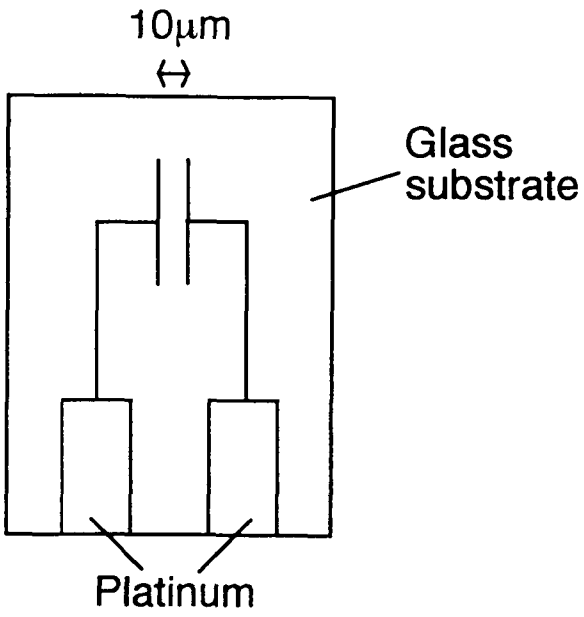

Fig. 1.1. Schematic diagram of a electrode substrate for a gas sensor.

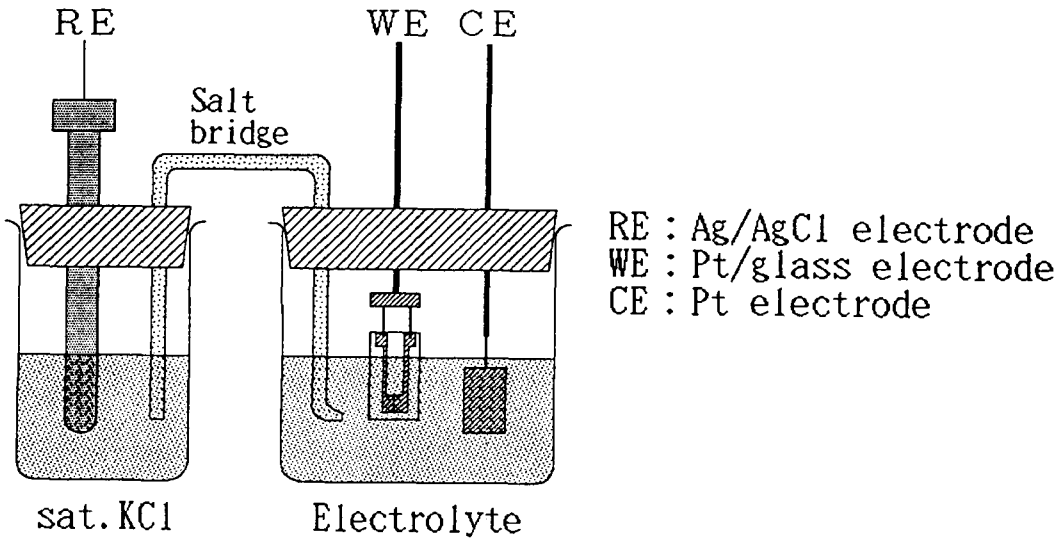

Fig. 1.2. Schematic diagram of an electrochemical cell for polymerization.

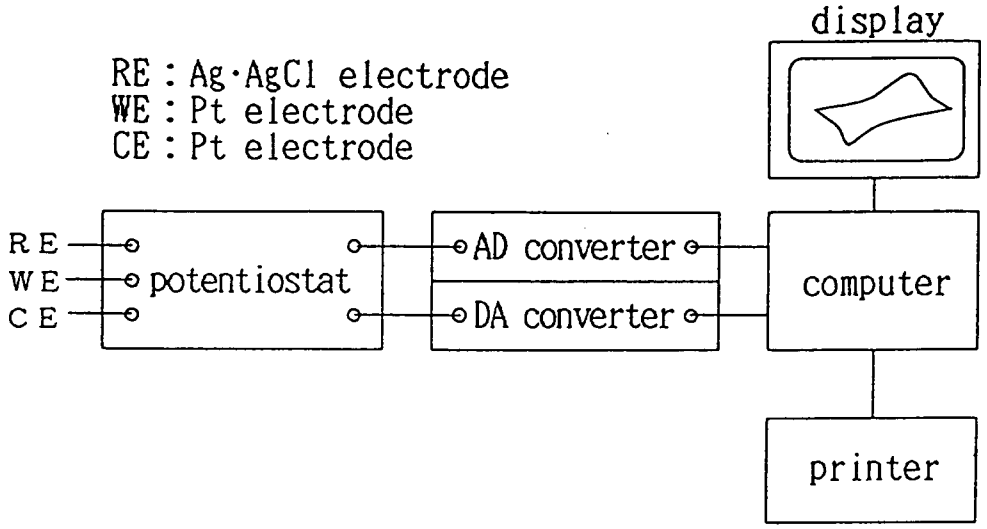

Fig. 1.3. Schematic diagram of an electrochemical polymerization system.

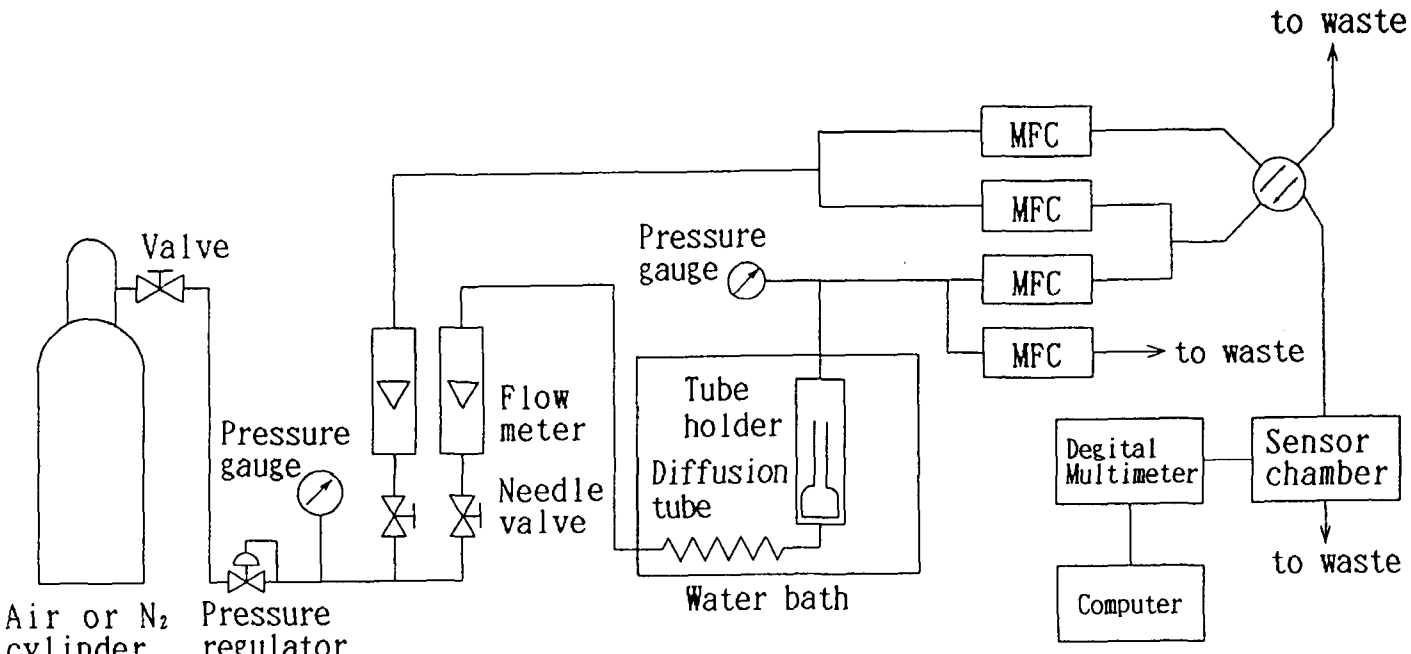

Fig. 1.4. Schematic diagram of a gas response measurement system.

polymerization. Before polymerization, the substrates were immersed in a 20 $mmoldm^{-3}$ octadecyltriethoxysilane/cyclohexane solution for 12 h to make the glass surface hydrophobic. This treatment is effective to promote the lateral growth of polymers on the glass surface during polymerization [20]. The substrate was then connected to a gold stem with a conductive silver resin. The electrochemical deposition of polypyrrole films on the substrate was performed using an electrochemical cell as shown in Fig. 1.2. A platinum plate (7mm × 7mm) was used as the counter electrode. The potentials were referred to an Ag/AgCl (3.33N KCl saturated by AgCl) electrode, which was separated from the electrolyte by a salt bridge and a Luggin capillary containing the background electrolyte. Polypyrrole films were grown on the substrate by sweeping the potential between −0.7 and +0.9 V (vs. Ag/AgCl) at the rate of $100mVs^{-1}$, typically for 10 sweep cycles. The potential was then held at 0.0 V vs. Ag/AgCl until the current decayed to less than 1 $mAcm^{-2}$. This treatment is important, because it determines the final oxidation state of the polymer and, hence, the conductivity. All electrochemical experiments were carried out using an HA−151 (Hokuto Denko) potentiostat/galvanostat, which was controlled by a computer (EPSON, PC−386V) via a 12−bit A/D and D/A converters, as shown in Fig. 1.3. After polymerization, the gap of the platinum was covered and bridged by deposited polymer films. The deposited polypyrrole films were rinsed with distilled water and dried in nitrogen for at least 24 h at room temperature.

1.2.2 Gas response measurements

Responses to organic vapors were measured in their concentration range from 10 to 10000 ppm. Nitrogen or synthetic air (nitrogen 79%, oxygen 21%) was used as the carrier gas. Low concentration organic vapors (from 10 to 1000 ppm) were obtained using a PD−1B permeator (Gastec), as shown in Fig.1.4. Liquid organic compounds were set in a diffusion tube maintained in

a thermostat. The desirable concentration of organic vapor was achieved by changing the temperature and the mass flow rate of the carrier gas. For concentrations higher than 1000 ppm, the organic vapors were obtained by bubbling carrier gas directly through the liquid organic compounds at 0° C. The resulting vapor flow was diluted using a second carrier gas line. The flow rate of the test gas was 1 dm^3min^{-1}. During measurements of gas response, samples were subjected successively to the carrier gas and an organic vapor diluted by the carrier gas.

The resistance of polypyrrole films between the two platinum stripes was measured using a 3478A digital multimeter (Hewlett–Packard) at room temperature. The obtained data were transferred to a computer (EPSON, PC–286VF) via an IEEE–488 interface.

1.3 Results and discussion

1.3.1 Electrochemical polymerization

Because the platinum electrodes used in the present study are small, they exhibit the enhanced mass transport characteristics of microelectrodes. This is advantageous for electrochemical polymerization of heterocyclic monomers, since the diffusion of species both towards and away from the electrode is enhanced.

Polypyrrole films were grown using the procedure described in the Experimental Section. Figure 1.5 shows a typical cyclic voltammogram for the growth of polypyrrole on the platinum substrates in $NaBF_4$ solution. The sharp increase in current at potentials above +0.7 V is due to the polymerization of pyrrole. The peaks that grow at −0.1 V on the cathodic scans and at +0.2 V on the anodic scans are assigned to reduction and oxidation of the deposited polymer.

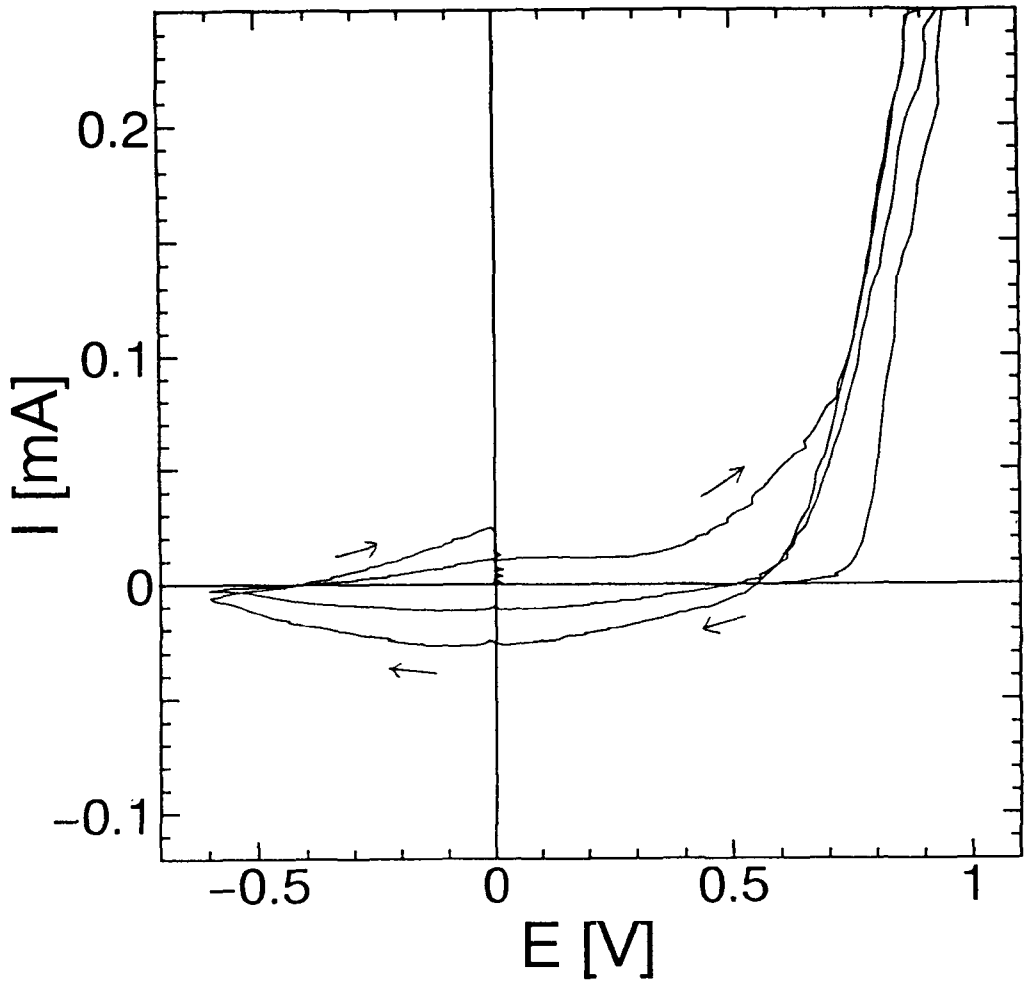

Fig. 1.5. Cyclic voltammogram for the deposition of polypyrrole on the substrate for a sensor. Polypyrrole is deposited from aqueous solution containing 0.1 $moldm^{-3}$ pyrrole and 0.1 $moldm^{-3}$ $NaBF_4$ by repeated potential sweep at 100 mVs^{-1}.

Since the sensor electrodes consist of two platinum strips separated by a 10 μm gap, we need to deposit a certain minimum amount of polymer in order to form a coherent film between the platinum electrodes. In order to investigate this amount, we measured the resistance between the electrodes as a function of the amount of polymer deposited. These measurements were made by measuring the resistance between the two platinum electrodes in air after the deposition of different amounts of the polymer. The amounts of films was controlled by controlling the number of potential sweeps. From the results, it was found that the 10 μm gap between the platinum patterns was interconnected with the polypyrrole thin film growing from each electrode, when the number of potential cycles was more than four. Consequently, subsequent experiments were carried out with the polypyrrole films deposited after five potential cycles.

1.3.2 Response to organic and water vapors

Figures 1.6–1.10 show typical response curves of polypyrrole films deposited from an Na_2SO_4 solution against various gas vapors. The films were repeatedly exposed to air and vapors, such as hexane, benzene, acetone, ethanol, methanol and water. The polypyrrole film showed no response to 500 ppm benzene, as shown in Fig. 1.6. On the other hand, the resistance of polypyrrole films changed when exposed to 1000 ppm acetone (in Fig. 1.7), 500 ppm ethanol (in Fig. 1.8), 1600 ppm methanol (in Fig. 1.9) and 400 ppm water (in Fig. 1.10). In the presence of acetone vapor, the resistance of the film decreased initially and then increased slowly, but the change of the resistance is small. The responses of polypyrrole to methanol and water are much larger than that to acetone. Their response patterns were similar, i.e., the resistance of the film decreased initially and then increased slowly by exposure to the vapors. In the case of ethanol, the resistance decreased, but the response at room temperature was much slower than that for the other vapors. From

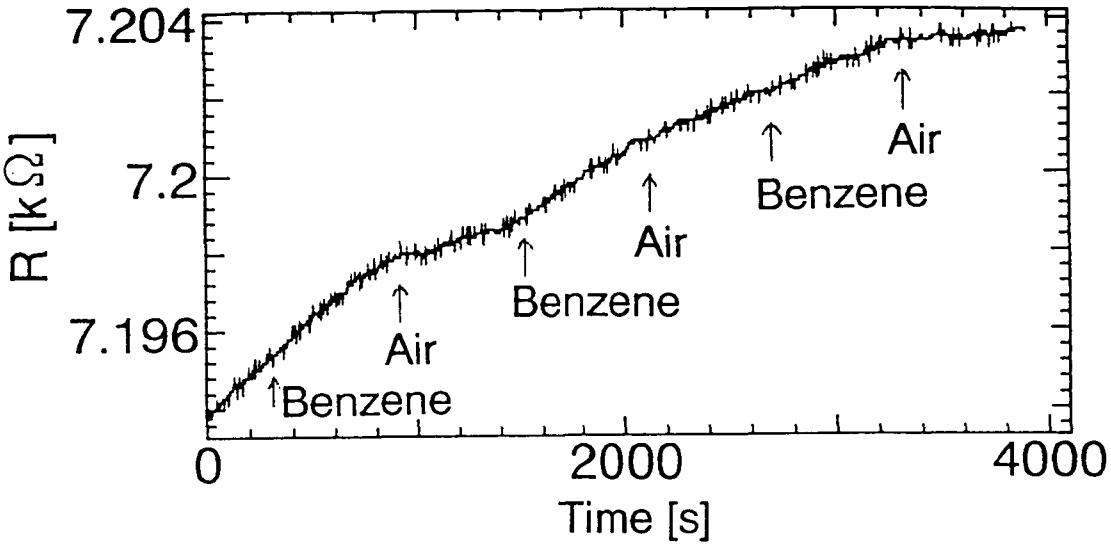

Fig. 1.6. Typical response of a SO_4^--doped polypyrrole film on exposure to 500 ppm benzene vapor at 25 °C in a flowing system. The gas was cycled repeatedly between vapor and clean air as indicated.

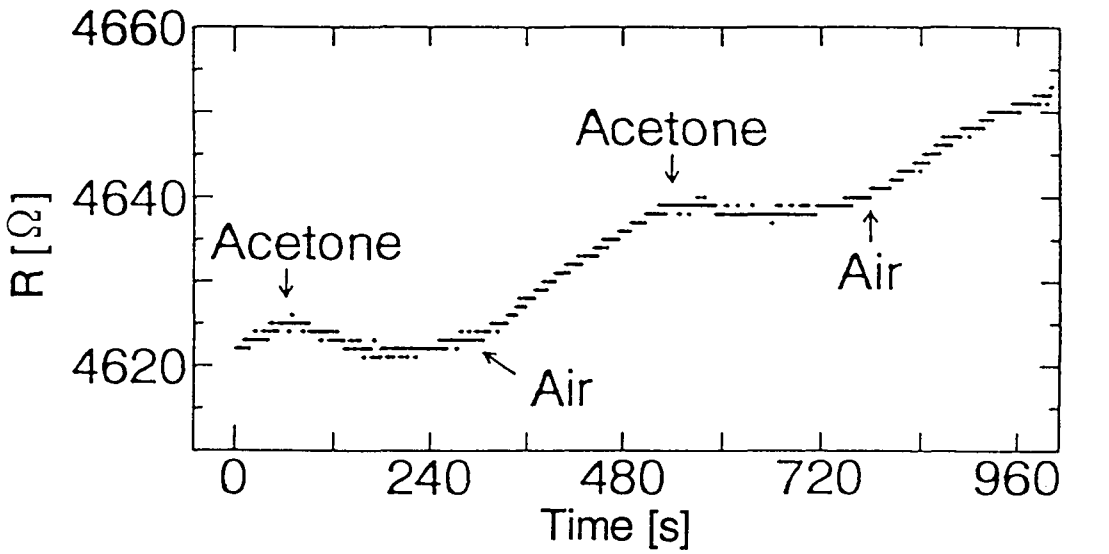

Fig. 1.7. Typical response of a SO_4^--doped polypyrrole film on exposure to 1000 ppm acetone vapor at 25 °C in a flowing system. The gas was cycled repeatedly between vapor and clean air as indicated.

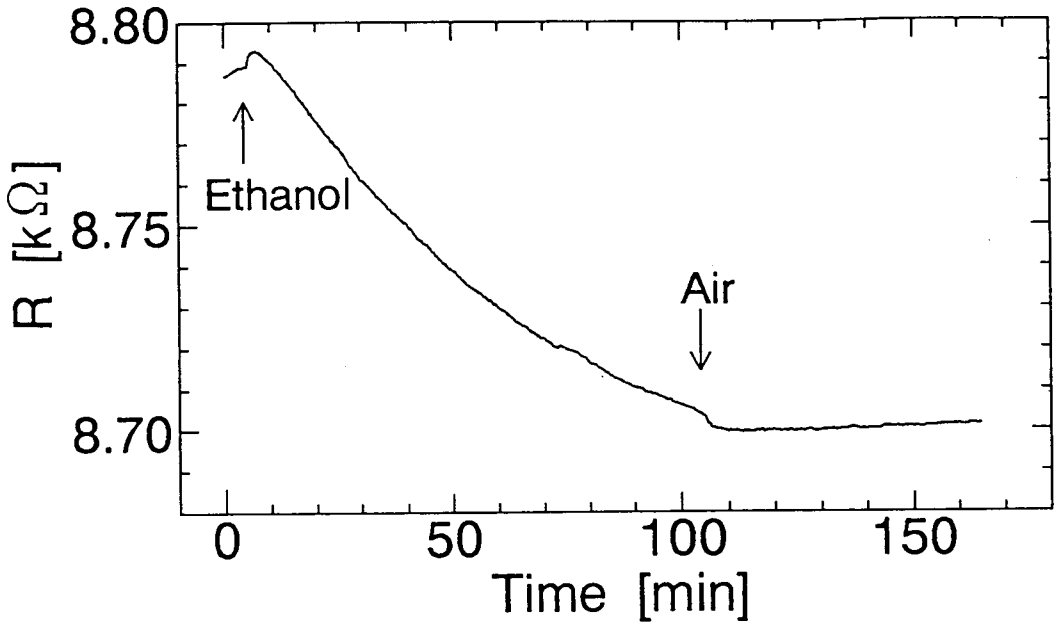

Fig. 1.8. Typical response of a SO_4^-–doped polypyrrole film on exposure to 500 ppm ethanol vapor at 25°C in a flowing system. The gas was cycled repeatedly between vapor and clean air as indicated.

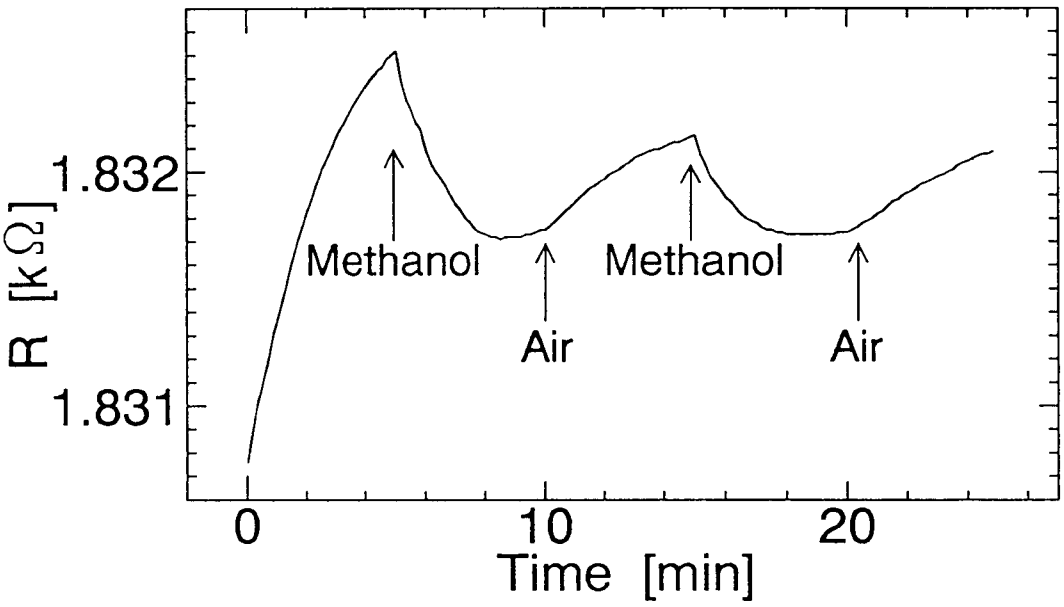

Fig. 1.9. Typical response of a SO_4^-–doped polypyrrole film on exposure to 1600 ppm methanol vapor at 25°C in a flowing system. The gas was cycled repeatedly between vapor and clean air as indicated.

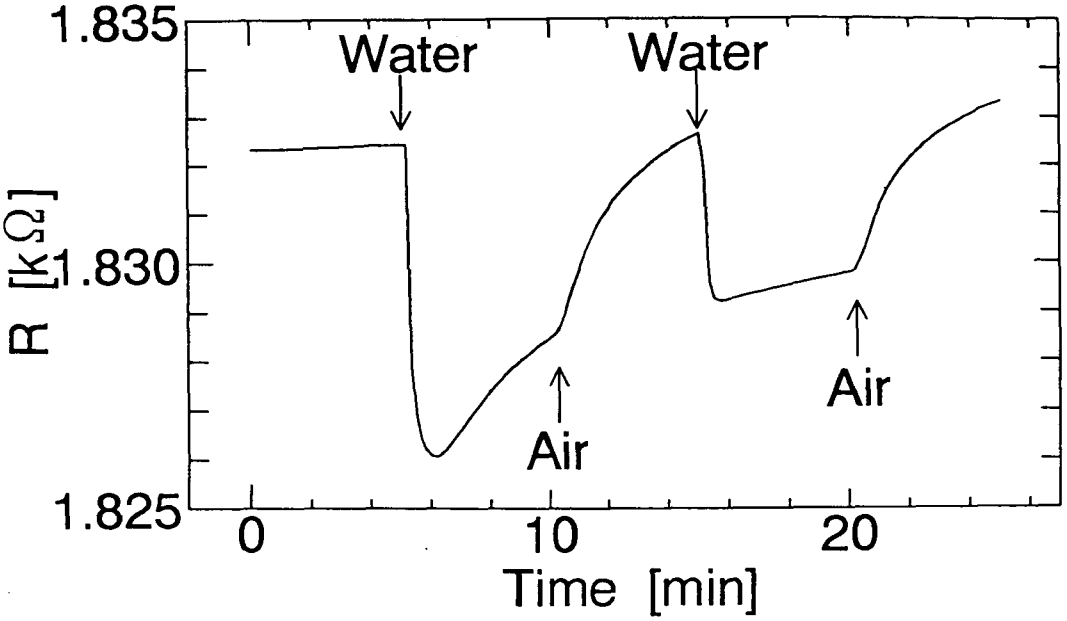

Fig. 1.10. Typical response of a SO_4^-–doped polypyrrole film on exposure to 400 ppm water vapor at 25°C in a flowing system. The gas was cycled repeatedly between vapor and clean air as indicated.

these results, it is concluded that the polypyrrole films have no response to non-polar molecules. On the contrary, the resistance decreases with an increase in polarity of molecules. The response becomes slower as the size of molecules increases. From the response patterns to water, methanol and acetone, it is considered that there are at least two components in the gas response of polypyrrole films; fast and slow components. The fast component decreases the resistance, and the slow component increases the resistance. It is assumed that the molecules are firstly adsorbed on the surface of the polymer and are then absorbed in the bulk of the polymer. These processes are expected to be related to the two responses. The details of gas sensing mechanism will be discussed in Chapters 3 and 5.

1.3.3 Effect of dopant anions on the response to methanol vapor

Among the organic vapors measured in this study, the response to methanol was especially large. Table 1.1 summarizes the initial resistance R_0, which is the resistance before exposure to methanol, and the maximum resistance change ΔR observed by exposure to 1700 ppm methanol. It is apparent that the nature of the gas response is dependent on the anions doped in polypyrrole. The resistance of polypyrrole films doped with SO_4^{2-} and BF_4^- decreased, while that of polypyrrole films doped with ClO_4^- and organic anions containing sulfonate group increased by exposure to methanol. The details will be discussed in the subsequent chapters.

1.4 Conclusion

The resistance of polypyrrole films changes when the films are exposed to polar molecules, such as methanol, ethanol or acetone. The sensitivity to methanol is especially high, and the response pattern of polymer films to

methanol changes with the anions doped in polypyrrole.

For array applications it is advantageous, if sensors having different response patterns toward sensing gases are combined. From our results it was found that we can make sensors with different responses against organic vapors. The response can also be modified by the anions doped in polymers. These sensors would be effectively adopted to the intelligent gas sensing system.

In subsequent chapters, we will characterize the polymer sensors and attempt to explain the gas response mechanisms.

Table 1.1 Resistance change in methanol (1700ppm)

Supporting electrolyte	$R_0/k\Omega$ [a]	$\Delta R/\Omega$ [b]	$\Delta R/R_0$
Na_2SO_4	12.9	-306	-2.37×10^{-2}
$NaBF_4$	8.39	-28.0	-3.34×10^{-3}
$NaClO_4$	7.87	4.80	6.10×10^{-4}
CF_3SO_3Na	9.59	200	2.08×10^{-2}
$C_2H_5SO_3Na$	788	37.8k	4.80×10^{-2}
$CH_3(CH_2)_5SO_3Na$	7.28	17.4	2.39×10^{-3}
$p\text{-}CH_3C_6H_4SO_3Na$	7.50	197	2.63×10^{-2}
NaPSS [c]	17.15	804	4.69×10^{-2}

a) Initial resistance of polypyrrole films.

b) Maximum resistance change by exposure to methanol.

c) Sodium poly(stylenesulfonate).

References

[1] J. J. Miasik, A. Hooper and B. C. Tofield, *J. Chem. Soc., Faraday Trans. 1*, **82**, 1117 (1986).

[2] G. Gustafsson And I. Lundstrom, *Synth. Met.*, **21**, 203 (1987).

[3] M. Hirata and J. Wu, *Technical Digest of 9th Sensor Symposium*, 1990, pp.113.

[4] J. P. Blanc, N. Derouiche, A. E. Hadri, P. Germain, C. Maleysson and H. Robert, *Sensors and Actuators B*, **1**, 130 (1990).

[5] F. J. G. Monreal and C. M. Mari, *Sensors and Actuators*, **12**, 129 (1987).

[6] T. Hanawa, S. Kuwabata and H. Yoneyama, *J. Chem. Soc., Faraday Trans. 1*, **84**, 1587 (1988).

[7] T. Hanawa and H. Yoneyama, *Synth. Met.*, **30**, 341 (1989).

[8] T. Hanawa, S. Kuwabata , H. Hashimoto and H. Yoneyama, *Synth. Met.*, **30**, 173 (1989).

[9] T. Hanawa and H. Yoneyama, *Bull. Chem. Soc. Jpn.*, **62**, 1710 (1989).

[10] P. N. Bartlett , P. B. M. Archer and S. K. Ling-Chung, *Sensors and Actuators*, **19**, 125 (1989).

[11] P. N. Bartlett and S. K. Ling-Chung, *Sensors and Actuators*, **19**, 141 (1989).

[12] P. N. Bartlett and S. K. Ling-Chung, *Sensors and Actuators*, **20**, 287 (1989).

[13] K. Ema, M. Yokoyama, T. Nakamoto and T. Moriizumi, *Sensors and Actuators*, **18**, 291 (1989).

[14] J. R. Stetter, P. C. Jurs and S. L. Rose, *Anal. Chem.*, **58**,860 (1986).

[15] M. Jasowicz and J. Janata, *Anal. Chem.*, **58**, 514 (1986).

[16] W. H. King, Jr., *Anal. Chem.*, **36**, 1735 (1964).

[17] J. Hlavay and G. G. Guilbault, *Anal. Chem.*, **49**, 1890 (1977).

[18] B. Bott and T. A. Jones, *Sensors and Actuators*, **9**, 19 (1986).

[19] H. Shurmer, A. Frad, J. Bartlett, G. Dodd and U. Hayat, *Phys. Technol.*, **18**, 170 (1987).

[20] M. Nishizawa, M. Shibuya, T. Sawaguchi, T. Matsue and I. Uchida, *J. Phys. Chem.*, **95**, 9042 (1991).

Chapter 2

Effect of Doping Anions in Polypyrrole Films on Sensing Methanol Vapor

Conductive polypyrrole films can be used to detect methanol vapors through changes in the film resistance. The resistance of ClO_4^--doped polypyrrole film increased in methanol vapor, while that of SO_4^{2-}-doped polypyrrole film decreased. When the doped SO_4^{2-} anions in polypyrrole films were replaced by ClO_4^- by an electrochemical treatment, its response pattern changed to that of ClO_4^--doped polypyrrole films. This means that finally-doped-anions decide the response patterns. From FT-IR and EPR measurements, it is found that the difference in gas responses of PP films doped with different anions is caused by their specific electronic properties.

2.1 Introduction

In Chapter 1, we prepared polypyrrole films containing various doped anions, such as BF_4^-, SO_4^{2-}, ClO_4^- and p-toluenesulfonate by electrochemical polymerization, and found that the resistance of polypyrrole films changed when the films were exposed to polar molecules, such as methanol, ethanol and acetone. Sensitivity for methanol was especially high, and the response patterns changed with the dopant anions.

Seemingly, there are more than two responses in resistance changes. These are considered to be related to the gas adsorption and absorption process. Namely, the molecules are first adsorbed onto the surface of the polymer and then absorbed in the bulk of the polymer. However, the detailed mechanism of gas sensing has not yet been fully explained.

It has been reported that the physical and electrochemical properties of polypyrrole vary with the anions used in the electrochemical polymerization [1-5]. In this chapter we discuss the effects of the anions doped in the polypyrrole on its response to methanol, and attempt to find the origin of the different gas responses.

Utilization of the quartz crystal microbalance (QCM) in conjunction with electrochemistry allows one to determine mass change on the electrode simultaneously with electrochemical reactions under *in situ* conditions. The method has been utilized to monitor the mass change due to electrochemical polymerization and the subsequent redox reactions of polypyrrole [6-8]. We adopted this measurement for the study of the doped anions in polypyrrole films for gas sensors.

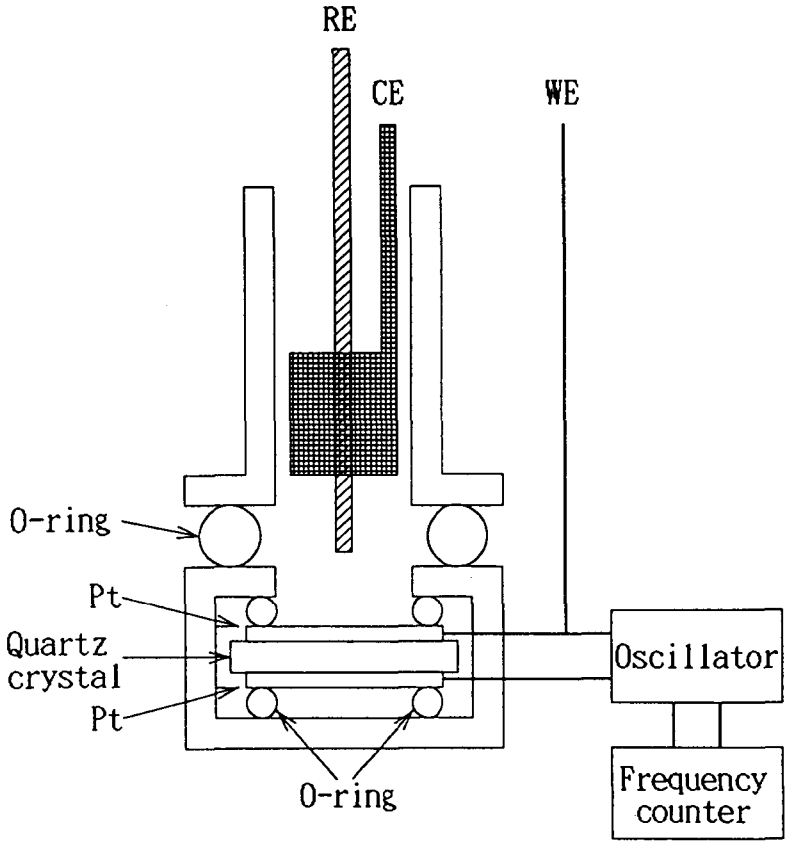

Fig. 2.1. Schematic diagram of an electrochemical quartz crystal microbalance system.

2.2 Experimental

2.2.1 Electrochemical polymerization

All chemicals used in this study were reagent grade. Deionized and then distilled water was used as solvent. The solution used for the preparation of polypyrrole films was water containing 0.1 moldm^{-3} pyrrole monomer and 0.1 moldm^{-3} electrolytes of $NaClO_4$ or Na_2SO_4. The solutions were purged with nitrogen gas before electrochemical polymerization.

The substrates used in the gas response measurements were Corning 7059 glass plates (10 mm × 20 mm), on which Niobium (10 nm) and platinum (40 nm) were evaporated. The substrates consists of two sets of platinum patterns separated by 10 μm gaps. The electrodes were immersed in a 20 mmoldm^{-3} octadecyltriethoxysilane/cyclohexane solution for 12 h before polymerization. Polypyrrole films were grown electrochemically on the substrate by cycling the potential between −0.7 and +0.9 V (vs. Ag/AgCl) using an HA−151 (Hokuto Denko) potentiostat. The deposited polypyrrole films were rinsed with distilled water and dried in nitrogen for at least 24 h before use. The details were given in Chapter 1.

2.2.2 EQCM measurement

Fig. 2.1 shows the schematic diagram of an electrochemical quartz crystal microbalance (EQCM) system. Shear mode quartz crystal plates deposited platinum electrodes on both sides were used as substrates (9 MHz AT−cut quartz crystals). The quartz plate was sealed with an O−ring and polypyrrole was deposited on one side of the platinum electrode (deposition area was 0.79cm^2).

Changes in the mass of the quartz crystal following the oxidation / reduction of attached electro−active polymer films are given by the Sauerbrey equation [9], which relates changes in resonant frequency, Δf, of the quartz

crystal to s changes, Δm, in the film :

$$\Delta f = -\frac{2f_0^2}{\sqrt{\rho\mu}}\frac{\Delta m}{A} \qquad (2.1)$$

where ρ is the density of quartz (2.68 gcm^{-3}), μ the shear modulus of quartz (2.947×10^{11} $dynecm^{-2}$; 1 dyne $\equiv 10^{-5}$ N), f_0 the resonance frequency of the unloaded quartz crystal (9 MHz), and A the piezoelectrically active area of the quartz (cm^2). A linear change of mass with charge passed electrochemically was seen during the course of polymer growth; hence we assume the polymer film as rigid substance free from elastomeric effects.

2.2.3 Gas response measurements

The responses of polymer films to methanol vapor was measured at a concentration of 1000 ppm. Synthetic air (nitrogen 79%, oxygen 21%) was used as the carrier gas. The resistance of polypyrrole films was measured at room temperature using a 3478A digital multimeter (Hewlett-Packard). This apparatus for gas response measurement is described in the experimental section of Chapter 1.

2.2.4 XPS, FT-IR and EPR measurements

Anion doping levels were decided using an ESCA 1000 spectrometer (Shimadzu). The infrared spectra were measured at room temperature on an FTS-3 infrared spectrometer (Bio-Rad) by the reflection method. The EPR apparatus was home-made and used at room temperature under nitrogen atmosphere or in 1000 ppm methanol diluted by nitrogen. Corning 7059 glass plates were used as substrates for XPS, FT-IR (10 mm × 20 mm) and in EPR experiments (3 mm × 20 mm), on which metal thin films were evaporated (50 nm of niobium and 400 nm of platinum). The substrate was mounted onto a

metallic holder. The conditions for electrochemical deposition of polypyrrole films were similar to those described above. The detailed procedure for these measurements will be given in the following chapters.

2.3 Results and discussion

2.3.1 Electrochemical polymerization

Figure 2.2 (a) shows a typical cyclic voltammogram for the growth of polypyrrole on platinum substrates in $NaClO_4$ solution. The film thickness was controlled by the number of potential-sweep cycles as described in Chapter 1. In all experiments, the total electric charge reached to 200 $mCcm^{-2}$. When this amount of charge was passed, the 10 μm gap between the platinum patterns was interconnected with the polypyrrole thin film growing from both electrodes, this was confirmed by measuring the resistance between two platinum electrodes after drying the polymer film. After electrochemical polymerization, the electrodes were washed with distilled water and then the potential was cycled in the background electrolyte until a stable voltammogram was obtained, and finally the potential was held at 0.0 V until the current decayed to less than 0.1 $mAcm^{-2}$, as shown in Fig. 2.2(b). This process is needed to control the degree of oxidation of the film. The sharp increase in current at potentials above +0.7 V is due to the polymerization (Fig. 2.2 (a)). The peaks that grow at −0.1 V on the cathodic and +0.2 V on the anodic scans are due to reduction and oxidation of the deposited polymer.

Figure 2.3 shows the cyclic voltammograms for the deposition of polypyrrole in Na_2SO_4 solution (a), and for the same polypyrrole film cycled in background electrolyte (b). A sharp increase in current for polymerization is observed at potentials above +0.7 V (Fig. 2.3 (a)). The reduction peaks of the film appear at −0.5 V on the cathodic scan. However, the oxidation peaks

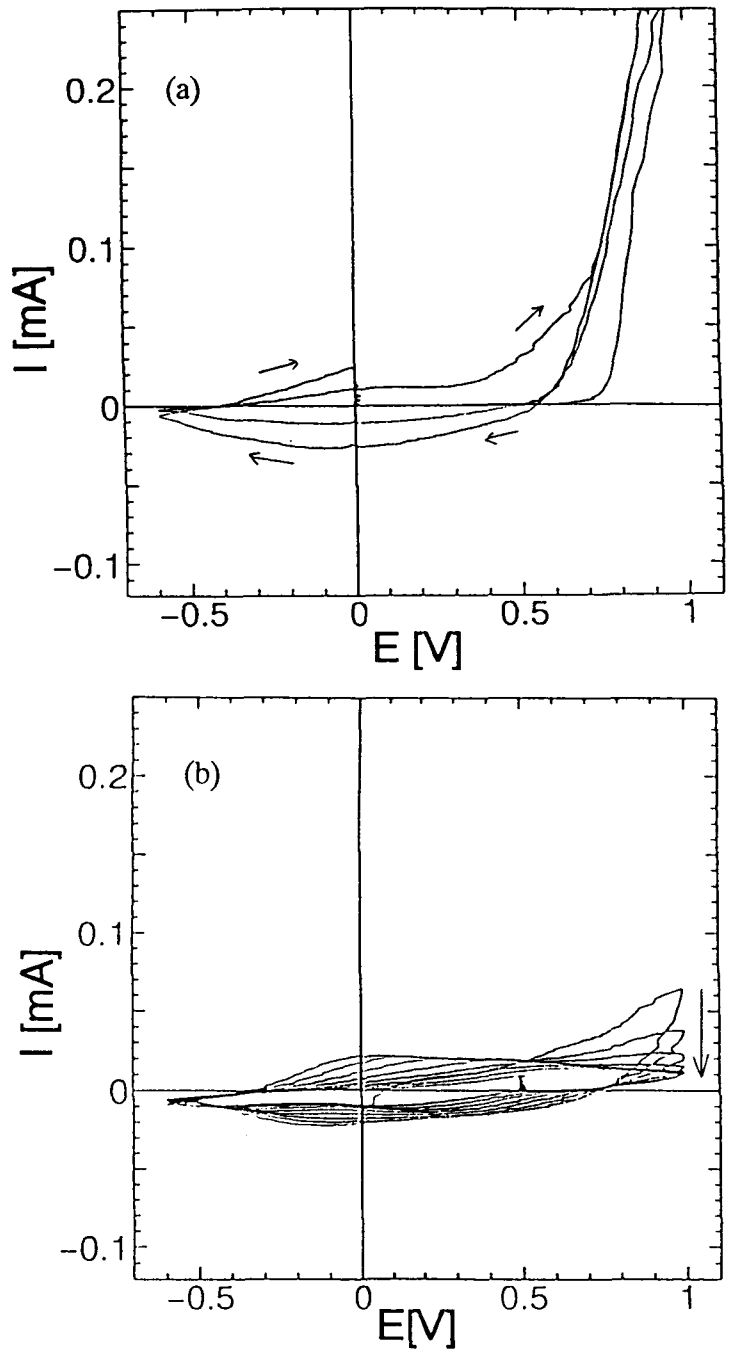

Fig. 2.2. Typical results of the electrochemical polymerization and subsequent cyclic voltammetry of the deposited polypyrrole films.

(a) Deposition of polymer from 0.1 moldm^{-3} pyrrole, 0.1 moldm^{-3} $NaClO_4$ in water by repeated cycling at 100 mVs^{-1}

(b) Cyclic voltammetry of the resulting film in 0.1 moldm^{-3} $NaClO_4$ at 100 mVs^{-1}

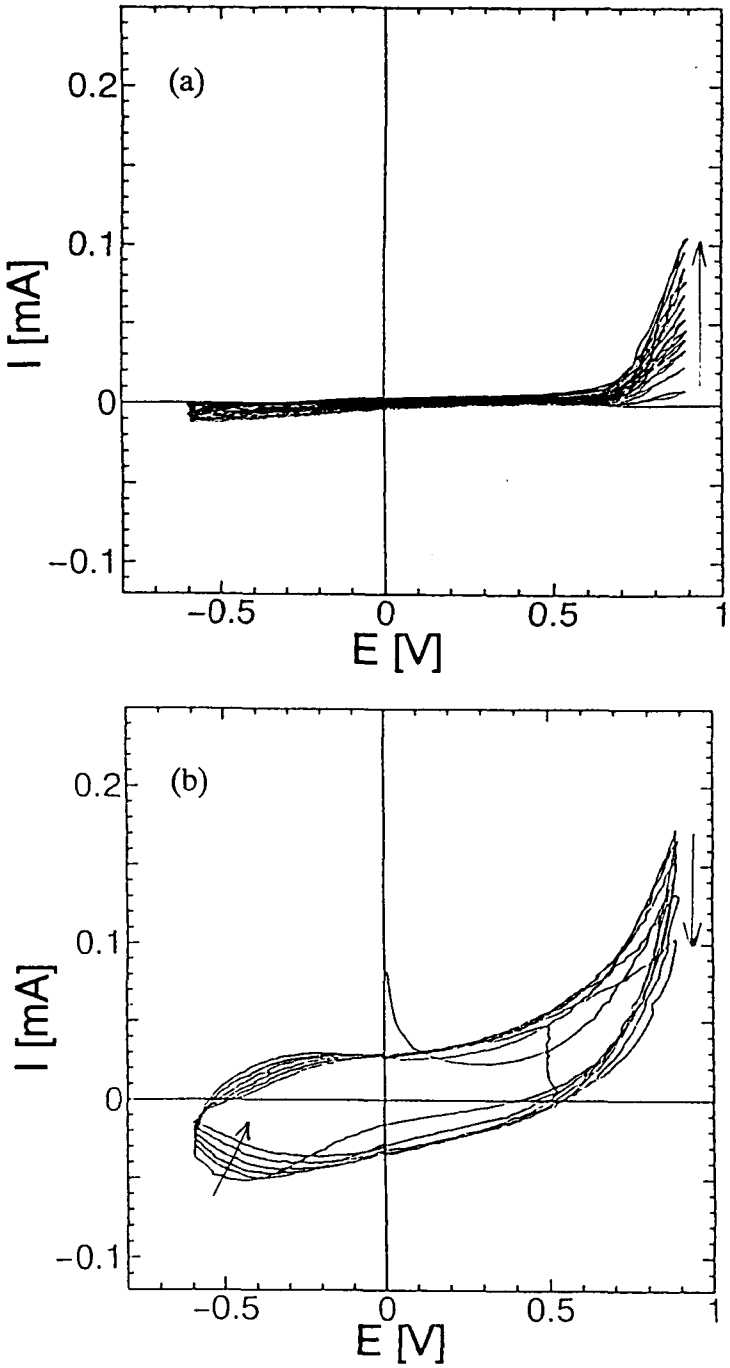

Fig. 2.3. Typical results of the electrochemical polymerization and subsequent cyclic voltammetry of the deposited polypyrrole films.

(a) Deposition of polymer from 0.1 moldm^{-3} pyrrole, 0.1 moldm^{-3} Na_2SO_4 in water by repeated cycling at 100 mVs^{-1}

(b) Cyclic voltammetry of the resulting film in 0.1 moldm^{-3} Na_2SO_4 at 100 mVs^{-1}

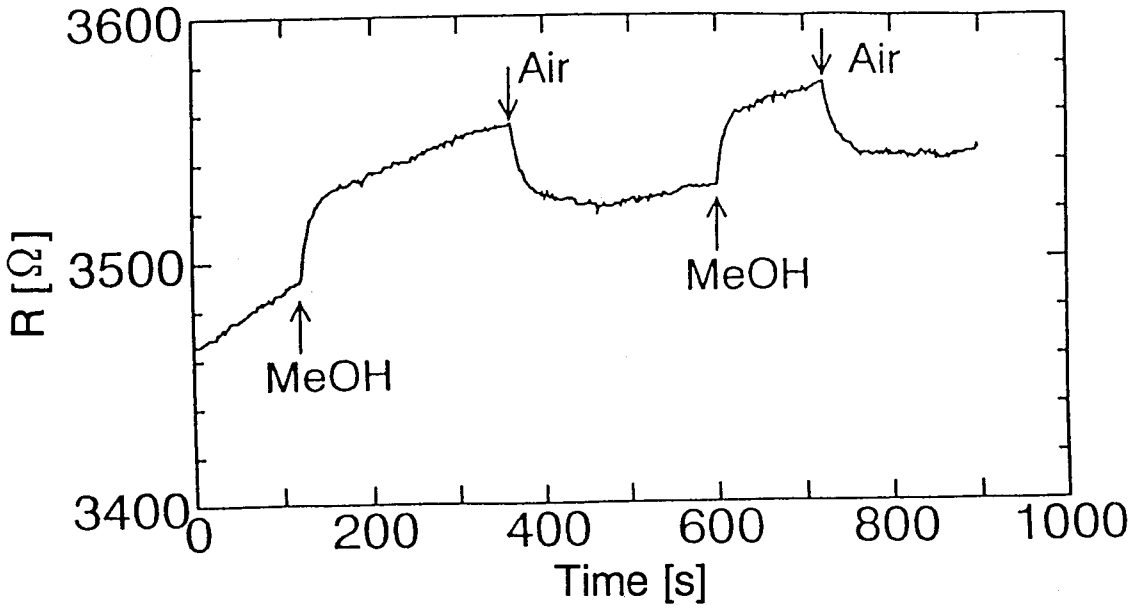

Fig. 2.4. Resistance change of the polypyrrole film polymerized in $NaClO_4$ and treated in $NaClO_4$ by the effect of methanol vapor (1000ppm).

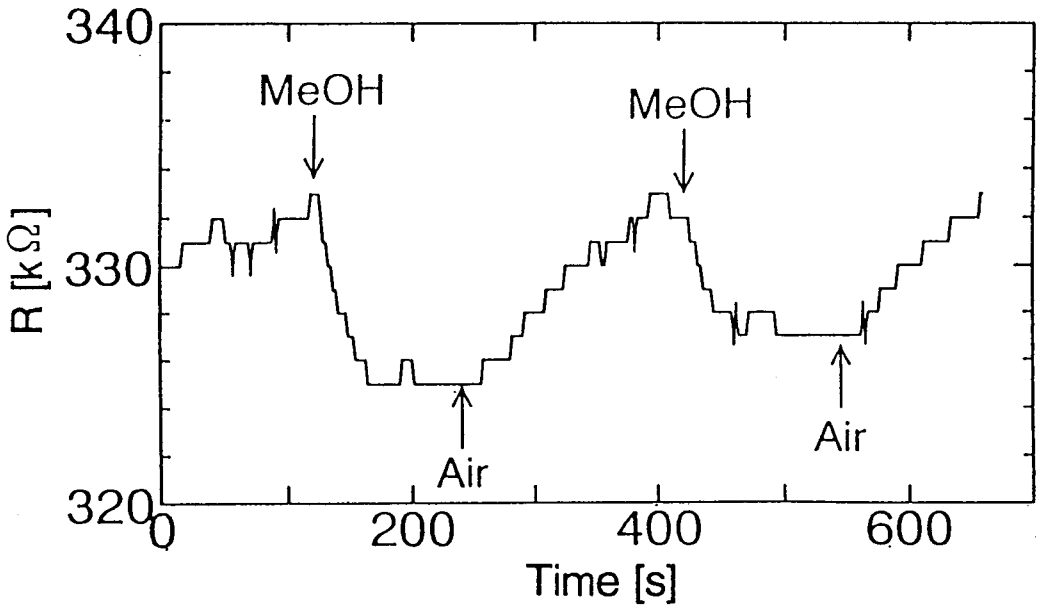

Fig. 2.5. Resistance change of the polypyrrole film polymerized in Na_2SO_4 and treated in Na_2SO_4 by the effect of methanol vapor (1000ppm).

of the film are not clearly observed on the anodic scans (Fig. 2.3 (b)). It is evident that the kind of electrolytes affects the cyclic voltammogram of polymerization and the properties of polymers. Further discussion will be presented later.

2.3.2 Response to methanol

Figure 2.4 shows a typical response curve for polypyrrole film deposited from $NaClO_4$ solution against methanol. The film was repeatedly exposed to air and methanol (1000 ppm) in air. The resistance of the film increased when the ambient gas was changed from dry air to methanol, then gradually reached a steady state. When the ambient gas was changed to dry air, the resistance decreased to its initial value. Figure 2.5 shows a typical response curve for polypyrrole film deposited from Na_2SO_4 solution. In this case, the resistance decreased suddenly and then gradually reached a steady state when the ambient gas was changed from dry air to methanol vapor. This response is different from that of Fig. 2.4; the resistance of these films changes in opposite directions. It is important to elucidate whether this difference results from their polymer structures or from the properties of the anions doped in polypyrrole.

2.3.3 Treatment for anion-exchange

In order to clarify the above point, a polypyrrole film polymerized in Na_2SO_4 was electrochemically treated by sweeping the potential in the $NaClO_4$ solution, as shown in Fig. 2.6 (a). This polypyrrole film is abbreviated as PP(SO_4 → ClO_4). The reduction peaks shown at −0.5 V on the cathodic scans decreased with the swept cycles. These peaks were characteristic to the SO_4^{2-}-doped polypyrrole film. they were observed when the potential was swept in Na_2SO_4, PP(SO_4 → SO_4), as shown in Fig. 2.3 (b). From the comparison of these voltammograms, it is expected that the doped anions were exchanged from SO_4^{2-} to ClO_4^-. Similarly a polypyrrole film polymerized in $NaClO_4$ was

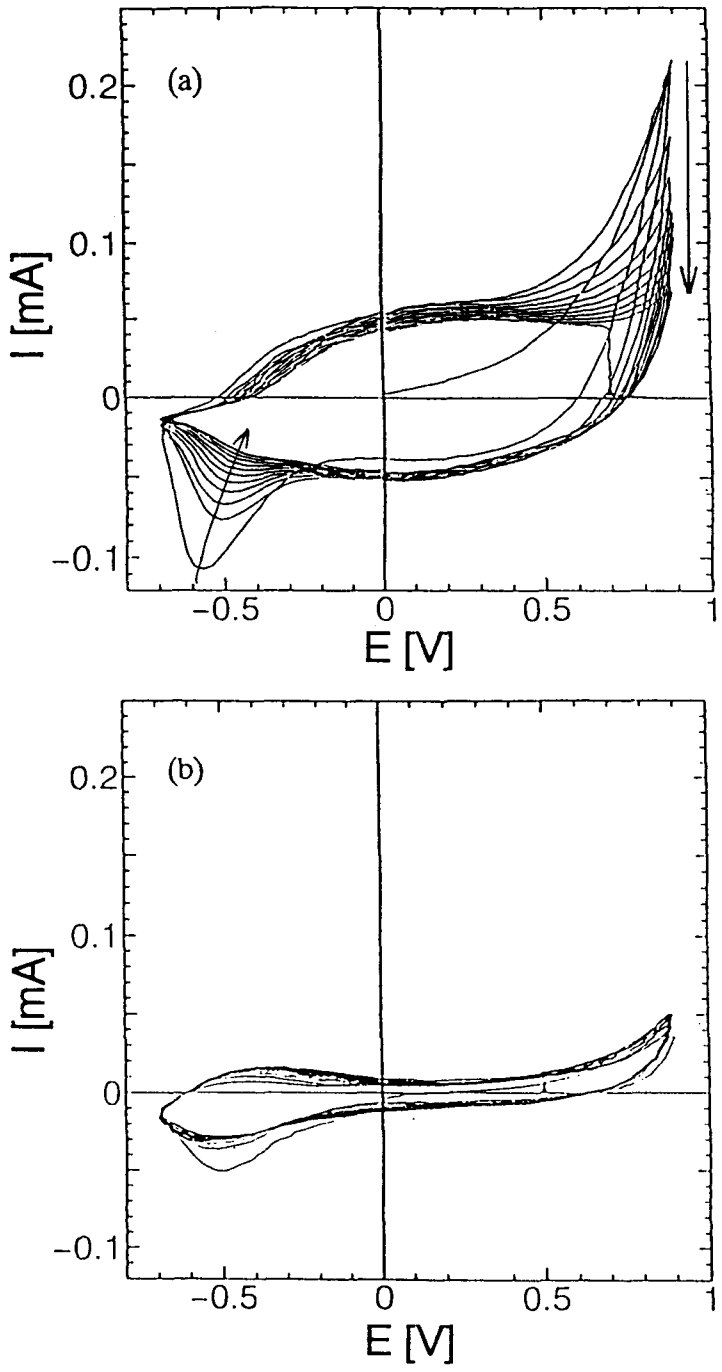

Fig. 2.6. Typical cyclic voltammograms recorded at 100 mVs^{-1}.
(a) SO_4^{2-}–doped polypyrrole recorded in 0.1 $moldm^{-3}$ $NaClO_4$
(b) ClO_4^-–doped polypyrrole recorded in 0.1 $moldm^{-3}$ Na_2SO_4

treated in the Na_2SO_4 solution as shown in Fig. 2.6 (b). In this case, the cyclic voltammogram of PP(ClO_4 → SO_4) has the properties of both PP(ClO_4 → ClO_4) and PP(SO_4 → SO_4), (in Fig. 2.2 (b) and 2.3 (b)).

2.3.4 Determination of doping level of anions by XPS

The doping level of anions was determined from the intensity of the N1s, S2p and Cl2p photoemission spectra. The detailed explanation on the method is described in Chapter 4. Table 2.1 shows the doping level of polypyrrole films polymerized in $NaClO_4$ and Na_2SO_4 solutions and post-treated in $NaClO_4$ and Na_2SO_4 solutions. The doping levels of anions in polypyrrole films polymerized in $NaClO_4$ and Na_2SO_4 were 0.34 and 0.16, respectively. Because sulfonate is divalent, the level of doped charge is calculated to be 0.32, which is equal to that of ClO_4^- within the limit of error. The doping level of PP(SO_4 → SO_4) was 0.17 and was nearly equal to that of polypyrrole polymerized in Na_2SO_4. On the other hand, the doping level of PP(ClO_4 → ClO_4) was 0.08 and was smaller than that of polypyrrole polymerized in $NaClO_4$ without the post-treatment. This indicates the fact that ClO_4^- is easily released from polypyrrole film. The doping level of ClO_4^- and SO_4^{2-} in PP(ClO_4 → SO_4) was 0.09 and 0.32. This means that most of ClO_4^- is released and SO_4^{2-} is doped in polypyrrole films, i.e., anions are exchanged. For PP(SO_4 → ClO_4), the doping level of ClO_4^- and SO_4^{2-} is 0.14 and 0.11. This suggests that SO_4^{2-} is more difficult to remove than ClO_4^-.

2.3.5 Study of anion-transfer by EQCM

Figure 2.7 shows the results of EQCM measurements for ClO_4^--doped polypyrrole film measured in 0.1 M $NaClO_4$ (b), and for SO_4^{2-}-doped polypyrrole film in 0.1 M $NaClO_4$ (c). The mass of the ClO_4^--doped polypyrrole film increased with the increase of potential. This means that ClO_4^- is incorporated into the polymer film during the anodic scan, and released from

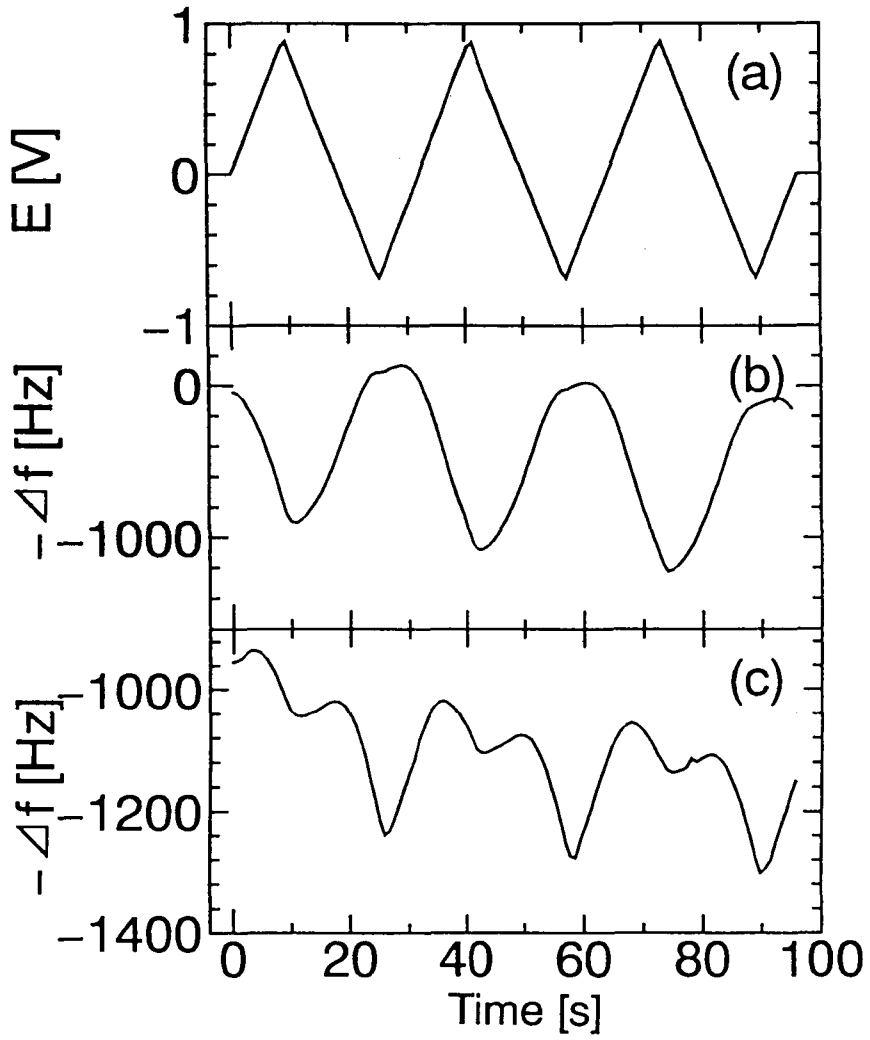

Fig. 2.7. EQCM measurements for polypyrrole films.

(a) Applied potential

(b) Frequency change for a ClO_4^--doped polypyrrole film in 0.1 M $NaClO_4$

(c) Frequency change for a SO_4^{2-}-doped polypyrrole film cycled in 0.1 M $NaClO_4$

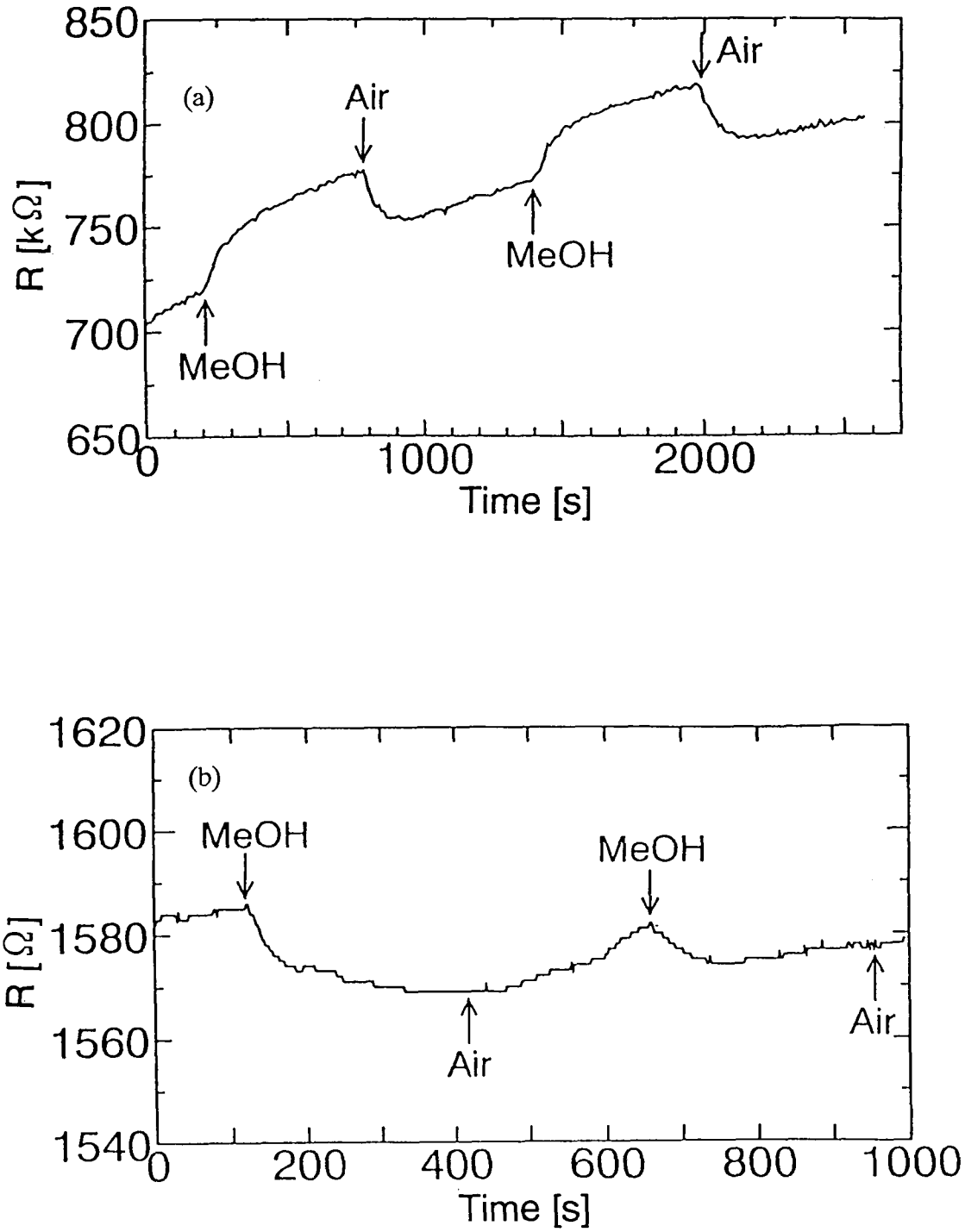

Fig. 2.8. Resistance change of polypyrrole films by the effect of methanol vapor (1000ppm).

(a) Polymerized in Na_2SO_4 and treated in $NaClO_4$

(b) Polymerized in $NaClO_4$ and treated in Na_2SO_4

the polymer film during the cathodic scan. The ClO_4^- ion is incorporated to compensate the positive charge formed in the PP film by the electrochemical oxidation of pyrrole rings, and released as the positive charge on the pyrrole rings are neutralized by their electrochemical reduction. Since the mass change returned to its initial value at the start of each potential cycle, these incorporated and released processes can be regarded as being reversible.

In the case of SO_4^{2-}-doped polypyrrole film, the EQCM results are complicated. There seems to be two pairs of ion incorporation-release process. They are observed during the potential change from 0.4 to -0.1 V with a smaller mass change and during the potential change from -0.1 to 0.4 V with a smaller mass change. The first incorporation-release process are attributed to the movement of SO_4^{2-} ions, which is incorporated into polypyrrole during the anodic potential shift and released during the cathodic shift. The second process have mass change opposite to the first process. Namely, the mass increases during the cathodic scan, and decreased during the anodic scan. Such mass change can only be explained by assuming that the mobile ions are cations, or sodium ions. this means that SO_4^{2-} ions are more difficult to move than ClO_4^- ions, and the charges formed in polypyrrole films by the electrochemical reactions are compensated with the help of incorporation and release of sodium ions. This explanation is in harmony with the results obtained from XPS measurements (see Section 3.3.2).

2.3.6 Gas response of anion-exchanged polypyrrole

The resistance change of polypyrrole films in which the anions are exchanged by applying the post-treatments is shown in Fig. 2.8. The resistance of PP($SO_4 \rightarrow ClO_4$) increased when the ambient gas was changed from dry air to methanol vapor, and decreased when the atmosphere was changed to dry air again, as shown in Fig. 2.8 (a). This response pattern is similar to that of PP($ClO_4 \rightarrow ClO_4$), as shown in Fig. 2.4. In the case of PP($ClO_4 \rightarrow SO_4$), the

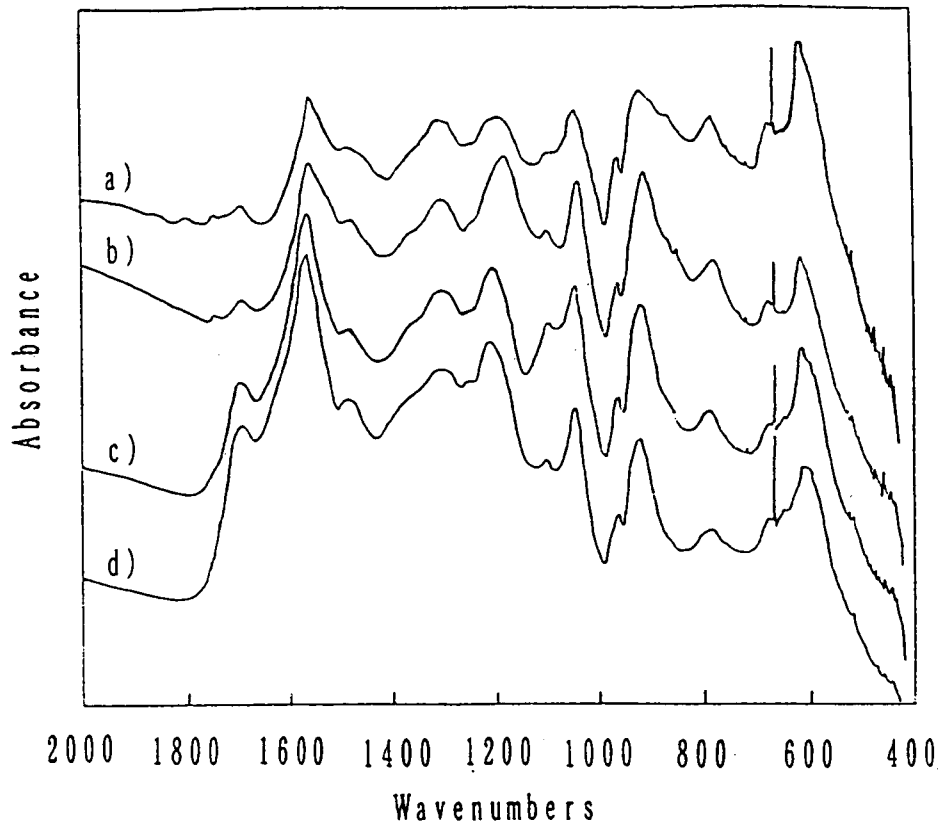

Fig. 2.9. FT-IR spectra of polypyrrole films.

(a) Polymerized in $NaClO_4$ and post-treated in $NaClO_4$

(b) Polymerized in $NaClO_4$ and post-treated in Na_2SO_4

(c) Polymerized in Na_2SO_4 and post-treated in $NaClO_4$

(d) Polymerized in Na_2SO_4 and post-treated in Na_2SO_4

Table 2.1 Anion doping levels of polypyrrole films

Electrolyte		Anion doping level	
Polymerization	Treatment	ClO_4^-	SO_4^{2-}
$NaClO_4$	–	0.34	–
$NaClO_4$	$NaClO_4$	0.08	–
$NaClO_4$	Na_2SO_4	0.09	0.32
Na_2SO_4	–	–	0.16
Na_2SO_4	Na_2SO_4	–	0.17
Na_2SO_4	$NaClO_4$	0.14	0.11

Table 2.2 EPR experimental parameters for polypyrrole films

Polymerization and treatment electrolyte	Ambient gas	Intensity ratio I_{gas}/I_{N_2} [c]	peak-to-peak line width W_{gas}/W_{N_2} [c]
$NaClO_4 \rightarrow NaClO_4$	$MeOH/N_2$ [a]	0.63	1.48
	N_2 [b]	0.81	1.00
$Na_2SO_4 \rightarrow NaClO_4$	$MeOH/N_2$ [a]	0.79	1.22
	N_2 [b]	0.99	1.00
$Na_2SO_4 \rightarrow Na_2SO_4$	$MeOH/N_2$ [a]	1.04	1.80
	N_2 [b]	1.03	1.00
$NaClO_4 \rightarrow Na_2SO_4$	$MeOH/N_2$ [a]	0.94	2.15
	N_2 [b]	1.20	1.12

a) In 1000ppm methanol diluted by N_2.
b) In N_2 after exposure to methanol.
c) Normalized by the value before exposure to methanol.

response shown in Fig. 2.8 (b) is similar to that of PP(SO_4 → SO_4) in Fig.2.5. From these results, it is concluded that the anions doped in polypyrrole films determine the gas response properties of PP films.

2.3.7 FT-IR studies of anion-exchanged polypyrrole

Figure 2.9 shows FT-IR spectra of the polypyrrole films; (a) PP(ClO_4 → ClO_4), (b) PP(ClO_4 → SO_4), (c) PP(SO_4 → ClO_4) and (d) PP(SO_4 → SO_4). The spectra of (b) is similar to that of (a), and that of (d) is similar to that of (c). This means that the molecular structures of polypyrrole films are determined by the anions used for their polymerization, but are not largely affected by the anions introduced in them by the post-electrochemical treatments. On the other hand, the gas response is dependent on the anions included in the films, or the anions introduced by the post-treatments. Therefore, it is concluded that the difference in gas response patterns among the polypyrrole films is not caused by a difference in their molecular structures, but is dependent on the anions introduced in them.

2.3.8 EPR studies

The EPR spectra of PP(SO_4 → ClO_4) were measured at room temperature in nitrogen before exposure to methanol, in 1000 ppm methanol diluted by nitrogen, and in N_2 after exposure to methanol. Peak-to-peak line width in methanol vapor is larger than that in nitrogen. In Table 2.2, spin intensity and peak-to-peak line width of several PP films measured in methanol vapor and in nitrogen after exposure to methanol are summarized. They are normalized by the values observed in N_2 before exposure to methanol vapor. The spin intensities of PP(ClO_4 → ClO_4) and PP(SO_4 → ClO_4) decreased in methanol vapor, while those of PP(SO_4 → SO_4) and PP(ClO_4 → SO_4) were virtually unchanged. That is to say, the concentration of unpaired electrons in polypyrrole films containing ClO_4^- decreased in the presence of methanol vapor,

and that was unchanged in the case of polypyrrole film containing SO_4^{2-}. The peak-to-peak line width increased in all cases. Further discussion on these results will be presented in Chapter 4.

2.4 Conclusion

It was found that dopant anions determine the methanol response pattern. The concentration of unpaired electrons in ClO_4^--doped polypyrrole films decreased, and its resistance increased, in methanol vapor. For SO_4^{2-}-doped polypyrrole film, the resistance decreased and the concentration of unpaired electrons was unchanged. From the measurements of FT-IR spectra, it was concluded that the difference in gas response of polypyrrole films is not attributable to the difference in their molecular structures. However, the gas-response pattern seems to be largely affected by the electronic interactions between polypyrrole, anion and methanol.

References

[1] M. Salmon, A. F. Diaz, A. J. Logan, M. Krounbi and J. Bargon, *Mol. Cryst. Liq. Cryst.*, **83**, 265 (1982).

[2] L. F. Warren and D. P. Anderson, *J. Electrochem. Soc.*, **134**, 105 (1987).

[3] R. J. Mammone and M. Binder, *J. Electrochem. Soc.*, **137**, 2135 (1990).

[4] M. Yamaura, T. Hagiwara and K. Iwata, *Synth. Met.*, **26**, 209 (1988).

[5] K. Sato, M. Yamaura, T. Hagiwara, K. Murata and M. Tokumoto, *Synth. Met.*, **40**, 35 (1991).

[6] K. Naoi, M. M. Lien and W. H. Smyrl, *J. Electroanal. Chem.*, **272, 273** (1989).

[7] K. Naoi, M. Lien and W. H. Smyrl, *J. Electrochem Soc.*, **138** (1991).

[8] M. Lien and W. H. Smyrl, *J. Electroanal. Chem.*, **309**, 333 (1991).

[9] G. Sauerberg, *Z. Phys.*, **155**, 206 (1959).

Chapter 3

XPS Investigations of Polypyrrole and Methyl Substituted Polypyrroles : Their Electronic Property and the Gas Sensing Mechanism

Polypyrrole films doped with BF_4^- or SO_4^{2-} showed a decrease in electric resistivity by exposing them to methanol vapor. On the other hand, those doped with p-toluenesulfonate or poly(4-styrenesulfonate) showed a increase in resistivity in the presence of methanol. On the basis of XPS measurements, it was found that there is strong electrostatic interaction between the cationic (or oxidized) sites of polypyrrole and doped small anions in polypyrrole. In this case, methanol absorbed in PP films screens the electrostatic force between them and delocalizing the positive charge over pyrrole rings, leading to lowered electric resistance. As for PP films doped with large anions, such as p-toluenesulfonate and poly(4-styrenesulfonate), the electrostatic interaction is weak. In this case, morphological change by the absorption of methanol plays the major role and the electric resistivity is increased by methanol. The gas-sensing properties of poly(3-methylpyrrole) and poly(N-methylpyrrole) films are also studied.

3.1 Introduction

We have studied the gas sensing properties of PP and its derivatives, and have found the following features; i) the resistance of polypyrrole films changes when the films were exposed to the organic vapors of polar molecules, such as methanol, ethanol or acetone [1], ii) the sensitivity for methanol was especially high, and the response depended largely on the doped anions [2], iii) response to gasses of conducting polymers made from N-methylpyrrole was different from that of PP [3]. These properties are favorable to construct an 'intelligent' gas-sensing system.

In spite of some promising results as gas sensors, only a few attempts have been made to clarify the gas sensing mechanism of conducting polymers. Josowicz *et al.* reported that there is weak interactions between the small vapor molecules and the polymer matrix on the basis of the linear relationship between the changes in work function and the amount of molecules absorbed in the PP film [4]. They concluded that sorption of organic vapors in polypyrrole is the driving force of the interaction, which is affected by the nature of anions incorporated in the polymer matrix.

The size of the anions has been reported to be an important factor for determining the structure and morphology of polymer films polymerized electrochemically. Several studies have recently been performed to determine the chemical state and nature of the conducting polymer doped with anions using X-ray photoemission spectroscopy (XPS) [6-11].

In this chapter, polypyrrole (PP), poly(3-methylpyrrole) (P3MP) and poly(N-methylpyrrole) (PNMP) thin films prepared by electrochemical polymerization are investigated with a view to utilizing them as gas sensors. The influences of doped anions and the methyl substituent of polypyrrole on the response of the films to methanol vapor will be discussed on the basis of resistivity and XPS measurements.

3.2 Experimental

3.2.1 Film Preparations

All chemicals used in the present study were reagent grade. Deionized and distilled water was used as a solvent for electrochemical polymerization. Pyrrole (Wako), 3-methylpyrrole (Sigma) and N-methylpyrrole (Wako) were doubly distilled and used as monomers. $NaClO_4$, $NaBF_4$, Na_2SO_4, sodium p-toluenesulfonate (NaTOS) and sodium poly(4-styrenesulfonate) (NaPSS) were used as the supporting electrolytes and as sources of anionic dopants.

The solutions used for the preparation of polymer films contained 0.1 $moldm^{-3}$ monomer and 0.1 $moldm^{-3}$ supporting electrolytes. For the preparation of PSS^--doped polymer films, we used the solutions containing 0.1 $moldm^{-3}$ monomer and 0.1 $moldm^{-3}$ sulfonate groups in NaPSS. The solutions were purged with N_2 gas before electrochemical polymerization. All polymer films were grown on substrate by applying potentials cycled between -0.7 and +0.9 V vs. an Ag/AgCl (3.33N KCl saturated with AgCl) reference electrode at the rate of 100 mV/s using a Hokuto Denko HA-151 potentiostat. The potential was controlled by a computer via a 12-bit D/A converter. The potential and current of the electrochemical experiment were also measured and stored using 12-bit A/D converter. The deposited polymer films were rinsed with distilled water and dried in a nitrogen atmosphere for more than 24 h at room temperature. Details of electrochemical polymerization have been given in the previous paper [2].

The substrates used for the gas response measurements were Corning 7059 glass plates ($10\times20mm^2$). On one side of the glass plate, two stripes of platinum ($10\times3000\mu m^2$) about 10μm apart were evaporated, as shown in Fig.1.1. The platinum stripes form the electrodes for polymerization. After polymerization, the gap of the Pt electrodes was covered and bridged by polymer films. In order to get good adherence of polymerized films to the

substrates, the substrates were immersed in 20 $mmoldm^{-3}$ octadecyltriethoxysilane/cyclohexane solution for 12h before polymerization [1].

3.2.2 Gas response

The response to methanol was measured using the apparatus described in Chapter 1. The resistance of polymer films between the two Pt stripes was measured using a Hewlett-Packard 3478A digital multimeter. The obtained data were transferred to a computer via an IEEE-488 interface. The response to organic vapors was measured at the vapor concentration of 1000 ppm. Nitrogen was used as the carrier gas.

3.2.3 XPS measurement

For the XPS experiments, Corning 7059 glass plates (10×20mm), on which metal thin films were evaporated (50 nm niobium and 400 nm platinum), were used as substrates. The XPS studies were performed using a Shimadzu ESCA 1000 spectrometer (Mg Kα X-ray source). The surface composition of doped polymer films was determined from the C1s, N1s, O1s, B1s, Cl2p, and S2p, Na_{KLL} photoelectron peaks, which were corrected using appropriate sensitivity factors. The energy calibration was checked using the $Pt4f_{7/2}$ line of platinum evaporated on glass substrate. Charging effects were not observed for the conductive samples. The photoemission data of N1s and B1s, Cl2p, or S2p were used to determine the doping level of BF_4^-, ClO_4^- and anions containing sulfonate groups in polymer films. The peak positions, peak height and full-width at half-maximum for the component Gaussians were provided by subtracting background signals and decomposing interactively the line-shape using the Gaussian function.

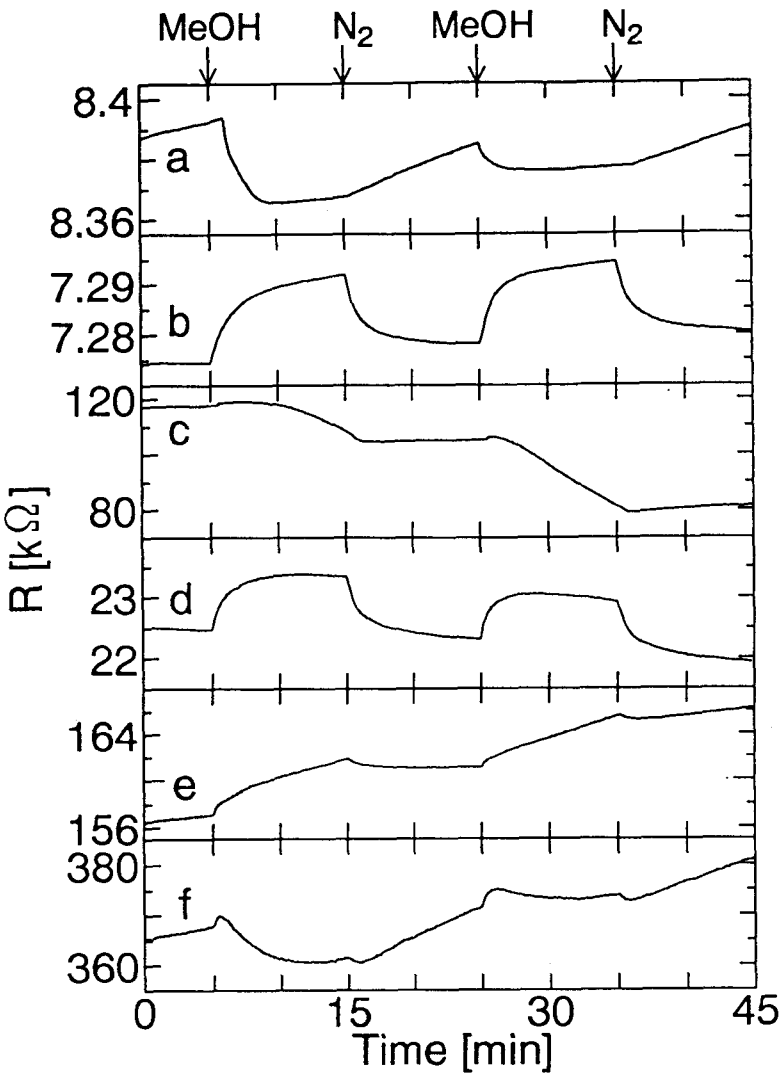

Fig. 3.1. Resistance change of polymer films by the effect of methanol vapor (1000ppm).

a) BF_4^-–doped PP b) TOS^-–doped PP

c) BF_4^-–doped P3MP d) TOS^-–doped P3MP

e) BF_4^-–doped PNMP f) TOS^-–doped PNMP

3.3 Results and discussion

3.3.1 Gas response

Figure 3.1 shows typical response curves of the resistance of PP, P3MP and PNMP films doped with BF_4^- or TOS^-. The films were repeatedly exposed to N_2 and methanol (1000ppm) in N_2. In the case of BF_4^-–doped PP and P3MP films, the resistance decreased when exposed to methanol vapor. For TOS^-–doped PP and P3MP, the resistance increased in methanol and decreased in N_2. PNMP films showed behavior different from that of PP and P3MP films. The resistance of BF_4^-–doped PNMP increased, while that of TOS^-–doped PNMP decreased, when exposed to methanol vapor.

Table 3.1 summarizes the resistivity of PP, P3MP and PNMP films doped with various kinds of anions. The initial resistance (R_0) was obtained before exposure to methanol and the sensitivity (S) is defined as $\Delta R/R_0 \times 100$ [%]; ΔR is the change in resistance observed when the films were exposed to methanol. Compared with PP and P3MP films, PNMP showed higher resistivity. SO_4^- or PSS^-–doped PNMP films were almost nonconducting. The increase and decrease of the resistance of the films by exposure to methanol can be related to the size of the anions doped in the films. Namely, the resistance of small–anion doped PP and P3MP films decreased in methanol vapor, while those doped with large anions, such as TOS^- or PSS^-, showed increase in resistivity in methanol vapor. On the other hand, for PNMP, an increase of resistance was obtained with small–anion doped films by exposing them to methanol .

3.3.2 Doping level of anions

The binding energy of the core levels of B1s, F1s, O1s, Cl2p and S2p appeared at about 193 eV, 686 eV, 531 eV, 207 eV and 167 eV, respectively. Pfluger and Street determined the anion doping levels of electrochemically polymerized PP–ClO_4 films from the analysis of N1s and Cl2p peak areas, and

Table 3.1 Initial resistance and sensitivity to methanol for various anion-doped conducting polymer films

Anion	R_0[a] [kΩ]			S[b] [%]		
	PP	P3MP	PNMP	PP	P3MP	PNMP
ClO_4^-	7.14	6.59	27.1	-0.171	-0.611	+1.55
SO_4^{2-}	12.89	7.52	∞	-2.37	-1.17	—
BF_4^-	8.39	7.02	157.1	-0.334	-0.638	+2.99
TOS^-	7.50	5.93	36.8	+0.263	+0.182	-1.94
PSS^-	17.15	20.18	∞	+0.469	+3.57	—

a) The resistance before exposure to methanol.

b) The sensitivity to 1000 ppm methanol, defined as $\Delta R/R_0$, where ΔR is the change in resistance on exposure to methanol.

Table 3.2 Anion doping level of conducting polymer films

Anion	Doping level[a]		
	PP	P3MP	PNMP
BF_4^-	0.25	0.25	0.31
ClO_4^-	0.34	0.34	0.30
SO_4^-	0.16	0.28	0.31
TOS^-	0.23	0.39	0.31
PSS^-	0.47	0.72	1.51

a) XPS spectra of B1s, C12p and S2p were employed to determine the doping level.

compared the results with those obtained by chemical analysis [8]. From the results, they concluded that XPS can be a reliable quantitative analytical tool for the doped ions, provided appropriate care is taken. According to their method, we measured the peak areas normalized by the area of N1s peak (see Table 3.2). The doping level of ClO_4^- thus determined was 0.34 in our experiment, which is in good agreement with the result reported by Pfluger and Street (0.35) [8]. For P3MP and PNMP, the doping levels of ClO_4^- was 0.34 and 0.30, respectively. These were close to the value for PP–ClO_4. Similar values were obtained for other anions, and it is concluded that a negative charge was produced per about 3 pyrrole ring units in the case of ClO_4^-, BF_4^-, SO_4^{2-} and TOS^-. The doping level of PSS^- was calculated as the number of sulfonate substituents in PSS^-. In this case, the doping level is higher than that of small anions. This can be explained by assuming that small anions can move easily in the polymer film to make ion pairs with pyrrole ring sites by electrostatic interaction. On the other hand, sulfonate groups in PSS^- cannot move easily, because PSS^- is a polymer anion and the sulfonate groups are fixed to polymer chain of polystyrene.

In order to verify the above discussion, we measured the amount of Na^+ ions incorporated into polymer films (PP, P3MP and PNMP doped with ClO_4^-, SO_4^{2-}, TOS^- and PSS^-; 12 samples) by XPS measurements. Polymer films doped with small anions, such as ClO_4^- and SO_4^{2-}, were free from Na^+ ions within the experimental error of XPS. Small Na_{KLL} peak was observed for PP–TOS film. In the case of PSS–doped PP, P3MP and PNMP films, large Na_{KLL} peaks were observed. This means that large amounts of Na^+ ions were incorporated into polymer films doped with polymer anions to neutralize the negative charge of sulfonate ions, which are not making ion pairs with the positive charges on pyrrole rings. From the above results, we conclude that the doping level is determined by the kind of anions and influenced a little by the monomers used for polymerization.

3.3.3 C1s line shape

Figure 3.2 shows the C1s photoemission of PP films doped with BF_4^-, SO_4^{2-} TOS^- and PSS^-. It can be seen that the C1s line is not symmetric, and that four components lie on the peak. Pflunger *et al.* have studied XPS spectra of conducting polymers and concluded that the asymmetry at higher binding energies of the C1s peak can be assigned to cross-linked, chain-terminating or non-α,α' bonded carbons [8], since it is known that the disorders caused by these carbons can lead to inhomogeneous broadening of core levels [12]. For line shape analysis based on Gaussian fitting, we used energy splitting of 0.9 eV for α and β carbon peaks, which is determined by Smyrl *et al.* for pyrrole monomers [13]. As the result, the C1s spectra of PP films can be decomposed into four component (I - IV) as shown in Fig. 3.2. The contributions from the four components to the C1s spectra of small-anion-doped PP films (i.e., PP-BF_4 and PP-SO_4) are C-I 32 %, C-II 41 %, C-III 18 % and C-IV 9 %.

These components have been assigned as follows: the component with the lowest binding energy (C-I), which is centered at 283.7 eV and has a line width of 1.5 eV, is due to the pyrrole β carbons. The C-II peak is centered at 284.6 eV and has a line width of 1.6 eV. This peak contains components of α carbons from neutral pyrrole units and β carbons from cationic pyrrole units. This is the reason for larger C-II than C-I [6]. The C-III peak comprises α carbons of cationic pyrrole units and disorder-type carbons, which are caused by the formation of single C-O bonds. The peak of C-IV has been attributed to carboxylation at polypyrrole chain termination or at the points of pyrrole ring cleavage, or due to formation of carbonyl bonds at α carbon sites.

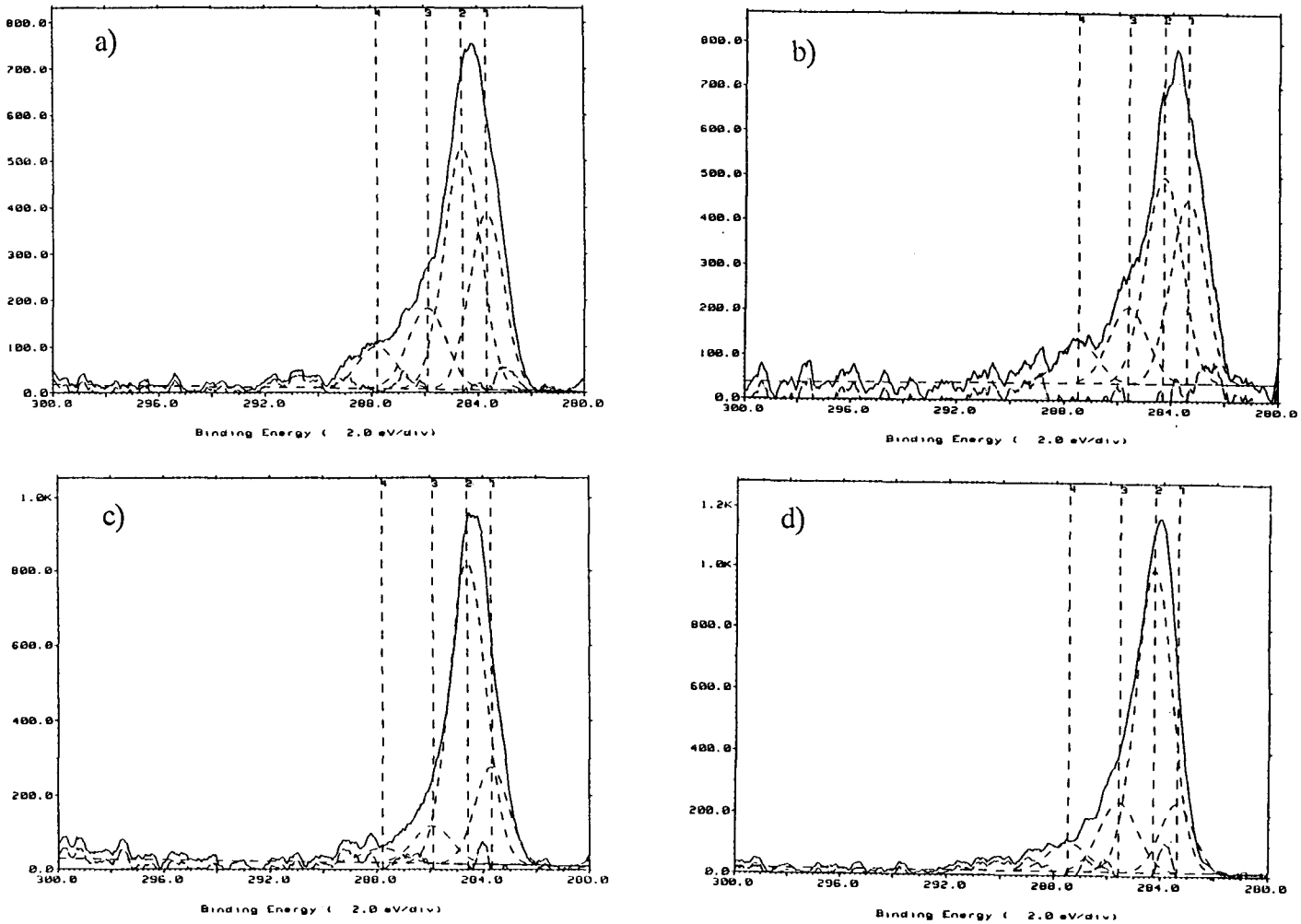

Fig. 3.2. C1s photoemission for polypyrrole films doped with a) BF_4^-, b) SO_4^{2-}, c) TOS^-, d) PSS^-.

3.3.4 N1s line shape

Typical N1s core level spectra of PP-BF_4, PP-SO_4, PP-TOS and PP-PSS are shown in Fig. 3.3. These spectra show shoulders on the higher binding energy side of the peaks. The shoulder of PP-BF_4 is larger than those of PP-TOS and PP-PSS. Besides PP-BF_4, large shoulders are observed for PP doped with small anions, i.e., PP-BF_4 and PP-SO_4. As has already been reported [6], the shoulder becomes larger for BF_4^--doped PP than for PSS^--doped PP [3]. The shoulder can be attributed to the nitrogen atom which is located close to anions, as shown in Fig. 3.4(a). Small anions doped in PP films have strong electrostatic interactions with pyrrole ring site, especially with nitrogen atom, on which positive charge is localized. This results in large binding energy. About 2-thirds of pyrrole rings are neutral as discussed before, and the main peak is attributed to the nitrogen atoms on them. In the case of large-anion-doped PP, the anion cannot easily approach the nitrogen atom of pyrrole ring. Hence the positive charge is less localized on the nitrogen atom. As a result, the intensity of the N1s shoulder of large-anion-doped PP films is less than that of small-anion-doped PP films, as shown in Fig. 3.3.

Figure 3.5 shows the typical N1s core level spectra of P3MP-BF_4, P3MP-SO_4, P3MP-TOS and P3MP-PSS films. These P3MP films show tendency similar to PP films, i.e., the peak is asymmetric on the higher binding energy side, and the shoulder of small-anion-doped P3MP films is larger than that of large-anion-doped P3MP films. From these results, it is concluded that the methyl substituent of P3MP has no inhibitory effect on the interaction between small anions and nitrogen atom, on which positive charge is localized, as shown in Fig. 3.6(a).

In the case of PNMP, the N1s core level photoemission spectra show a single peak, as shown in Fig. 3.7. The binding energy of the N1s core level for PNMP-BF_4 and PNMP-TOS is 399.7 eV. This binding energy is slightly larger than that of the major peak of anion-doped PP and P3MP films. This

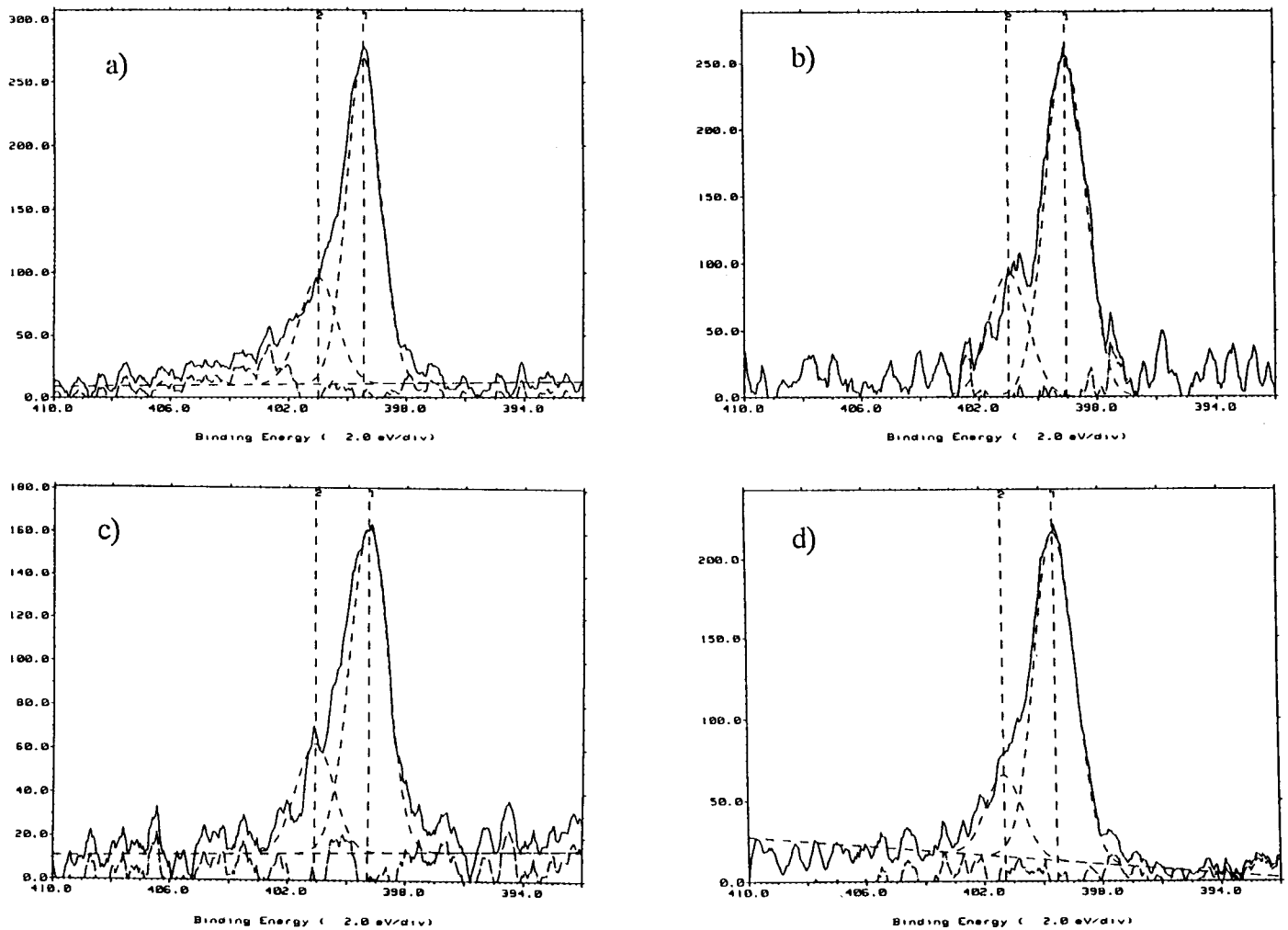

Fig. 3.3. N1s photoemission for polypyrrole films doped with a) BF_4^-, b) SO_4^{2-}, c) TOS^-, d) PSS^-.

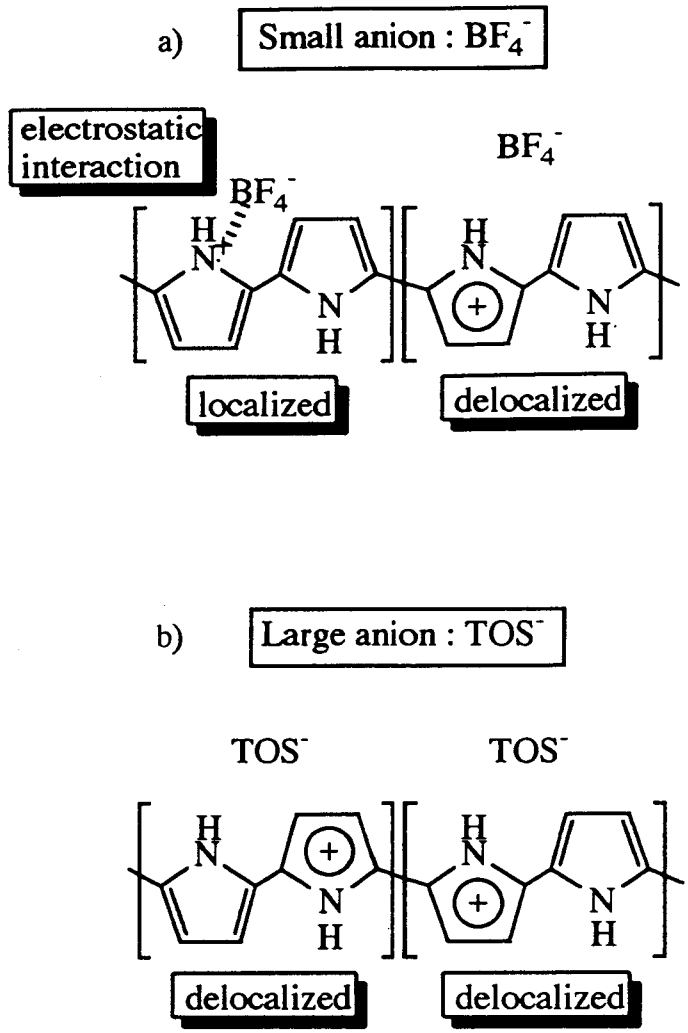

Fig. 3.4. Proposed models for the interaction between pyrrole rings and anions.
a) PP–BF_4 b) PP–TOS

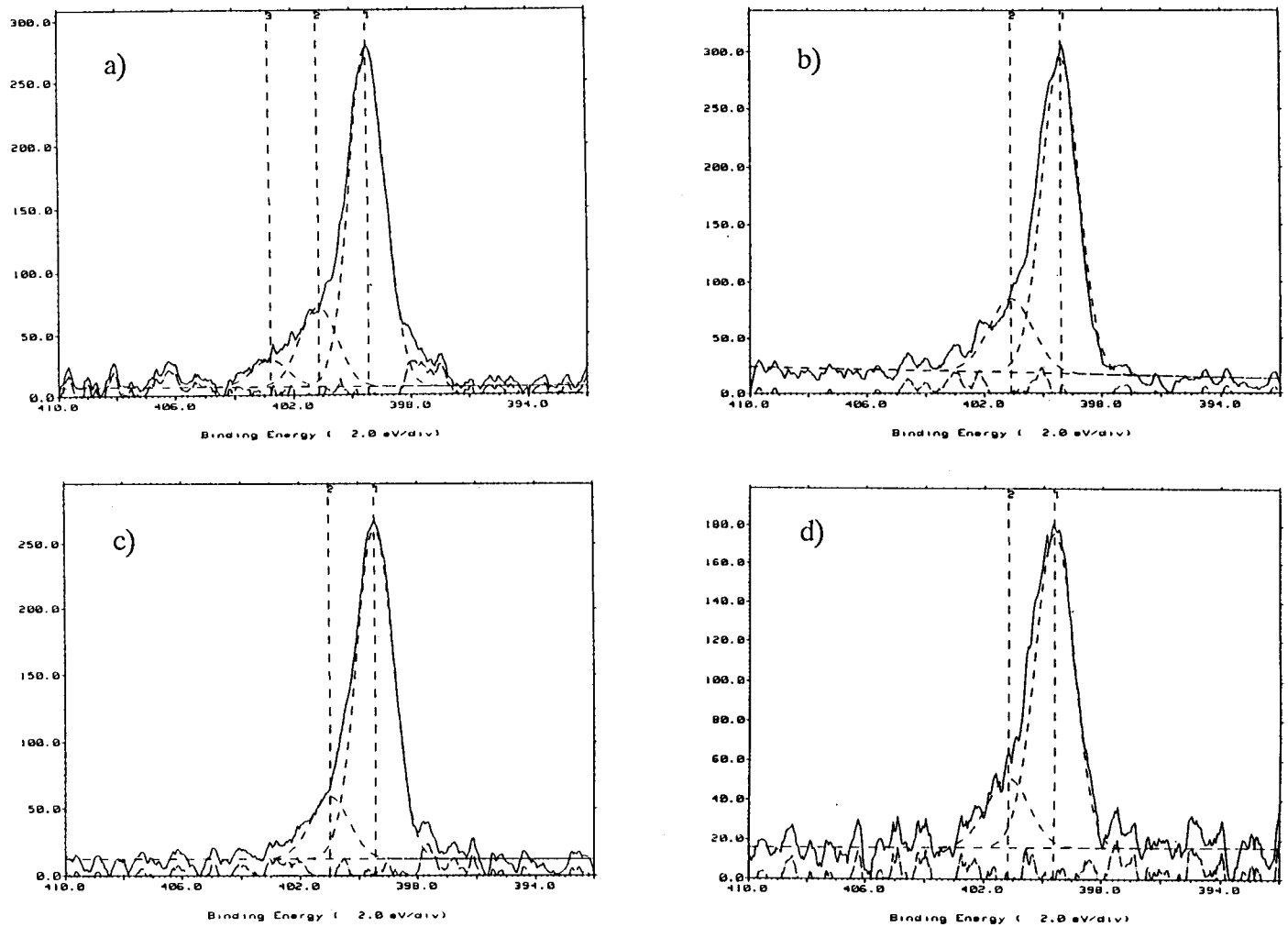

Fig. 3.5. N1s photoemission for poly(3-methylpyrrole) films doped with a) BF_4^-, b) SO_4^{2-}, c) TOS^-, d) PSS^-.

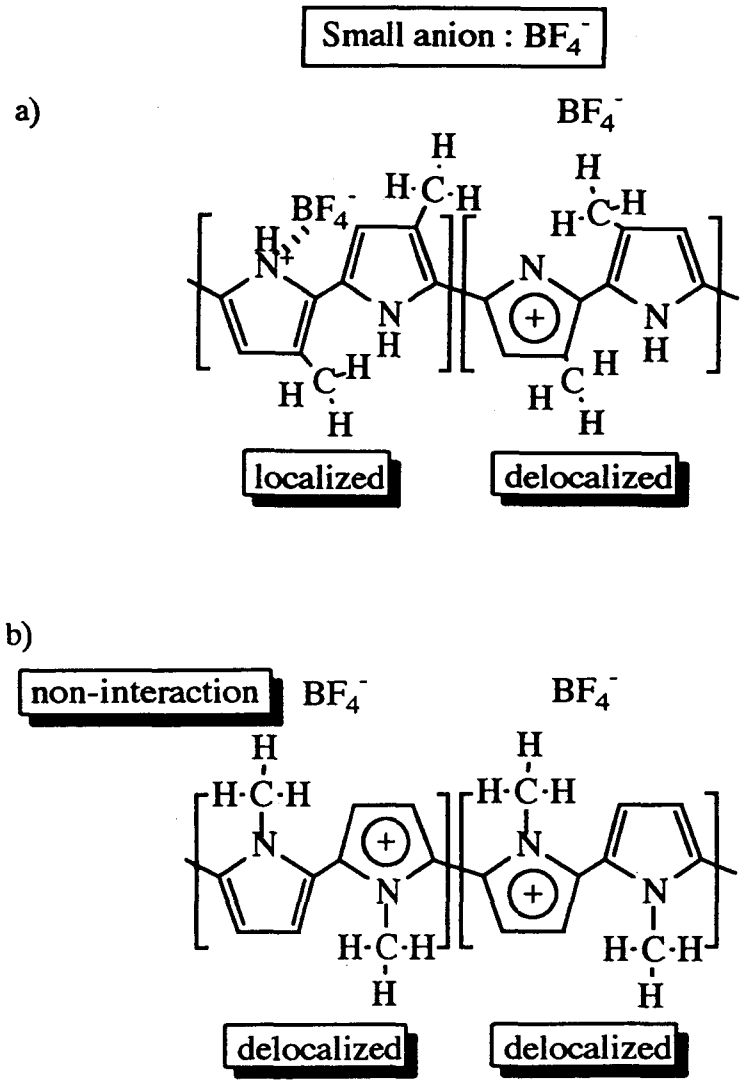

Fig. 3.6. Proposed models for the interaction between pyrrole rings and anions.
a) P3MP–BF_4 b) PNMP–BF_4

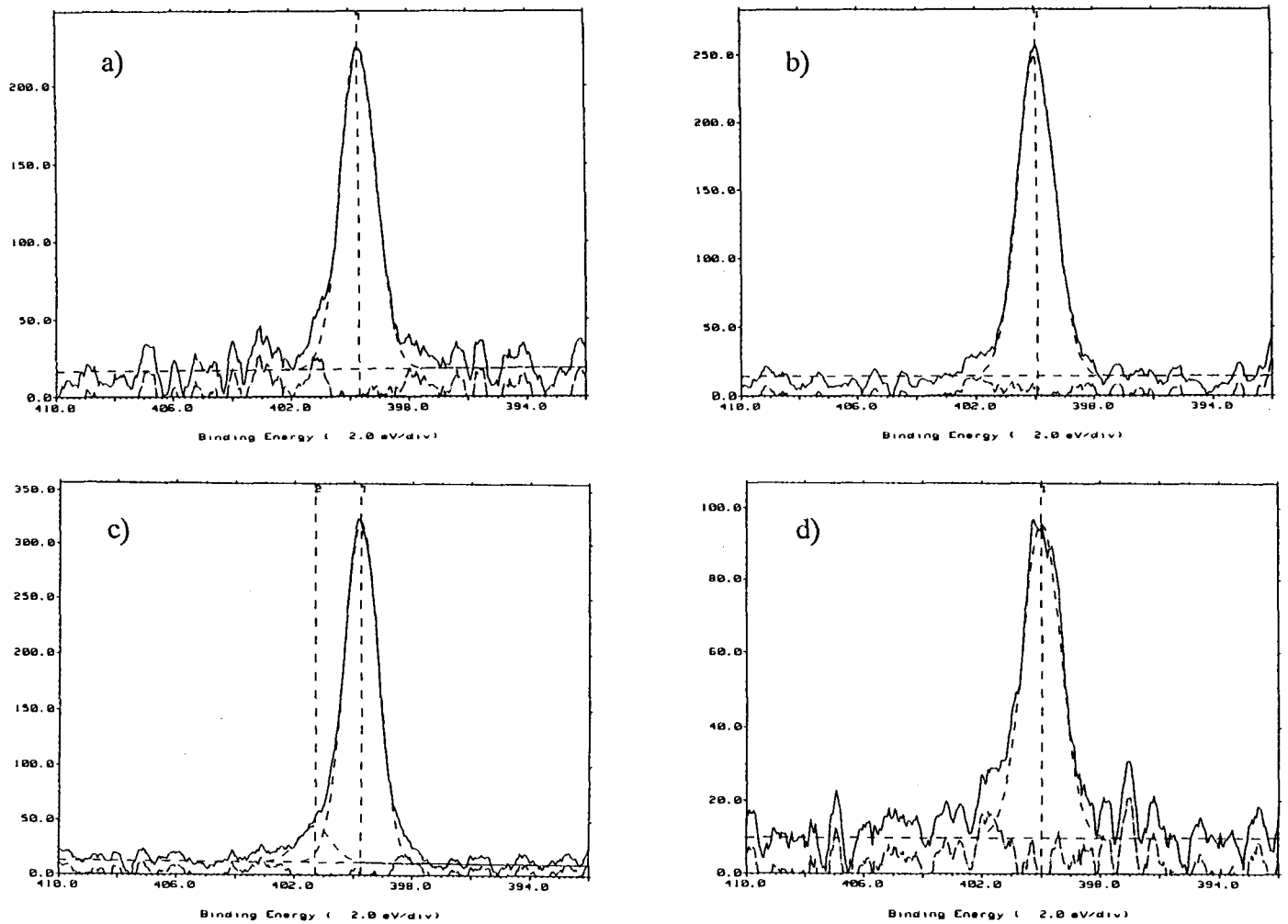

Fig. 3.7. N1s photoemission for poly(N-methylpyrrole) films doped with a) BF_4^-, b) SO_4^{2-}, c) TOS^-, d) PSS^-.

can be explained by considering that the N-substituted methyl group has a steric effect, and anions doped into PNMP films cannot approach the nitrogen atom as shown in Fig. 3.6(b). In this case, there are no strong interactions between nitrogen atoms and anions, and positive charges are delocalized over the pyrrole rings.

The N1s core energy level of PNMP-SO_4 and PNMP-PSS is about 400.0 eV; higher than the N1s core level of the other-anion-doped PNMP. This is probably because PNMP-SO_4 and PNMP-PSS films are insulators.

3.3.5 Gas response mechanism

The gas response mechanism can be discussed on the basis of the above models of anion doped PP, P3MP and PNMP. The decrease in the electric resistance of small-anion-doped PP films under exposure to methanol vapor can be explained, if we assume that a part of the absorbed methanol is located between the cationic pyrrole rings and doped small anions, as shown in Fig. 3.8(a). As mentioned above, small anions doped in PP films have strong electrostatic interactions with the nitrogen atom, on which positive charge is localized. In this case, methanol screens the electric potential between the anion and the nitrogen atom. As a result, the electrostatic interaction between this ion pair weakens, and the positive charge on the nitrogen atom is delocalized over the pyrrole rings. This favorably affects the mobility of positive charge on the polypyrrole and lowers the resistivity.

For large-anion-doped PP films, the cationic pyrrole rings are probably loosely paired with the anions, as shown in Fig. 3.4(b). In this case, the increase of the resistance by exposure to methanol is attributable to the morphological changes in conducting polymer chains, as shown in Fig. 3.8(b). Detailed descriptions of morphological effects were reported in the previous paper [1]. The morphological changes are also expected for small-anion-doped PP films. But in this case, the change of electrostatic interaction seems to have

a)

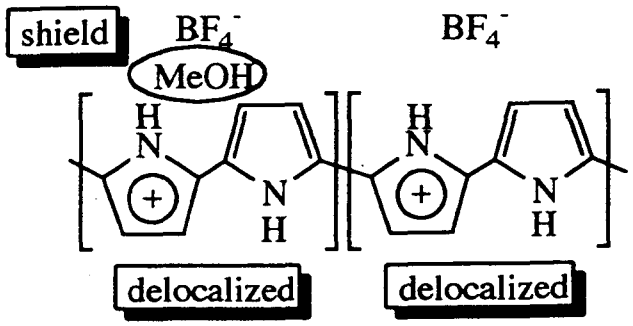

b)

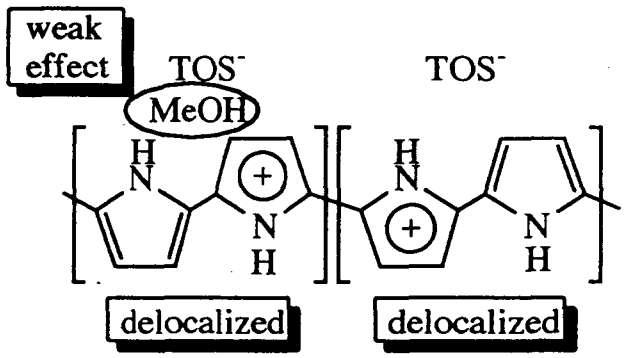

Fig. 3.8. Proposed models for the interaction between methanol and anion-doped pyrrole.
a) PP-BF_4 b) PNMP-TOS

stronger effects than the morphological changes. As shown in Fig. 3.1(a), under exposure to methanol vapor, the resistance of PP–BF_4 film decreases initially, then increases slowly. This response suggests the presence of both mechanisms. The details of the morphological changes by the effect of methanol will be discussed in the next chapter.

3.4 Conclusion

The resistance of small–anion–doped PP and P3MP decreases when exposed to methanol vapor. This is attributed to the delocalization of the positive charge existing in polypyrrole rings by methanol. The cationic sites of PP films doped with small anions have strong electrostatic interactions with anions. Methanol is assumed to be located reversibly between cationic sites and anions, and to weaken the electrostatic interaction. This leads to the reduced resistance. In the case of PNMP and large–anion–doped PP and P3MP, the anions cannot easily approach the cationic sites of pyrrole rings. Hence, the above mechanism does not play the major role, but the morphological change of conducting polymer chains by exposure to methanol gives the dominant effect. As a result, the resistance increases on exposure to methanol vapor.

References

[1] H. Nagase, K. Wakabayashi, T. Imanaka, *Sensors and Actuators B*, **13-14**, 596 (1993).

[2] H. Nagase, H. Abe and T. Imanaka, *Proc. of the Symposium on Chemical Sensors II*, Honolulu, (1993) p.317.

[3] H. Nagase, H. Abe, M. Matsumura and T. Imanaka, *Proc. of the East Asia Conference on Chemical Sensors*, Fukuoka, (1993) p.57.

[4] Patrice Topart and Mira Josowicz, *J. Phys. Chem.*, **96**, 8662 (1992).

[5] K. Naoi, M. Lien and W. H. Smyrl, *J. Electrochem. Soc.*, **138**, 440 (1991).

[6] L. Atanasoska, K. Naoi and W. H. Smyrl, *Chem. Matter.*, **4**, 988 (1992).

[7] P. Pfluger, M. Krounbi, G. B. Street and G. Weiser, *J. Chem. Phys.*, **78**, 3212 (1983).

[8] P. Pfluger and G. B. Street, *J. Chem. Phys.*, **80**, 544 (1984).

[9] J. Lei, Z. Cai and C. R. Martin, *Synth. Met.*, **46**, 53 (1992).

[10] T. A. Skotheim, M. I. Florit, A. Melo and W. E. O'Grady, *Phys. Rev. B*, **30**, 4846 (1984).

[11] A. J. Nelson, S. Glenis and A. J. Frank, *J. Vac. Sci. Technol. A*, **6**, 954 (1988).

[12] W. H. Smyrl, R. T. Atanasoski, L. Atanasoska, L. Hartshorn, K. Nygren and E. A. Fletcher, *J. Electroanal. Chem.*, **267**, 67 (1989).

[13] D. T. Clark and D. M. J. Lilley, *Chem. Phys. Lett.*, **9**, 234 (1971).

Chapter 4

FT-IR and EPR Investigations of Polypyrrole and Methyl Substituted Polypyrroles : Their Physical and Structural Properties

The structures of polypyrrole and methyl substituted polypyrrole were studied by FT-IR. From the results, it was found that the structures are dependent on the monomers and are influenced a little by dopant anions, which were used in the electrochemical polymerization. The very low conductivity of PNMP doped with SO_4^- and PSS^- films is explained by the existence of carboxyl groups in the polymer structure, which cause the interruption of the π-conjugation system. PNMP-TOS is found to have a specific structure, and the structure is considered to be one of the reasons for its unique response to methanol.

The EPR spectra of polypyrrole films show very narrow line width, which implies the presence of highly mobile spins in these polymers. Methanol has immediate effect on the conductivity and the EPR spectrum of the films. The decrease in EPR intensity and the broadening of the line shapes in methanol vapor indicate that methanol molecules impede the movement of charge carrier through polymer chains.

4.1 INTRODUCTION

In Chapter 2, it is described that i) the gas response of polypyrrole (PP) films to methanol vapor is largely dependent on the dopant anions, and ii) the nature of the dopant anions employed in the electrochemical synthesis of polypyrrole can significantly affect the conductivity of the resulting materials [1, 2]. From these studies, however, it was impossible to determine whether these effects of dopant anions were due to the difference in their size, polarizability, solvation effects, or to a difference in the structure of the doped polypyrrole films.

The vibrational infrared spectrum plays an important role in the study of polyconjugated electrically conducting organic polymers, since it provides information directly related to the molecular structures of insulating and conducting materials. The spectra of conducting polymers have been studied in various ways in search of their structures in connection with the mechanism of their electric conduction [3-10].

Electron paramagnetic resonance (EPR) is also a useful method for the study of conducting polymers. From studies carried out by means of EPR together with UV-vis, the presence of both polarons and bipolarons in PP has been determined quantitatively [3, 11-18]. Although both polaron and bipolaron are the charge carriers in conducting polymers, only polaron contributes to the EPR signal, because it has an un-paired electron. EPR is also expected to be a useful method for clarifying the mechanism of gas response of PP films.

In this chapter, the states of polymers doped with anions and the interaction between the polymer backbone and dopant anions were investigated from the analysis of the Fourier transform infrared reflection absorption spectra (FT-IR RAS) and EPR spectra for polypyrrole (PP), poly(3-methylpyrrole) (P3MP) and poly(N-methylpyrrole) (PNMP) doped with BF_4^-, ClO_4^-, SO_4^{2-}, p-toluenesulfonate (TOS^-) and polystylenesulfonate (PSS^-).

4.2 Experimental

Pyrrole, N-methylpyrrole (Wako) and 3-methylpyrrole (Sigma) were purified by distillation. Other chemicals were used as received from commercial sources.

Electrochemical experiments were carried out using a Hokuto Denko HA151 potentiostat/galvanostat. Pyrrole, 3-methylpyrrole and N-methylpyrrole were polymerized electrochemically in aqueous solutions of $NaBF_4$, $NaClO_4$, Na_2SO_4, sodium toluenesulfonate (NaTOS) and sodium poly(p-stylenesulfonate) (NaPSS). Before polymerization, nitrogen was bubbled through the solutions for more than 30 min in order to remove dissolved air. In each case, the monomer concentration was 0.10 M and that of the electrolyte was 0.10 M. Corning 7059 glass plates, on which metal thin films were evaporated (50 nm niobium and 400 nm of platinum), were used as substrates. The polymer films were electrochemically deposited on the substrate. The areas of substrates were 10 mm × 20 mm and 3 mm × 20 mm for FT-IR and EPR measurements, respectively. A platinum plate (10 mm × 20 mm) was used as a counter electrode, and Ag/AgCl (3.33M KCl) as a reference electrode. The potential of the working electrode was cycled between -0.7 V and 0.9 V at the rate of 100 mV/s. The number of swept cycles was 10-20. When the charge of polymerization current reached about 200 mC/cm^2, the electrode potential was switched to and held at 0.0 V until the current dropped to less than 0.01 mA. The films thus prepared were expected to have a thickness of about 500 nm on the basis of the reported thickness of ~25 nm per 10 mC/cm^2 for the deposition of polypyrrole from $LiClO_4$ and $(Et_4N)BF_4$ electrolytes [19]. The polymer films were thoroughly washed in distilled water and dried in vacuum for 1 h and then stored under dry nitrogen gas before measurements.

The FT-IR spectra were obtained using a FTS-3 infrared spectrometer (Bio-Rad) with a unit for RAS at a resolution of 4 cm^{-1}. Each spectrum

represents 64 scans. The spectrometer was driven by an SPC 3200 computer. Enhanced FT-IR software was used to analyze the spectra.

The EPR measurements were carried out at X-band (9.35 GHz) microwave frequencies using a Varian cavity with a home-built spectrometer with 100-kHz field modulation at room temperature [20]. The sample was contained in a quartz EPR tube.

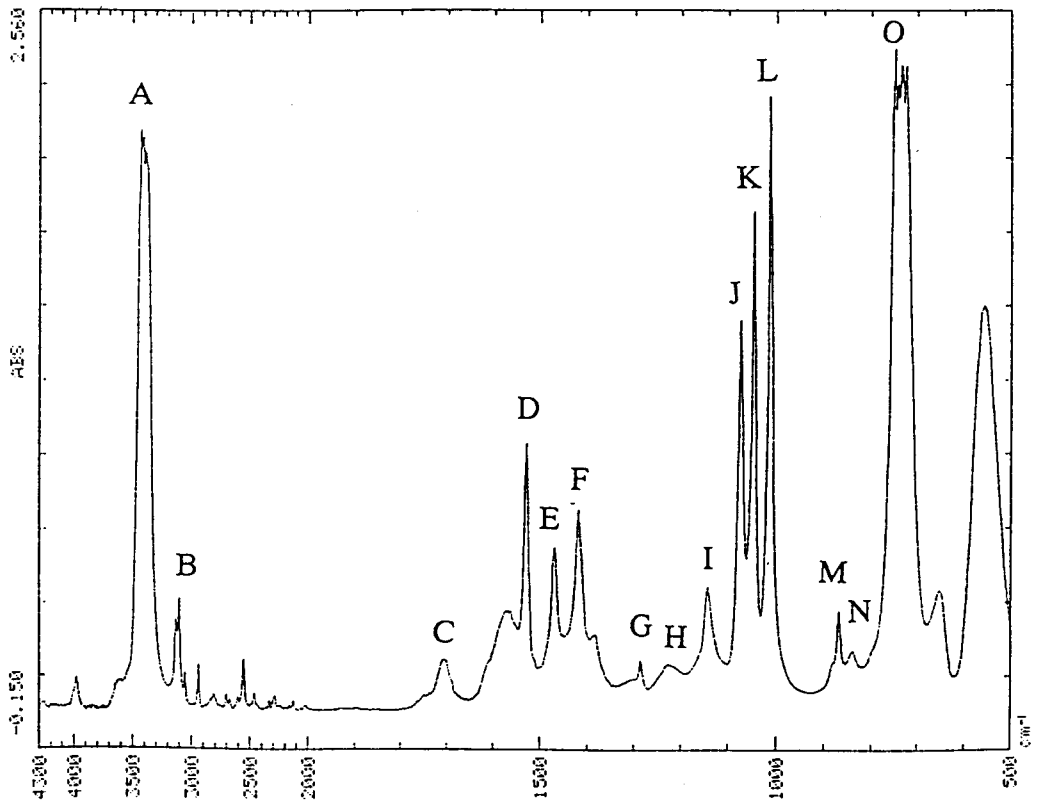

Fig. 4.1. FT-IR spectrum of pyrrole monomer.

4.3 Results and discussion

4.3.1 FT-IR studies

The FT-IR spectra of pyrrole monomer and PP, P3MP and PNMP doped with BF_4^- are shown in Fig. 4.1 and 4.2 (a), (b), (c), respectively. The 14 peaks were observed, and they are labeled from A through O.

The assignment of these absorption peaks was as follows [3-9];

A: N-H stretching
B: C-H stretching
C: C=O stretching
D: asymmetric ring stretching
E: symmetric ring stretching
F: asymmetric ring stretching
G: symmetric ring stretching
H: N-H in-plane
I: C-H out-of-plane
J: symmetric C-H in-plane
K: asymmetric C-H in-plane
L: un-known
M: un-known
N: ring out-of-plane
O: C-H out-of-plane

Figure 4.3 and Table 4.1 show FT-IR RAS spectra of polypyrrole synthesized by the electrochemical polymerization of pyrrole in an aqueous solutions of (a) 0.1 M $NaBF_4$, (b) 0.1 M $NaClO_4$, (c) 0.1 M Na_2SO_4, (d) 0.1 M NaTOS and (e) 0.1 M (the concentration of the sulfonate group)

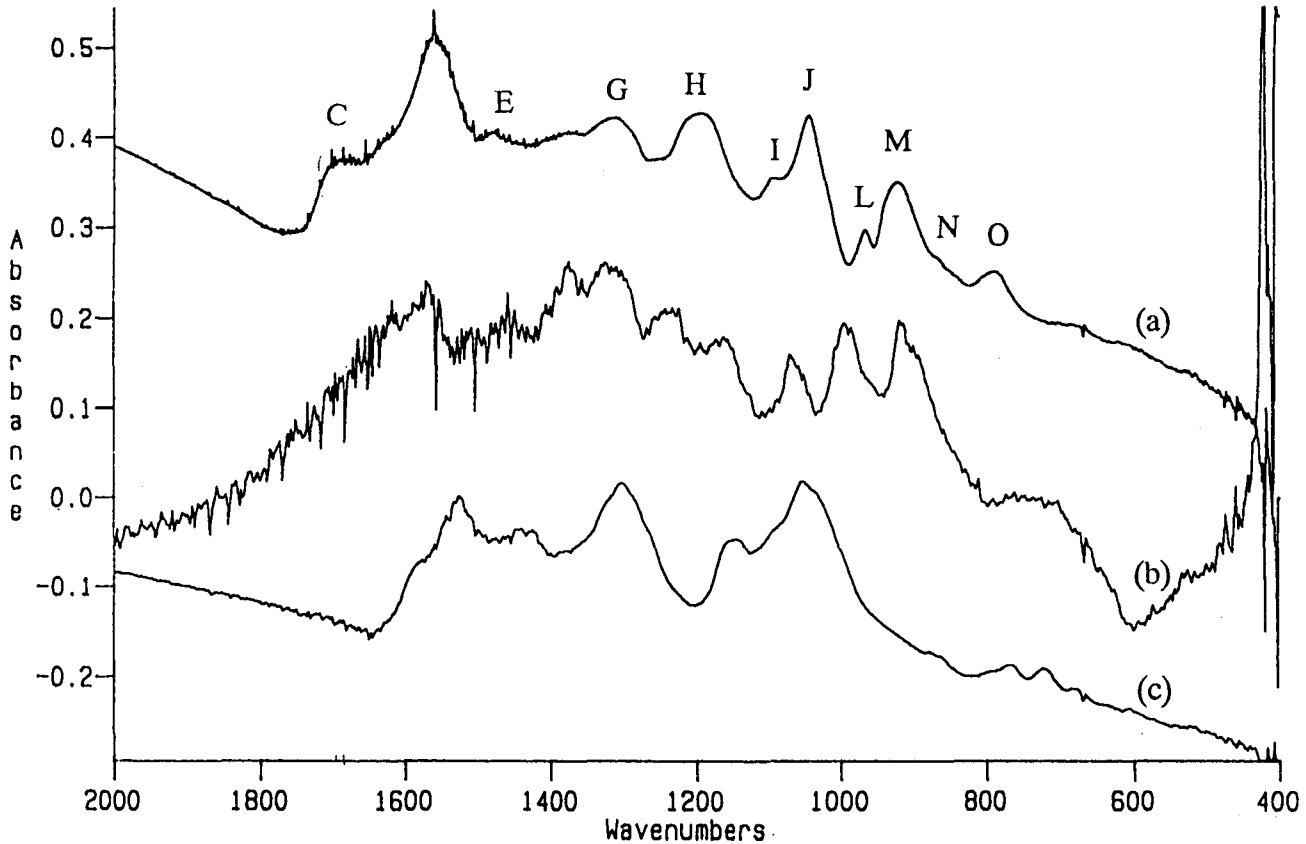

Fig. 4.2. FT–IR spectra of polymer films with BF_4^-.

(a) polypyrrole,

(b) poly(3–methylpyrrole),

(c) poly(N–methylpyrrole).

NaPSS, respectively. Though it is not shown here, essentially the same spectra were obtained for the polymer films of PP–BF_4, PP–ClO_4, PP–SO_4, PP–TOS and PP–PSS in the region above 2000 cm^{-1}. The 610 cm^{-1} peak in Fig. 4.3(b) and 605 cm^{-1} peak in Fig. 4.3(c) are assigned to ClO_4^- and SO_4^{2-}, respectively, which are reported to have characteristic absorptions at 625 cm^{-1} (m) and 611 cm^{-1} (m) [8, 9]. Absorption attributable to BF_4^-, which is expected to appear at 1052 cm^{-1}, was not significantly observed. This is perhaps because its absorption is obscured by the polypyrrole bands, as has been suggested by Street *et al.*[3]. The spectra of PP films doped with various anions, such as (a) BF_4^-, (b) ClO_4^-, (c) SO_4^{2-}, (d) TOS^- and (e) PSS^- show similar absorption bands in the energy region between 700 cm^{-1} and 2000 cm^{-1}. The positions of D, G, J and M bands depend on the kind of dopant anions. These bands shifted to smaller wavenumbers with the increase of anion size. It is reported that blue shifts for particular bands might be expected, however, if the order for the bond associated with the vibration increased upon doping (e.g. going from the benzenoid to the quinoid configuration). Because the D and G bands are due to stretching of pyrrole rings, the benzenoid character of pyrrole rings for the large–anion–doped PP is larger than that for small–anion–doped PP. The electrostatic interaction between pyrrole ring site and dopant anion was discussed in detail in Chapter 3. The shift of J and M bands is considered to be caused by the interaction between C–H and the pyrrole ring. However, further theoretical work concerning the specific molecular assignments for IR bands in PP is required before these shifts in peak positions can be fully interpreted.

Figure 4.4 and Table 4.2 show FT–IR spectra of poly(3–methylpyrrole) synthesized by the electrochemical polymerization of 3–methylpyrrole in an aqueous solution of (a) 0.1 M $NaBF_4$, (b) 0.1 M $NaClO_4$, (c) 0.1 M Na_2SO_4, (d) 0.1 M NaTOS and (e) 0.1 M (the concentration of sulfonate group) NaPSS, respectively. Similar spectra were obtained in the region below 2000 cm^{-1} for

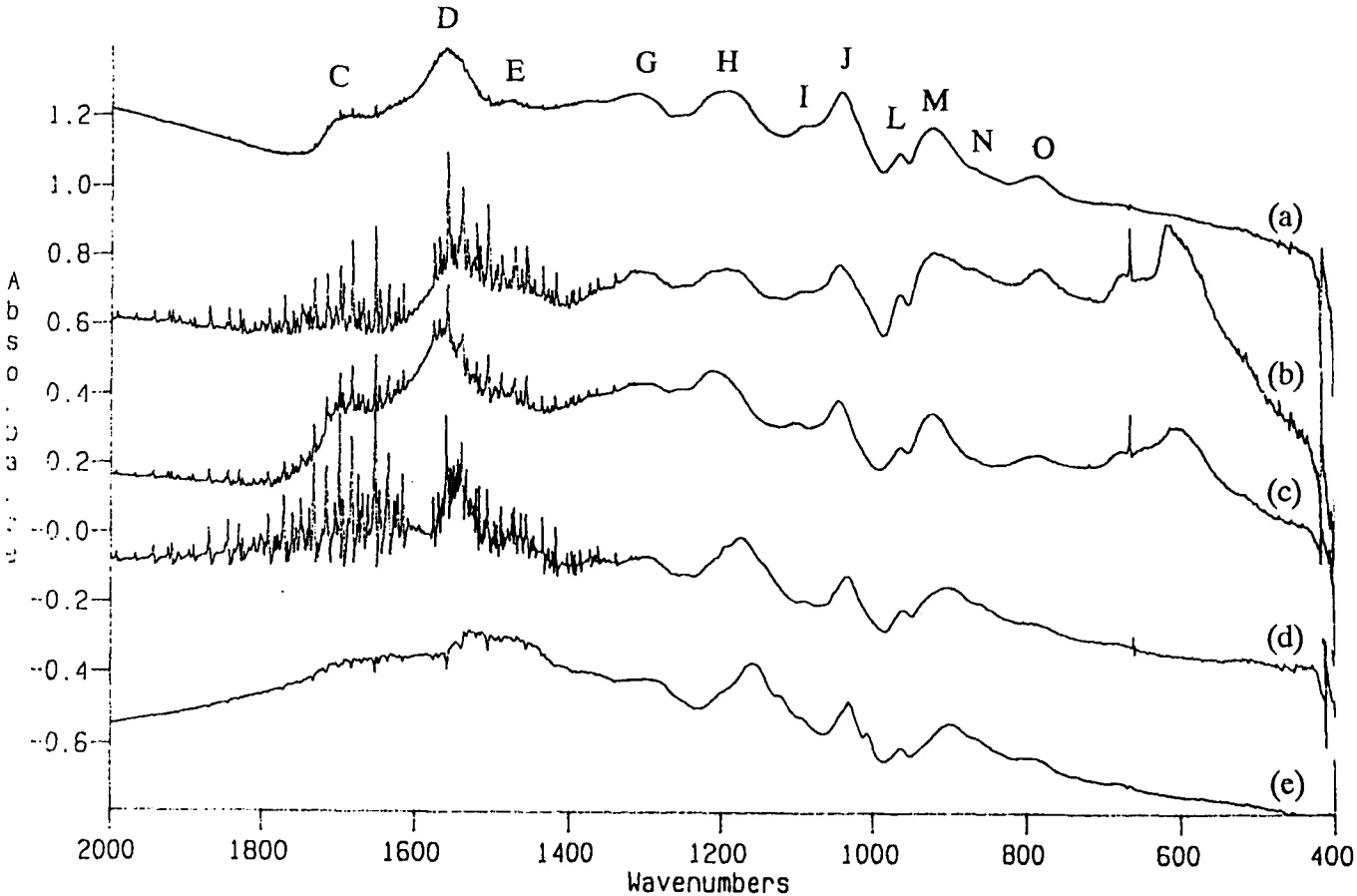

Fig. 4.3. FT–IR spectra of polypyrrole synthesized in aqueous solution of (a) 0.1 M $NaBF_4$, (b) 0.1 M $NaClO_4$, (c) 0.1 M Na_2SO_4, (d) 0.1 M sodium p–toluenesulfonate, (e) 0.1 M sodium poly(stylenesulfonate).

Table 4.1

FT-IR band positions (cm^{-1}) of polypyrroles doped with various anions

polymer	Band designation							
	A	B	C	D	E	F	G	H
PP-BF_4	3574	–	1697	1552	1465	–	1304	1186
	(w)		(m)	(s)	(w)		(m)	(s)
PP-ClO_4	3402	–	1697	1541	1465	–	1304	1186
	(m)		(w)	(s)	(w)		(m)	(s)
PP-SO_4	3402	–	1697	1552	1465	–	1304	1207
	(s)		(m)	(s)	(w)		(w)	(s)
PP-TOS	3402	–	–	1541	1465	–	1290	1166
	(s)			(s)	(w)		(w)	(s)
PP-PSS	3574	–	–	1541	1465	–	1276	1152
	(w)			(m)	(w)		(w)	(s)

polymer	Band designation						
	I	J	K	L	M	N	O
PP-BF_4	1090	1041	–	966	924	869	779
	(w)	(s)		(w)	(s)	(vw)	(m)
PP-ClO_4	1090	1041	–	966	924	869	779
	(w)	(s)		(w)	(s)	(vw)	(s)
PP-SO_4	1090	1041	–	966	924	869	779
	(w)	(s)		(w)	(s)	(vw)	(w)
PP-TOS	1090	1028	–	966	910	869	779
	(w)	(s)		(w)	(m)	(vw)	(w)
PP-PSS	1090	1028	–	966	897	869	779
	(w)	(s)		(w)	(s)	(vw)	(w)

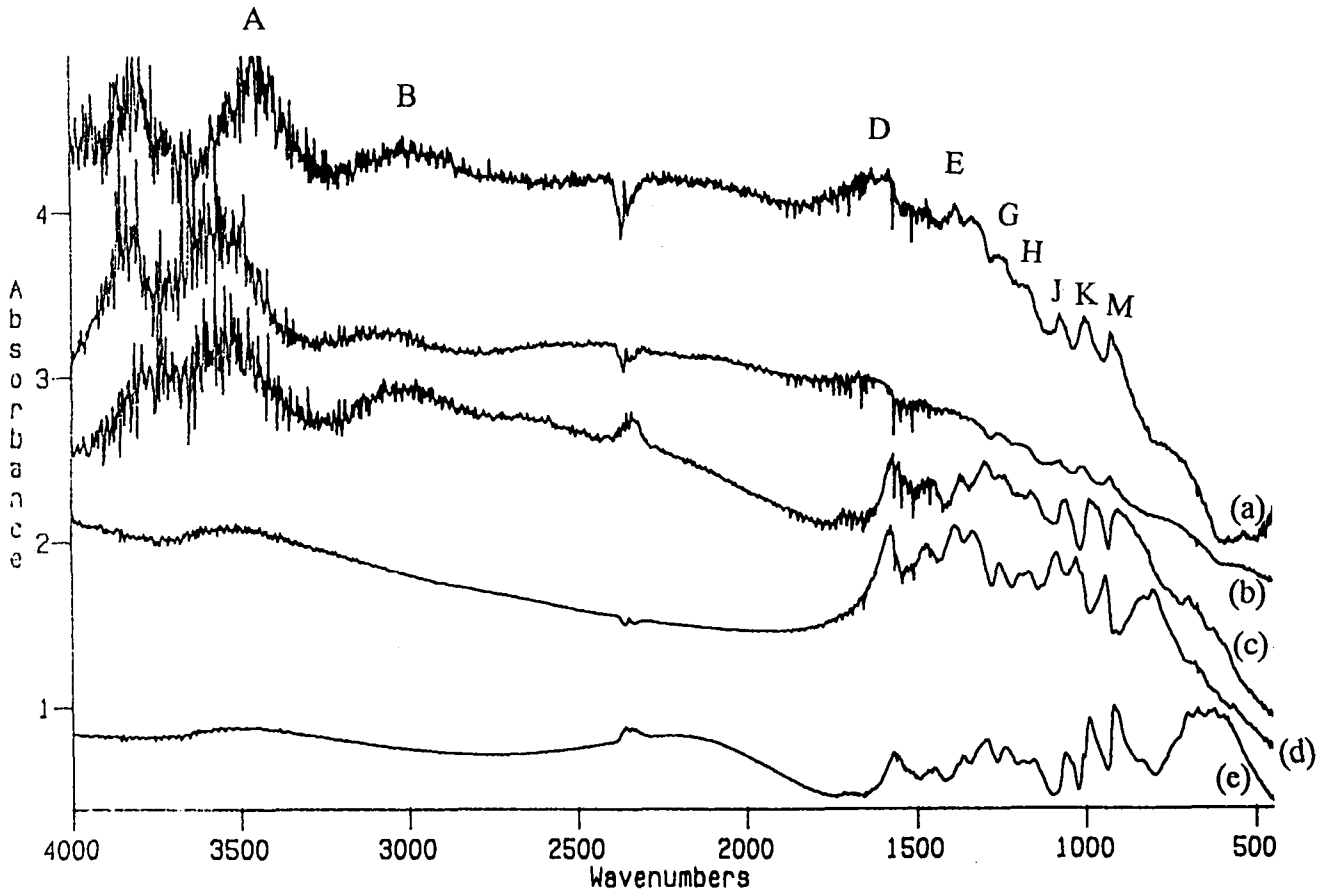

Fig. 4.4. FT–IR spectra of poly(3–methylpyrrole) synthesized in aqueous solution of (a) 0.1 M $NaBF_4$, (b) 0.1 M $NaClO_4$, (c) 0.1 M Na_2SO_4, (d) 0.1 M sodium p–toluenesulfonate,
(e) 0.1 M sodium poly(stylenesulfonate).

Table 4.2

FT-IR band positions (cm^{-1}) of poly(3-methylpyrrole)s doped with various anions

polymer	Band designation							
	A	B	C	D	E	F	G	H
P3MP-BF_4	3429 (s)	3000 (w)	–	1552 (w)	1455 (w)	–	1317 (m)	1155 (w)
P3MP-ClO_4	3532 (s)	3030 (w)	–	1573 (w)	1466 (w)	–	1314 (w)	1155 (w)
P3MP-SO_4	3532 (m)	3000 (m)	–	1559 (s)	1455 (w)	–	1286 (s)	1148 (w)
P3MP-TOS	3532 (w)	–	–	1569 (s)	1462 (m)	–	1324 (m)	1155 (w)
P3MP-PSS	3574 (w)	–	–	1562 (m)	1448 (w)	–	1286 (m)	1148 (vw)

polymer	Band designation						
	I	J	K	L	M	N	O
P3MP-BF_4	–	1062 (m)	990 (s)	–	917 (s)	–	–
P3MP-ClO_4	–	1062 (w)	1000 (m)	–	917 (m)	–	–
P3MP-SO_4	–	1048 (s)	983 (s)	–	900 (s)	–	–
P3MP-TOS	–	1076 (s)	1017 (m)	–	938 (s)	–	–
P3MP-PSS	–	1062 (s)	990 (s)	–	917 (s)	–	–

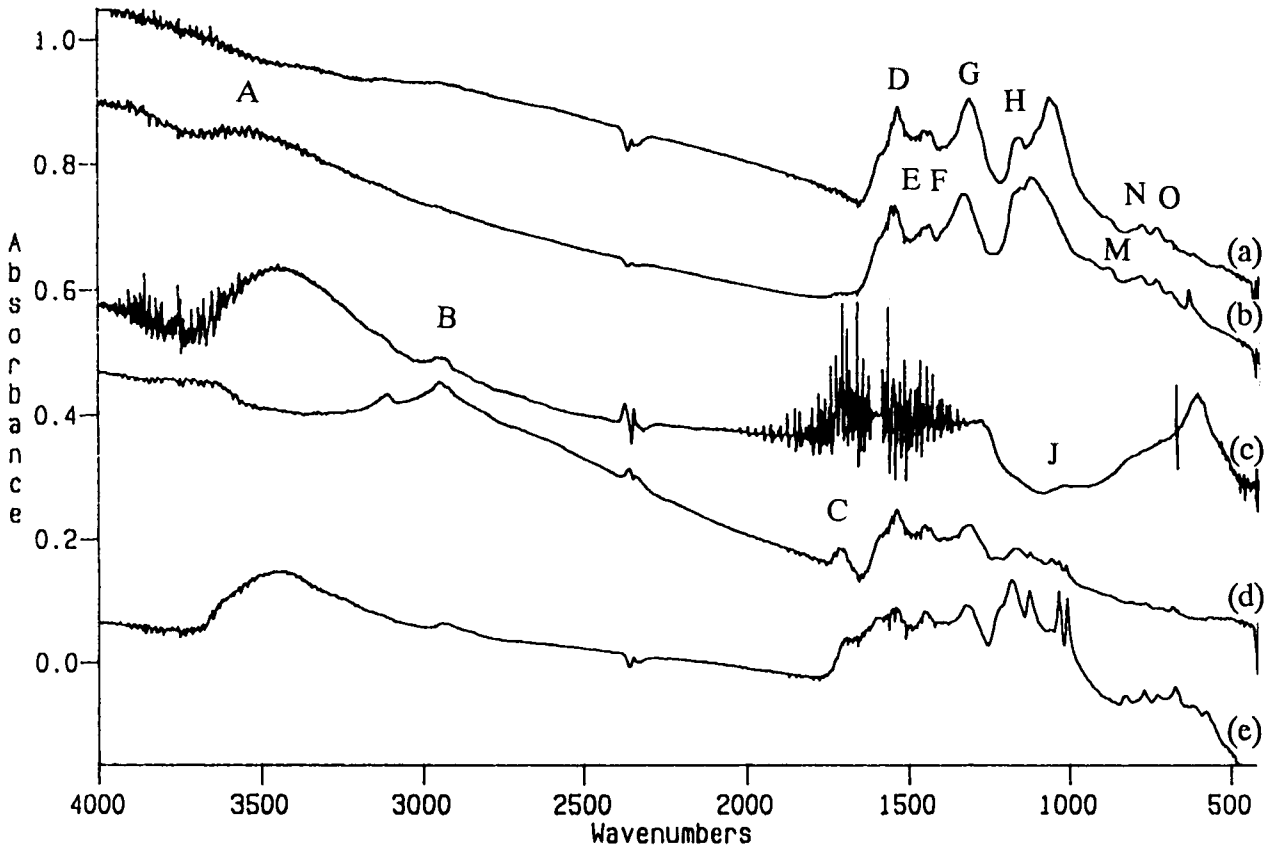

Fig. 4.5. FT-IR spectra of poly(N-methylpyrrole) synthesized in aqueous solution of (a) 0.1 M $NaBF_4$, (b) 0.1 M $NaClO_4$, (c) 0.1 M Na_2SO_4, (d) 0.1 M sodium p-toluenesulfonate,
(e) 0.1 M sodium poly(stylenesulfonate).

Table 4.3

FT-IR band positions (cm^{-1}) of poly(N-methylpyrrole)s doped with various aniions

polymer	Band designation							
	A	B	C	D	E	F	G	H
PNMP-BF_4	3317 (vw)	2934 (vw)	–	1525 (s)	1444 (w)	1418 (w)	1296 (s)	1137 (m)
PNMP-ClO_4	3517 (w)	2934 (vw)	–	1533 (s)	1444 (w)	1418 (w)	1318 (s)	1126 (m)
PNMP-SO_4	3300 (vw)	2934 (w)	1714 (m)	1533 (m)	1433 (m)	1430 (w)	1304 (w)	1126 (w)
PNMP-TOS	3650 (w)	2934 (w)	1714 (w)	1533 (m)	1444 (w)	1430 (w)	1304 (m)	1126 (w)
PNMP-PSS	3434 (s)	2934 (w)	1689 (w)	1533 (w	1444 (w)	1430 (w)	1304 (m)	1126 (m)

polymer	Band designation						
	I	J	K	L	M	N	O
PNMP-BF_4	–	–	–	–	–	867 (w)	774 (w)
PNMP-ClO_4	–	–	–	–	927 (vw)	867 (w)	774 (w)
PNMP-SO_4	–	1052 (w)	–	–	937 (w)	867 (w)	774 (w)
PNMP-TOS	–	1052 (w)	–	–	–	867 (w)	774 (w)
PNMP-PSS	–	1059 (w)	–	–	–	–	774 (w)

the polymer films of P3MP–BF_4, P3MP–ClO_4, P3MP–SO_4, P3MP–TOS and P3MP–PSS. Conversely, in the region between 2500 cm^{-1} and 4000 cm^{-1} apparent differences were observed among them. Three absorption bands at about 3800 cm^{-1}, 3400 cm^{-1} and 3100 cm^{-1} ((a) P3MP–BF_4, (b) P3MP–ClO_4 and (c) P3MP–SO_4) are not observed in the spectra of (d) P3MP–TOS and (e) P3MP–PSS. The absorption at 3400 cm^{-1} is undoubtedly attributable to the A band, namely N–H stretching mode. It is reported that un–doped material shows a very distinct band at 3400 cm^{-1}, which becomes weaker when the dopant anion increases, because this band is buried in the free carrier absorbance of the doped material [4]. The very weak band at 3100 cm^{-1} in the spectra of (a), (b) and (c) is undoubtedly attributable to the B band, namely C–H stretching mode. This band is also completely hidden by the free carrier absorption, if the concentration of dopants is high. Therefore, the P3MP films of (a), (b) and (c) are considered to have a low doping level. The origin of the band at 3800 cm^{-1} is not clear yet.

Figure 4.5 and Table 4.3 show FT–IR spectra of poly(N–methylpyrrole) synthesized by the electrochemical polymerization of N–methylpyrrole in an aqueous solution of (a) 0.1 M $NaBF_4$, (b) 0.1 M $NaClO_4$, (c) 0.1 M Na_2SO_4, (d) 0.1 M NaTOS and (e) 0.1 M (the concentration of sulfonate group) NaPSS, respectively. For PNMP–BF_4, PNMP–ClO_4 and PNMP–SO_4, absorptions possibly due to the dopant anions are observed at 1051 cm^{-1} for BF_4^-, at 621 cm^{-1} for ClO_4^- and at 611 cm^{-1} for SO_4^{2-}. Except for these bands, essentially the same spectra were obtained for PNMP–BF_4 and PNMP–ClO_4. Because the films of PNMP–BF_4 and PNMP–ClO_4 exhibit high conductivity, the A and B bands were concealed in the free carrier absorption of the doped material, as described before. On the other hand, the spectra of (c) PNMP–SO_4 and (e) PNMP–PSS show the A and B bands at 3400 cm^{-1} and 2900 cm^{-1}, respectively. It is considered that these polymers show the absorption of A and B bands, because films of PNMP–SO_4 and PNMP–PSS have very low

conductivity, as described in Chapter 2. The spectra of PNMP–SO_4 and PNMP–PSS show absorption at 1706 cm^{-1}, which is characteristic of the carbonyl group [5]. Besides the low doping level of these materials, the presence of carbonyl group is considered to be another reason for their very low conductivity. Hyodo and Mac Diarmid reported [10] that PNMP–SO_4 contains structures of [I] and/or [II] at their polymer ends together with a structure like [III] within the polymer chain.

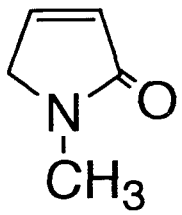

[I]

$\nu_{C=O}$ = 1675 cm^{-1}

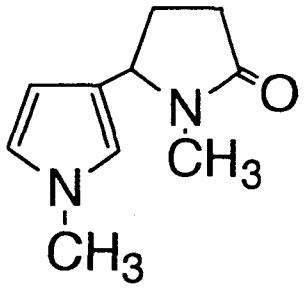

[II]

$\nu_{C=O}$ = 1689 cm^{-1}

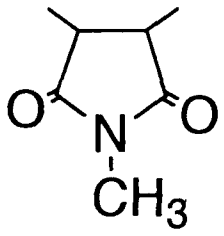

[III]

$\nu_{C=O}$ = 1701 cm^{-1}

The polymers involving these structures are susceptible to interruption of the π–conjugation system due to the formation of sp^3 hybridized carbon linkages. This leads to reduced conductivity.

The spectra of (c) PNMP–SO_4 and (e) PNMP–PSS also show a C–H stretching vibration due to the CH_3 group at 2934 cm^{-1}. Conversely, the C–H vibration is not clearly defined in the spectra of (a) PNMP–BF_4 and (b) PNMP–ClO_4, probably because of the high density of free carriers in these polymers, which have high conductivity. The spectrum of (d) PNMP–TOS shows very different properties from the other polymers. In spite of the high conductivity of PNMP–TOS, a C–H stretching vibration due to the CH_3 group at 2934 cm^{-1}, and a vibration due to the ring CH groups at 3150 cm^{-1} were observed, while the A band is not apparent. This suggests that PNMP–TOS has a very specific structure. One of the reasons for the unique response of

PNMP–TOS films to methanol, as shown in Table 1.1, is considered to be due to this special structure.

4.3.2 EPR studies

The EPR spectra of PP and PNMP were measured at room temperature. Figure 4.6 shows the EPR spectra of PP–SO_4 obtained in nitrogen before exposure to methanol (a), in 1000 ppm methanol (b) and in nitrogen after exposure to methanol (c), respectively. The g value of the spectrum was approximately equal to that of a free electron, 2.0005, and also close to that of a π–radical in the aromatic compounds. The peak–to–peak line width of 1.39 G is larger than that reported for PP–ClO_4 (0.2–0.3 G) [3] and PP–TOS (0.38 G) [11], which are prepared in acetonitrile solution under an argon atmosphere [3]. The broadening of our PP–SO_4 sample arises mainly from solvent water [12] and exposure to air for 1 h before EPR measurement. In our experiment, the sample was exposed to air to get the information about the polymer sensor under the working conditions, which is used in the air atmosphere. Scott *et al.* reported that the line width of polypyrrole doped with perchlorate ion increased to 1.3–1.7 G when exposed to oxygen [13]. This agrees with the line width of our sample measured in air. Broadening of the line width by oxygen was also observed by Street for PP–TOS, where line width became as narrow as 0.9 G by evacuating oxygen [11]. Although the line width of PP–SO_4 is broadened by the effect of water and oxygen, it can be compared with 0.7 G of *trans*–polyacetylene, which is a highly conducting polymeric material, where the carriers are presumed to be highly mobile solitons [14]. This implies that there are highly mobile spins in PP–SO_4. Exposure to methanol vapor broadens the line to 2.5 G as shown in Fig. 4.6 (b). By pumping out methanol and re–introducing nitrogen, the EPR intensity increased to almost initial level, as shown Fig. 4.6 (c).

EPR spectra were also measured for PP and PNMP doped with BF_4^-,

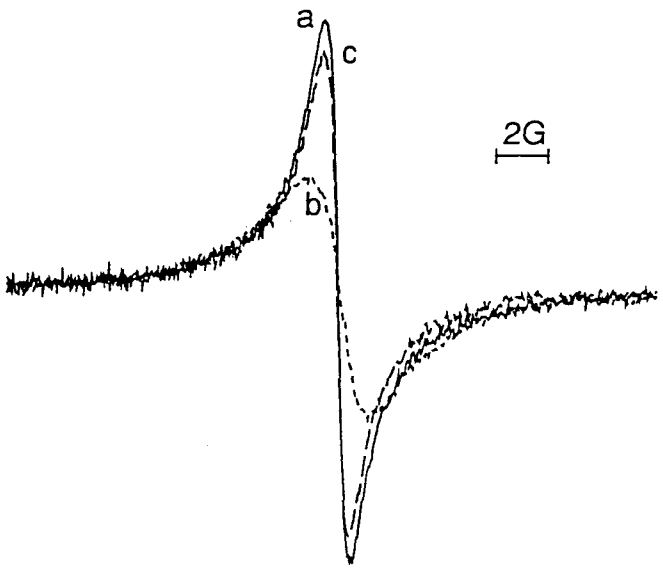

Fig. 4.6. EPR spectra of polypyrrole film polymerized in aqueous solution of 0.1 M Na_2SO_4 and measured at room temperature in
(a) N_2 before exposure to methanol,
(b) 1000 ppm methanol diluted by N_2,
(c) N_2 after exposure to methanol.

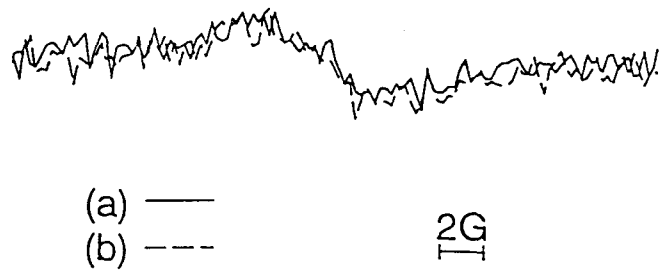

Fig. 4.7. EPR spectra of poly(N-methylpyrrole) film polymerized in aqueous solution of 0.1 M Na_2SO_4 and measured at room temperature in
(a) N_2 before exposure to methanol,
(b) 1000 ppm methanol diluted by N_2.

ClO_4^-, SO_4^{2-}, TOS^- and PSS^-. The EPR line width of these samples measured in nitrogen before and after exposure to methanol, and in 1000 ppm methanol, is compared in Table 4.4. The line width increased in methanol in all cases. When the sample tube was evacuated and nitrogen was re-introduced in it, the line width returned to its initial value. The spin intensity of the samples observed in 1000 ppm methanol was compared with that measured before exposure to methanol, and the ratio is summarized in Table 4.5. The spin intensity in N_2 after exposure to methanol is also shown in the table. In methanol atmosphere, the spin intensity of the films decreased except for PP-SO_4 and PNMP-SO_4. The decrease indicates that the concentration of polarons decreased by exposure to methanol. The spin intensities of PP-SO_4 was unchanged and that of PNMP-SO_4 increased by exposing to methanol vapor. Although the spin intensities of PP films doped with BF_4^-, ClO_4^-, TOS^-, PSS^-, and PNMP films doped with BF_4^-, ClO_4^-, TOS^- did not recovered completely to the initial value, they grew back when the methanol vapor was pumped out and replaced with nitrogen.

The EPR spectra for PNMP-SO_4 are very different as shown in Fig. 4.7. The intensity for PNMP-SO_4 is much weaker than that for the others, and it increases in a methanol atmosphere. The spectra are rather broad and the line width is about 5-7 G. The EPR signal of PNMP-PSS is so weak that the intensity and line width cannot be determined.

The mechanism of transport of electrical charge has been receiving much interest. The conduction mechanism has been postulated that it occurs through the movement of charge carriers along the polymer chain. The two possible charge carriers of PP are polaron and bipolaron [21]. It has been reported that the spin concentration becomes a maximum for the removal of one electron from a unit of six pyrrole monomers in the PP chain [16]. From the steady-state experiments, the EPR signals were interpreted in terms of a model involving quasi-equilibrium populations of polarons and bipolarons formed in

Table 4.4 EPR intensity ratio of poly(pyrrole)s and poly(N-methylpyrrole)s

Polymer	Intensity ratio [-]	
	I_2/I_1 [a]	I_3/I_1 [a]
PP -BF_4	0.77	0.87
PP -SO_4	1.04	1.03
PP -ClO_4	0.63	0.81
PP -TOS	0.43	0.86
PP -PSS	0.76	0.83
PNMP-BF_4	0.76	1.07
PNMP-SO_4	1.61	1.59
PNMP-ClO_4	0.96	1.07
PNMP-TOS	0.84	0.98
PNMP-PSS [b]	—	—

a) I_1, I_2, I_3 are the EPR intensities before exposure to methanol, in 1000 ppm methanol, and after exposure to methanol, respectively.
b) EPR signal was too weak to decide the intensity.

Table 4.5 The peak-to-peak line width of EPR signal of poly(pyrrole)s and poly(N-methylpyrrole)s

Polymer	Line width [G]		
	W_1 [a]	W_2 [b]	W_3 [c]
PP -BF_4	1.21	2.38	1.32
PP -SO_4	1.39	2.50	1.39
PP -ClO_4	0.97	1.44	0.97
PP -TOS	1.29	4.14	1.32
PP -PSS	1.52	2.84	1.48
PNMP-BF_4	1.09	1.71	1.03
PNMP-SO_4	5.40	5.90	7.3
PNMP-ClO_4	1.02	1.52	1.00
PNMP-TOS	1.32	1.36	1.30

a) The line width before exposure to methanol.
b) The line width in 1000 ppm methanol.
c) The line width after exposure to methanol.

the following two step redox process [16, 18] :

$$PP^0 \overset{E_1}{\rightleftharpoons} PP^{\bullet+} \overset{E_2}{\rightleftharpoons} PP^{2+} \qquad (3.1)$$

where E_1 and E_2 are the quasi-standard potentials for the formation of polarons ($PP^{\bullet+}$) and bipolarons (PP^{2+}).

Theoretical calculation of the energies of polaron and bipolaron formation in PP has led to the conclusion that the formation of a bipolaron is favorable by 0.45 eV as compared to the formation of two polarons [21, 22]. It has also been concluded that the charged species responsible for the charge transport in PP is bipolaron from the EPR experiment [13]. From the a.c. impedance/*in-situ* EPR experiment, however, it is indicated that conduction within PP cannot be solely attributed to the bipolaron, and that the polaron can be the dominant carrier at low doping levels [16, 17]. In our experiment, the ratio of anions doped in polymer films to a pyrrole ring is about 1/3 - 1/4, which will be discussed in Chapter 5. This means that the doping level is rather high, and the main carrier is bipolaron. This is consistent with the result that the observed spin intensities for the various conducting polymers in our experiment were irrelevant to their conductivity. The change of the spin intensity of polymers by methanol does not have direct relationship with the change of their conductivity by methanol, either. However, the EPR results gives us some insights into the electronic properties of conducting polymers. First, the decrease of spin intensity by exposure to methanol, which is observed for most of the polymers, suggest that the equilibrium between polaron and bipolaron states shifts favorably for bipolaron side by the effect of methanol. This can be explained by taking into account the reduction of the repulsive coulombic force between two positive charges of bipolaron by the potential screening effect of methanol. Secondly, the insensitiveness of the spin intensity against

methanol in the case of PP–SO_4 can be explained by considering the interaction between bivalent SO_4^{2-} ion and positive charges of polypyrrole. In this case, because two positive charges are stabilized near SO_4^{2-} ion, bipolaron state is favorable formed near the ion. This will blur the screening effect by methanol. Thirdly, the slower component of the resistance change by methanol, which was attributed to the morphological change of PP polymers in Chapter 5, may be related to the shift of the equilibrium between polaron and bipolaron states by the effect of methanol.

4.4 Conclusion

It was found that apparently minor changes in synthesis of conducting polymers can lead to considerable modification of the conjugation of polymer backbone, with attendant changes in their conductivity and related properties. The polymer structures are dependent on the monomer and are influenced a little by dopant anions, which were used in the electrochemical polymerization. In the case of PNMP films doped with SO_4^- and PSS^-, their exceptionally low conductivity is explained by the existence of carboxyl groups in the polymer structure, which involves the interruption of the π–system. The specific structure of PNMP–TOS is one of the reasons for its unique response to methanol.

EPR gives us information about polarons, which are not the major carrier in the conducting polymers. From the spectra, however, we could obtain insights into their electronic properties. 1) The EPR spectra showed the presence of highly mobile spins in these polymers. 2) Methanol molecules absorbed in conducting polymers seem to favorably affect the formation of bipolaron from polaron.

References

[1] H. Nagase, H. Abe, M. Matsumura, and T. Imanaka, *Proc. of the East Asia Conference on Chemical Sensors*, Fukuoka, (1993) p.57.

[2] R. Qian and J. Qiu, *Polymer Journal*, **19**, 157 (1987).

[3] G. B. Street, T. C. Clarke, M. Krounbi, K. Kanazawa, V. Lee, P. Pfluger, J. C. Scott and G. Weiser, *Mol. Cryst. Liq. Cryst.*, **83**, 253 (1982).

[4] J. Lei, W. Liang and C. R. Martin, *Synth. Met.*, **48**, 301 (1992).

[5] J. Lei, Z. Cai and C. R. Martin, *Synth. Met.*, **46**, 53 (1992).

[6] H. Kato, O. Nishikawa, T. Matsui, S. Honma and H. Kokado, *J. Phys. Chem.*, **95**, 6011 (1991).

[7] H. Kato, O. Nishikawa, T. Matsui, S. Honma and H. Kokado, *J. Phys. Chem.*, **95**, 6014 (1991).

[8] B. Tian and G. Zerbi, *J. Chem. Phys.*, **92**, 3886 (1990).

[9] C. A. Ferreira, S. Aeiyach, M. Delamar, and P. C. Lacaze, *J. Electroanal. Chem.*, **284**, 351 (1990).

[10] K. Hyodo and G. Macdiarmid, *Synth. Met.*, **11**, 167 (1985).

[11] K. J. Wynne and G. B. Street, *Macromolecules*, **18**, 2361 (1985).

[12] S. Dong, J. Ding and R. Zhan, *J. Chem. Soc., Faraday Trans. 1*, **85**, 1599 (1989).

[13] J. C. Scott, P. Pfluger, M. T. Krounbi and G. B. Street, *Phys. Rev. B*, **28**, 2140 (1983).

[14] A. J. Heeger and A. G. MacDiarmid, *Chem. Scr.*, **17**, 115 (1981).

[15] M. Ogasawara, K. Funahashi, T. Demura, T. Hagiwara and K. Iwata, *Synth. Met.*, **14**, 61 (1986).

[16] F. Genoud, M. Guglielmi and M. Nechtschein, *Phys. Rev. Lett.*, **55**, 118 (1985).

[17] A. M. Waller and R. G. Compton, *J. Chem. Soc., Faraday Trans. 1*, **85**, 977 (1989).

[18] C. J. Zhong, Z. Q. Tian and Z. W. Tian, *J. Phys Chem.*, **94**, 2171 (1990).

[19] A. F. Diaz, J. I. Castillo, J. A. Logan and W. Y. Lee, *J. Electroanal. Chem. Interfacial Chem.*, **129**, 115 (1981).

[20] H. Hori, M. Fujii, Y. Shiro, T. Iizuka, S. Adachi and I. Morishima, *J. Biological Chem.*, **264**, 5715 (1989).

[21] J. L. Bredas, R. R. Chance and R. Silbey, *Phys. Rev. B*, **26**, 5843 (1982).

[22] J. L. Bredas, B. Themans, J. G. Fripiat, J. M. Andre and R. R. Chance, *Phys. Rev. B*, **29**, 6761 (1984).

Chapter 5

Quartz Crystal Microbalance Measurements of Polypyrrole Thin Films : Sorption of Exposed Vapor in the Films

The sorption process of methanol, ethanol and water vapor to polypyrrole films is investigated using the QCM method. The sorption of methanol can be described by a one-dimensional Fickian diffusion. From the analysis of sorption curve, diffusion coefficient in the film was determined. Small molecules have large diffusion coefficient, and hence, the response speed is fast. Diffusion coefficient depends on the size of molecules. It is revealed that diffusion of molecules considerably affects the gas response.

5.1 Introduction

The quartz crystal microbalance (QCM) method is very useful for measuring micro-changes in mass. The relationship between mass change and the resulting frequency change is known as the Sauerbrey equation [1], as shown in Eq. (2.1). This method has been applied to thickness monitors. Hlavay *et al.* [2] and Ema *et al.* [3] demonstrated that quartz crystals coated with various polymers can be used as gas sensors. In Chapter 2, we used the QCM method to measure mass changes during electrochemical processes. It is expected that the adsorption process in polypyrrole films may be analyzed by using the QCM method [4-6].

In Chapter 1, it is shown that the response speed is different with the kind of vapor. The response becomes slower as the size of molecules increases. It is supposed that the molecules absorbed in polymers affect the resistance of polypyrrole films. In this chapter we will investigate the absorption process of substances from vapor phase into polypyrrole films using QCM method.

5.2 Experimental

5.2.1 Electrochemical polymerization

All chemicals used in this study were reagent grade. Deionized and then distilled water was used as the solvent. Solutions used for the preparation of polypyrrole films were water containing 0.1 moldm^{-3} pyrrole monomer and 0.1 moldm^{-3} of $NaClO_4$ or Na_2SO_4 electrolytes. The solutions were purged with nitrogen gas before electrochemical polymerization.

The substrates used in the QCM experiments were shear mode AT-cut quartz crystal (INFICON). The resonant frequency of the quartz crystal changes with the mass of adsorbed methanol in the film, as shown by Eq. (2.1). Since

the resonant frequency of the unloaded quartz crystal (f_0) is 6 MHz, the quartz crystal has the sensitivity of 12.3 $ngHz^{-1}cm^{-2}$. On both side of the crystals gold electrodes were vacuum-deposited. The quartz plate was sealed with an o-ring and one side of the gold electrode was used as the working electrode for the deposition of polypyrrole. The mass sensitive area was 0.79 cm^2. A platinum disk with an area of 2.54 cm^2 served as the counter electrode, which was placed in parallel to the working electrode. This electrodes arrangement in the cell was useful to eliminate the edge effects of the working electrode. The electrochemical deposition of the polypyrrole films on the quartz crystals was carried out as described in the previous chapters. The deposited polypyrrole films were rinsed with distilled water and dried in nitrogen for at least for 24 h before use.

5.2.2 QCM measurement

Figure 5.1 shows the schematic diagram of the QCM apparatus. The quartz crystal was placed in the sensor chamber as shown in Fig. 1.4. The shift of the resonance frequency was measured with a 5384A frequency counter (Hewlett Packard), and the data were stored in a computer (PC-286VF, EPSON). The sorption amounts of substances to the polymer film were measured from vapor, such as methanol, ethanol, water, at concentrations from 0 to 1600 ppm, 0 to 1000 ppm, and 0 to 2000 ppm, respectively. Synthetic air (nitrogen 79%, oxygen 21%) was used as a carrier gas. The resistance of the polypyrrole gas sensor was measured simultaneously. The apparatus for gas response measurement was described in Chapter 1.

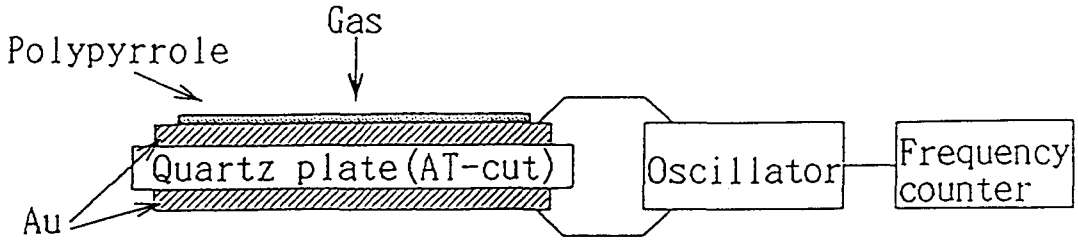

Fig. 5.1. Schematic diagram of quartz crystal microbalance apparatus.

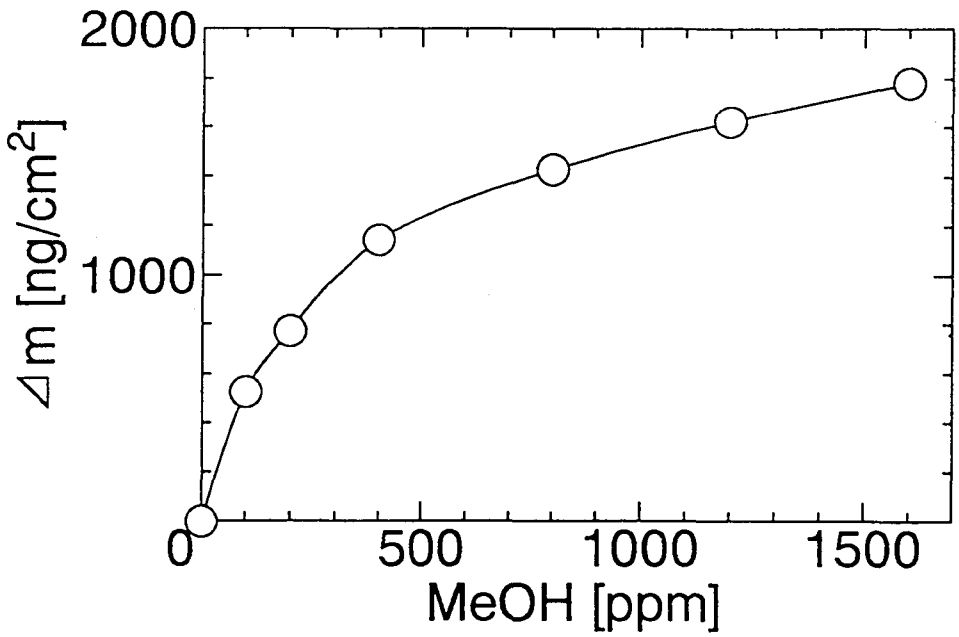

Fig. 5.2. Typical sorption isotherm of methanol to a SO_4^{2-}-doped polypyrrole film.

5.3 Results and discussion

5.3.1 Sorption isotherm of methanol to polypyrrole

Figure 5.2 shows a typical sorption isotherm of methanol into SO_4^{2-}-doped polypyrrole (PP) films. The amount of adsorbed methanol increased steeply with the concentration of methanol in the low concentration range, and then linearly increased in the range above 800 ppm. The same results were obtained for other anions-doped PP films.

From the simultaneous measurements of resistance and mass by QCM, it has been confirmed that there are linear relationship between the amount of absorbed methanol and resistance change of PP. It is apparent that the gas response is influenced by the absorption of molecules. We will consider the absorption process of methanol in the next section, and other molecules in subsequent sections.

5.3.2 Absorption of methanol

To clarify the absorption process, we have analyzed the time-course of the mass change of the crystals coated with polymers exposed to methanol vapor. Figure 5.3 shows typical sorption curves of methanol into SO_4^{2-}-doped PP films at the concentration of 400 ppm (a), and 1200 ppm (b). The sorption rate increases with the methanol concentration.

It is considered that molecules may dissolve in the polymer film according to Henry's law and that this process may be described by a one-dimensional Fickian diffusion equation [7]. The system is assimilated to a plane sheet[8]. Initially, the concentration in the polymer film is taken as C_1. The surface concentration, C_0, of which is in equilibrium with a given vapor concentration [8]. The differential equation is expressed as

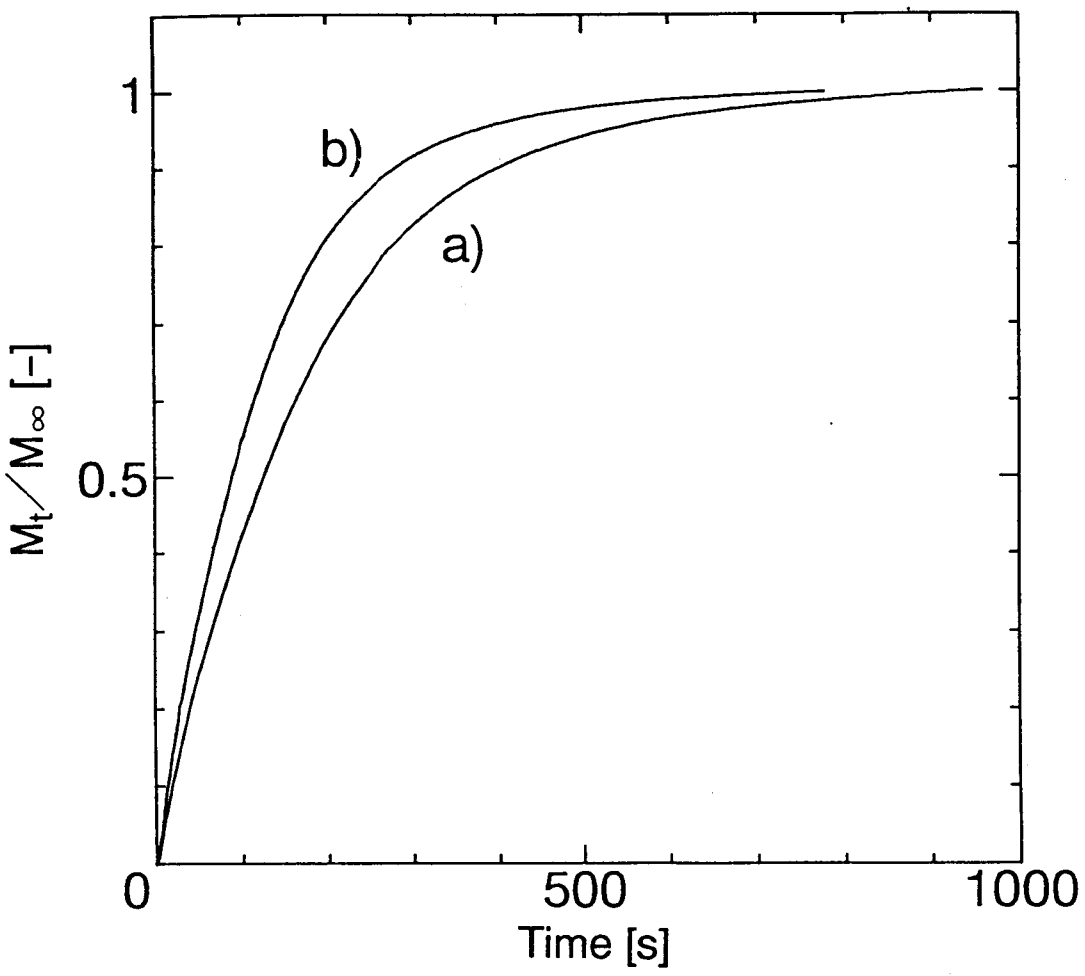

Fig. 5.3. Typical sorption curves of methanol to a SO_4^{2-}–doped polypyrrole film at the concentrations of (a) 400 ppm, (b) 1200 ppm.

$$\frac{\partial C}{\partial t} = D\frac{\partial^2 C}{\partial x^2} \tag{5.1}$$

Initial condition : $C = C_1 \quad -l < x < l \quad t = 0$

Boundary condition : $C = C_0 \quad x = \pm l \quad t > 0$

Eq. (5.1) can be solved as

$$\frac{C-C_0}{C_1-C_0} = 1-\frac{4}{\pi}\sum_{n=0}^{\infty}\frac{(-1)^n}{2n+1}\exp[-\frac{D(2n+1)^2\pi^2 t}{4l^2}]\cos\frac{(2n+1)\pi x}{2l} \tag{5.2}$$

The amount of vapor absorbed in the polymer, M_t, at time t, can be expressed by

$$\frac{M_t}{M_\infty} = 1-\sum_{n=0}^{\infty}\frac{8}{(2n+1)^2\pi^2}\exp[-\frac{D(2n+1)^2\pi^2 t}{4l^2}] \tag{5.3}$$

where M_∞ refers to the amount of vapor absorbed in the film at equilibrium with the vapor. For large t, the equation can be reduced to

$$\ln(1-\frac{M_t}{M_\infty}) = \ln\frac{8}{\pi^2}-\frac{D\pi^2 t}{4l^2} \tag{5.4}$$

because the terms of sum is negligible except for $n = 0$. Fig. 5.4 shows typical plots of $\ln(1-M_t/M_\infty)$ *vs.* t, in which good agreement with Eq. (5.4) was obtained. When t is large, the absorption of methanol in the polymer films obeys the Fickian diffusion. The diffusion coefficient was determined from the slope of the dotted line using Eq. (5.4).

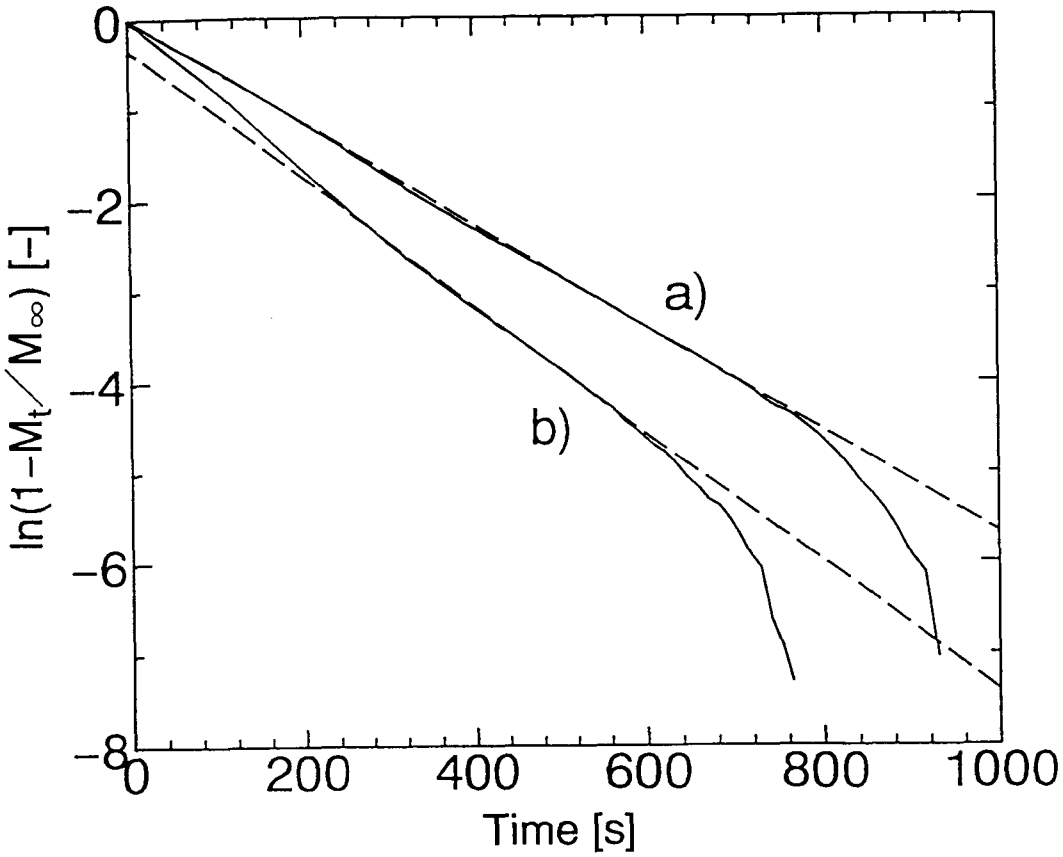

Fig. 5.4. $\ln(1-M_t/M_\infty)$ *vs.* t plots according to Eq. (5.4) at the methanol concentrations of (a) 400 ppm, (b) 1200 ppm.

Table 5.1 summarizes the diffusion coefficients, D, which were determined for the films with different thickness. The film thickness was estimated from the electric charge passed during the electrochemical polymerization, on the basis of Baed *et al.*'s report which describes that charge of 24 $mCcm^{-2}$ produces a PP coating 0.1 μm thick [9]. The value of D is approximately constant, being independent of film thickness, while the diffusion coefficients at 1200 ppm are a little larger than those at 400 ppm.

In the region of very large t (more than 600 s), a deviation between the plots and Eq. (5.4) is apparent. This deviation seems to be caused by the morphological changes of the polypyrrole film.

Table 5.1 Diffusion coefficient of methanol in polypyrrole films

Polymerization charge [mC]	Thickness[a] [μm]	Diffusion coefficient D[b] [$10^{-13}cm^2s^{-1}$] 400ppm[c]	1200ppm[c]
74.7	0.39	1.64	2.28
166.9	0.88	1.82	2.47
287.8	1.52	1.91	2.33

a) Esstimated from polymerization charge.
b) Determined from sorption curves using Eq. (5.13).
c) Concentration of methanol vapor.

5.3.3 Relationship between gas response and diffusion of molecules

As described Chapter 1, the speed of resistance change is different with the kind of vapor. Figures 1.8–1.10 show the response to ethanol, methanol and water, respectively. The time required for the resistance to stop decreasing is about 1 min for water, 3 min for methanol, and more than 100 min for ethanol, respectively. The response becomes slower with increasing molecule size. Such behavior may be due to that the diffusion speed of molecules in the film is different among these substances. To clarify this, the diffusion coefficient was determined using the method described in the previous section.

Figures 5.5–5.7 show typical plots of $\ln(1-M_t/M_\infty)$ *vs.* t, which were obtained for the same quartz crystal plate coated SO_4^{2-}–doped PP film of about 0.58 μm thick by exposing it to ethanol, methanol and water vapor, respectively. Dotted lines were drawn according to Eq. (5.4). In the case of water vapor, the line was fitted in relatively small t region, because sharp variations in the resistance took place in the region of small t. Diffusion coefficients, which were determined from the slope of the lines, were summarized in Table 5.2. It is apparent that the diffusion coefficient becomes smaller with decreasing molecular size. This corresponds to the difference in the speed of resistance change. The sorption amount at steady state, m_s, is also related to the size of molecules. The variation of resistance is influenced by the absorbed amount of molecules, and polypyrrole films have high sensitivity to small molecules.

Table 5.2 Sorption parameters of an SO_4^{2-}-doped polypyrrole film

Vapor	Molecular weight	D $[10^{-13}cm^2s^{-1}]$	t_s [min]	m_s $[ngcm^{-2}]$
Water	18	643	1	600
Methanol	32	4.91	130	152
Ethanol	46	1.34	230	60

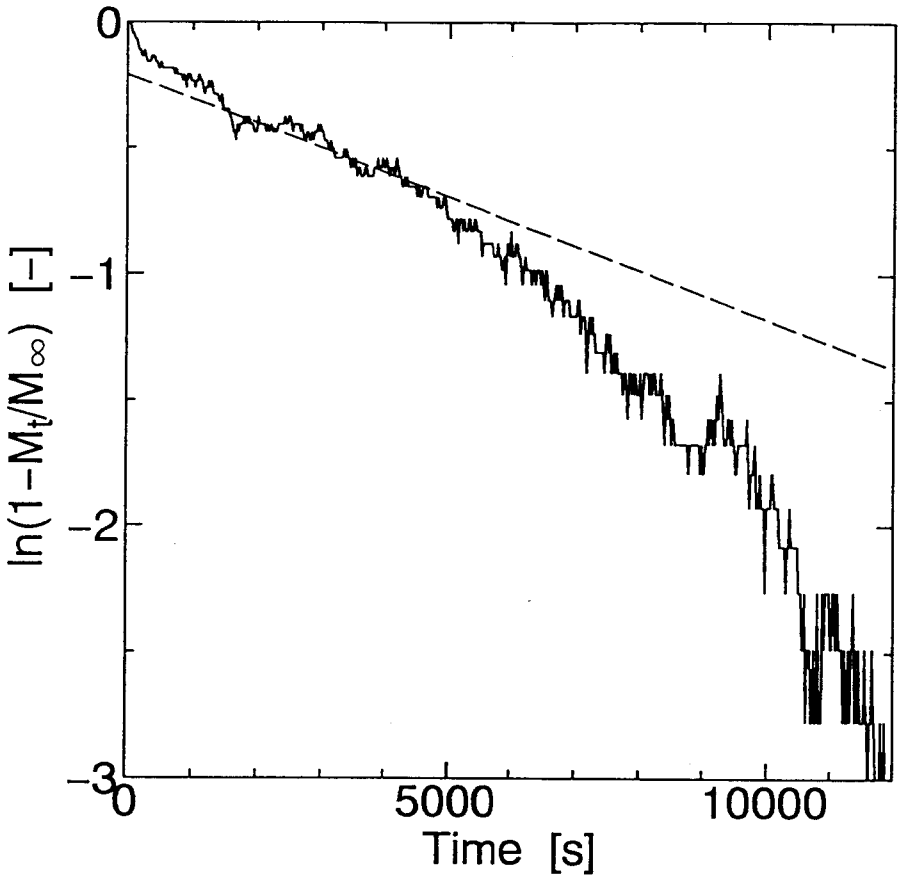

Fig. 5.5. $\ln(1-M_t/M_\infty)$ *vs.* t plots of a SO_4^{2-}–doped polypyllole film exposed to ethanol (100 ppm) according to Eq. (5.4).

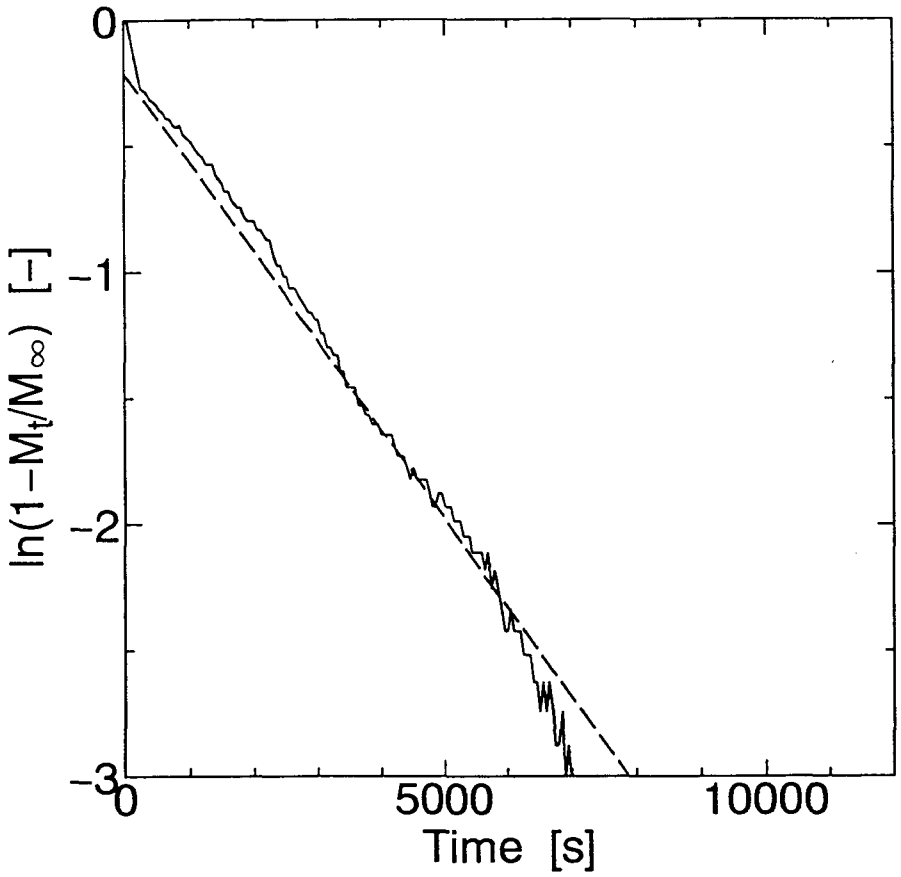

Fig. 5.6. $\ln(1-M_t/M_\infty)$ *vs.* t plots of a SO_4^{2-}–doped polypyllole film exposed to methanol (100 ppm) according to Eq. (5.4).

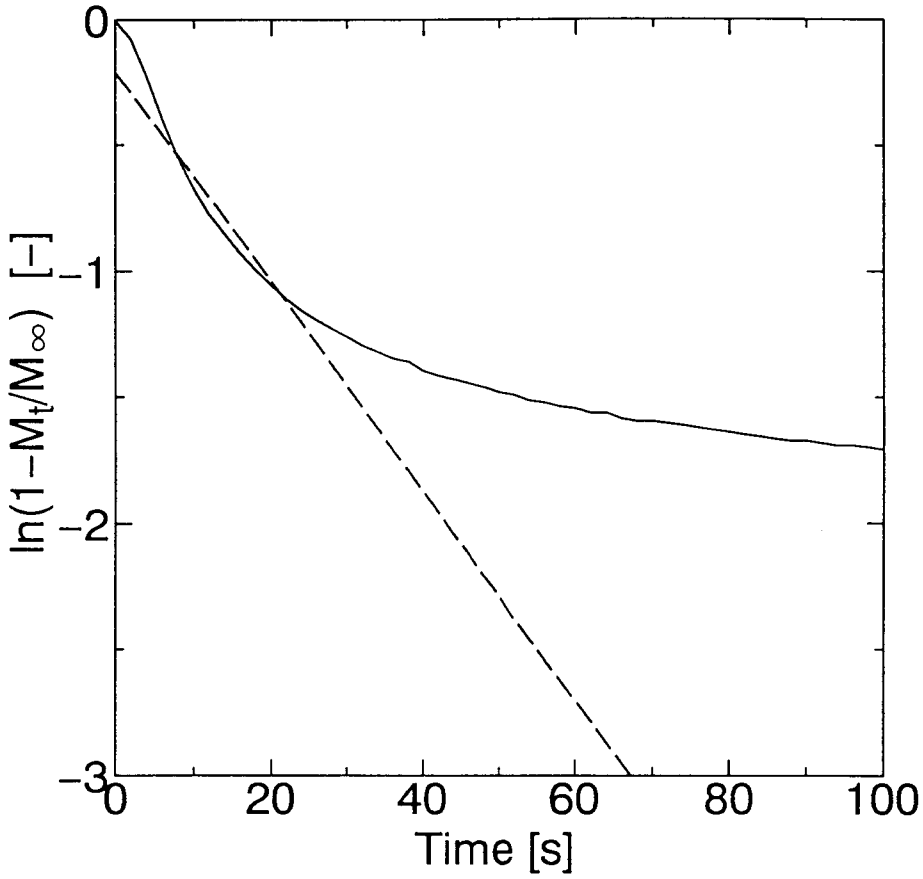

Fig. 5.7. $\ln(1-M_t/M_\infty)$ *vs.* t plots of a SO_4^{2-}-doped polypyllole film exposed to water vapor (500 ppm) according to Eq. (5.4).

5.4 Conclusion

The sorption of vapor molecules into polypyrrole films was investigated using QCM methods. The absorption process was described by one-dimensional Fickian diffusion. Small molecules are easily absorbed into polypyrrole films and have large diffusion coefficients, and hence the response speed is fast. It has been confirmed that the diffusion of molecules in the films considerably affects the gas response.

References

[1] *Chemical Sensors*, ed. Edmonds. T. E., Blackie, Glasgow, 1988, pp. 295–317.

[2] J. Hlavay and G. G. Guilbault, *Anal. Chem.*, **49**, 1890 (1977).

[3] K. Ema, M. Yokoyama, T. Nakamoto and T. Moriizumi, *Sensors and Actuators*, **18**, 291 (1989).

[4] J. M. Slater and E. J. Watt, *Analyst*, **116**, 1125 (1991).

[5] J. M. Slater and E. J. Watt, *Anal. Proc.*, **29**, 53 (1992).

[6] P. Topart and M. Josowicz, *J. Phys. Chem.*, **96**, 8662 (1992).

[7] J. Crank, *The Mathematics of Diffusion*, 2nd ed., Clarendon Press, Oxford, 1975, p. 238.

[8] P. N. Bartlett and S. K. Ling-Chung, *Sensors and Actuators*, **19**, 141 (1989).

[9] B. A. F. Diaz and J. I. Castillo, *J. Chem. Soc., Chem. Comm.*, **1980**, 397.

Part 2

SnO_X Thin Films for Sensing NO_X Prepared by Microwave Plasma CVD

Chapter 6

Preparation and Characterization of SnO_X Thin Films

Tin oxide thin films were prepared from tetramethyltin (TMT) and oxygen by means of the microwave plasma CVD method. The optical transmittance and the conductivity of the tin oxide films have been found to be sensitive to the partial pressures of TMT and O_2. Conductive films were obtained with a partial pressure ratio, O_2 to TMT, of above 4.

6.1 Introduction

Recently, much attention has been focused on the plasma enhanced chemical vapor deposition (CVD) method for semiconductor device fabrication. By the CVD methods, it is possible to prepare nonstoichiometric thin films at low temperatures. A deposition technique using microwave discharge and a plasma transport has attracted strong interest as a new preparation method for semiconductor thin films, since the damage to the substrate and the incorporation of electrode elements into the films can be avoided [1].

Since a tin oxide thin film has the properties of both optical transparency and electrical conductivity, it is widely used in the electronics industry as transparent electrodes and as sensors. This film is prepared by heat CVD [2], RF sputtering [3], DC [4] or RF [5] plasma CVD. However, few studies have been carried out so far on the preparation of tin oxide thin films by utilizing the microwave plasma CVD method.

In this chapter, the preparation of transparent tin oxide thin films by a microwave plasma CVD method from tetramethyltin (TMT) mixed with oxygen and argon is reported. The effects of gas pressure on the thickness, surface condition, electrical and optical properties of the films are examined.

6.2 Experimental

A diagram of the plasma CVD apparatus is shown in Fig. 6.1. Ar and O_2 gases were introduced into the plasma chamber, and TMT vapor was introduced into the deposition chamber. The partial pressure of Ar was constant at 0.40 Torr, and those of TMT and O_2 were varied in the range from 0.005 to 0.10 Torr and from 0.01 to 0.20 Torr, respectively. Quartz plates (10x20mm) and silicon plate (10x10mm) were used as substrates for the optical and

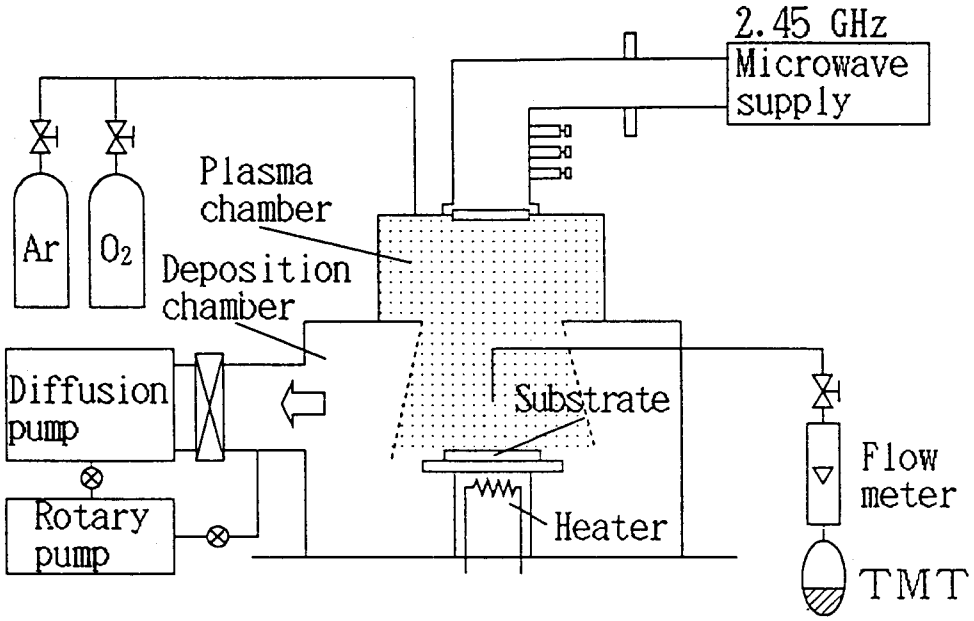

Fig. 6.1. Schematic diagram of the microwave plasma CVD system.

thickness measurements, respectively, and Corning 7059 glass plates (10x20mm) for the other measurements. The temperature of these substrates was kept at 250°C, and the microwave power (frequency 2.45GHz) was maintained at 100W during depositions (1h).

The composition of the films was determined by means of X-ray photoelectron spectroscopy (XPS) with an ESCA 750 spectrometer (Shimadzu). The UV-visible spectrum (200 to 900 nm) was measured with a UV-360 double beam spectrometer (Shimadzu). The thickness of the films was evaluated by ellipsometry. Resistivity was measured with a K-705RD 4-probe resistance meter (Kyowariken).

6.3 Results and discussion

Figure 6.2 shows the dependence of film thickness deposited by microwave plasma CVD on the partial pressure of TMT (P_{TMT}). The partial pressure of O_2 (P_{O_2}) was kept constant at 0.20 Torr. The film thickness reached a maximum at P_{TMT} around 0.05 Torr. In the range of P_{TMT} lower than 0.05 Torr, the film thickness increased with increasing P_{TMT} as oxygen exists in excess. The thickness of films decreased for higher P_{TMT} because of the lack of oxygen, which is required to decompose TMT.

The resistivity of films prepared in the P_{TMT} range from 0.01 to 0.05 Torr was about $2x10^{-4}\Omega cm$, but it approached infinity for P_{TMT} higher than 0.05 Torr. The resistivity of the films deposited under constant P_{TMT} of 0.01 Torr was infinity at P_{O_2} below 0.02 Torr. The resistivity decreased with increase of P_{O_2} above 0.20 Torr. It is therefore apparent that the partial pressure ratio of O_2 to TMT (P_{O_2}/P_{TMT}) influences the property of the deposited films.

The O/Sn atomic ratio of the films, determined from the XPS intensity of Sn_{3d} and O_{1s}, is shown in Fig. 6.3 as a function of P_{O_2}/P_{TMT}. Above

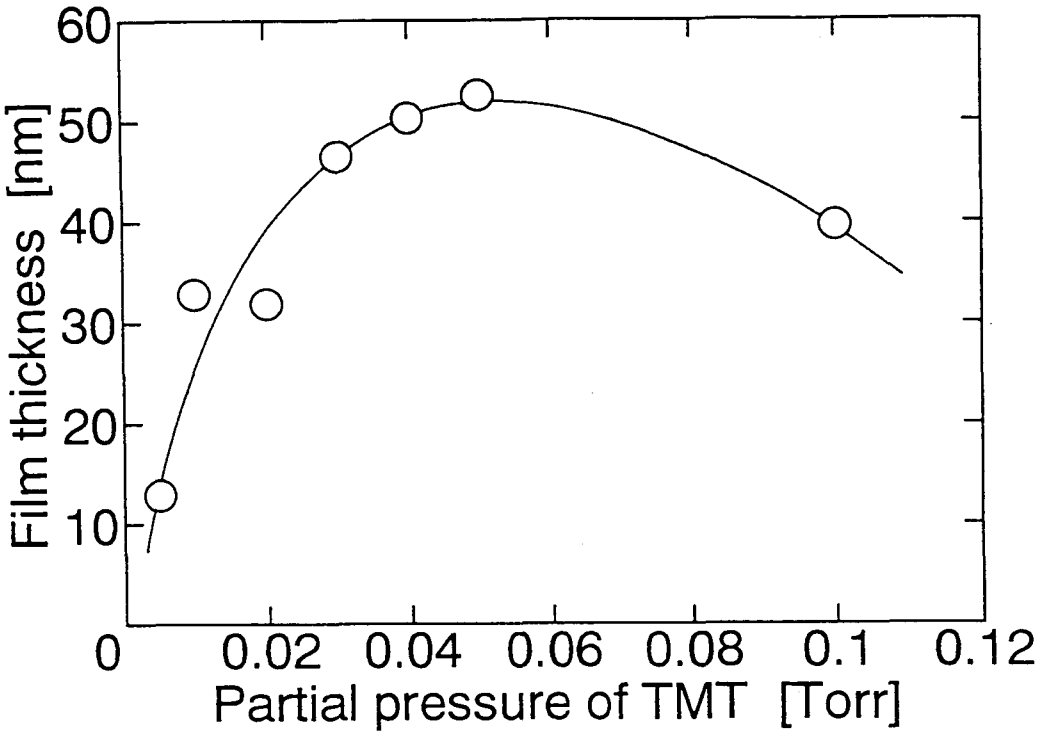

Fig. 6.2. Dependence of the film thickness on the partial pressure of TMT.
Partial pressure of O_2 : 0.20 Torr
Substrate temperature : 250 °C
Deposition time : 1h

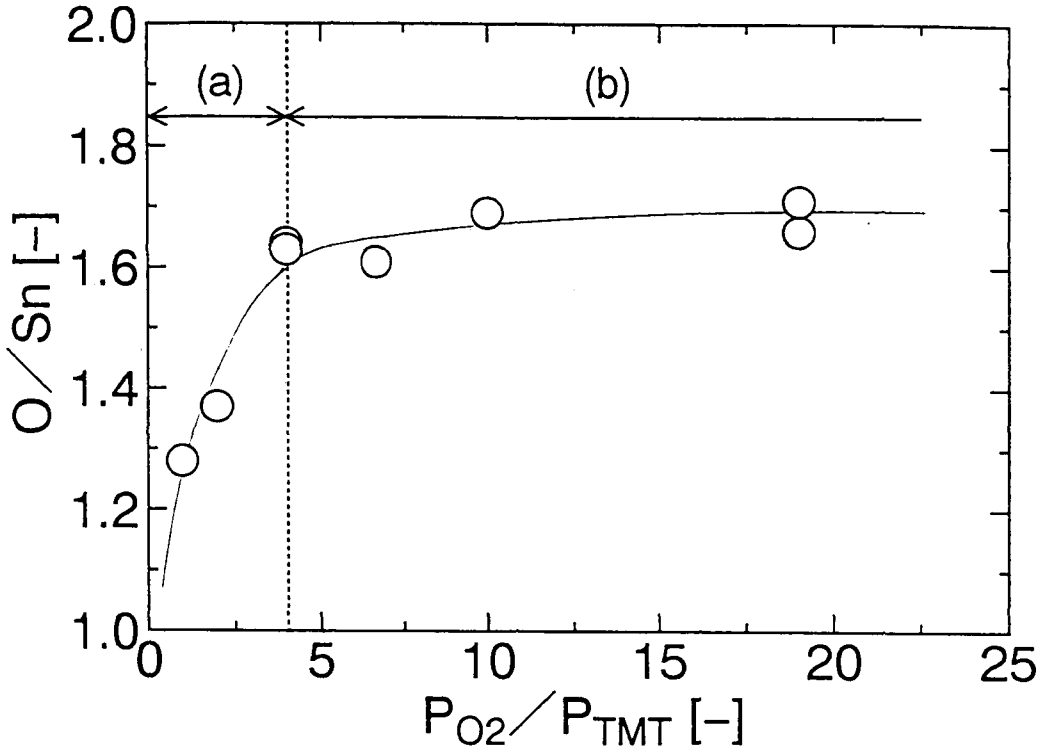

Fig. 6.3. O/Sn atomic ratio of SnO_x thin films prepared at 250 °C as a function of partial pressure ratio O_2/TMT.
(a) and (b) show insulating and conducting regions, respectively.

P_{O_2}/P_{TMT}=4, the atomic ratio of O/Sn is constant at about 1.7. This is smaller than the value of 2 expected for SnO_2. The films deposited at P_{O_2}/P_{TMT} above 4 are conductive. Below P_{O_2}/P_{TMT}=4, the atomic ratio of O/Sn is smaller, and the films are non-conductive. This is probably due to the lack of oxygen.

Figure 6.4 shows the UV-visible spectra of films prepared at various P_{TMT}. The transmittance of the films was larger than 80% at the wavelengths above 430nm. It became lower for the wavelengths shorter than 400nm, owing to the electron transition from the valence band to the conduction band. The shape of spectra for the films prepared at P_{TMT}=0.005, 0.01 and 0.03 Torr were similar to each other; the transmittance decreased with increase of P_{TMT} in all the range of wavelength measured. This is mainly due to the increasing thickness of the films as shown in Fig. 6.2. For higher P_{TMT} (0.05 and 0.10 Torr), where the films are insulator, the shapes of the spectra were different from those of the others.

6.4 Conclusion

We found that the tin oxide thin films prepared by microwave plasma CVD methods provide good conductivity and transmittance. Films prepared at P_{TMT}=0.01 Torr and P_{O_2}=0.20 Torr showed satisfactorily high conductivity and transmittance. The study on the application of such a film to a gas sensor is described in the next chapter.

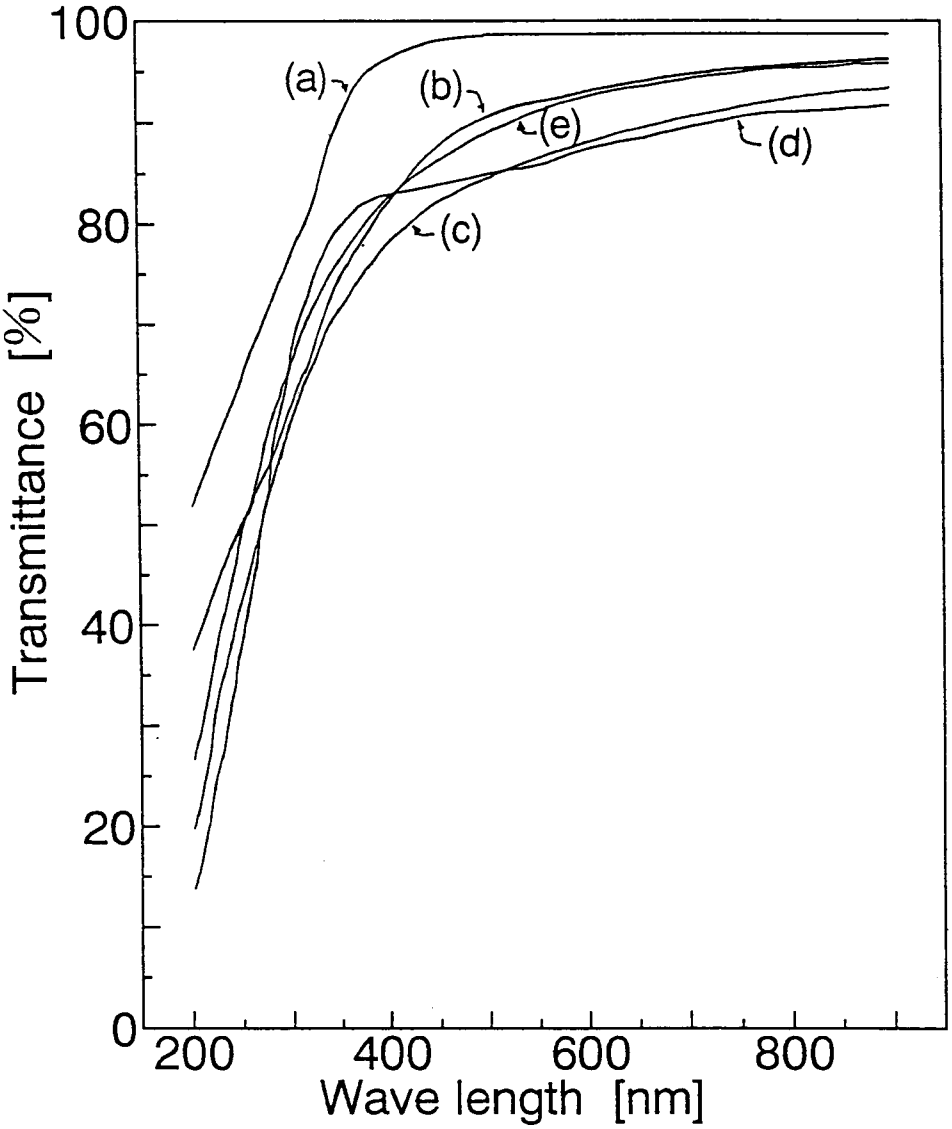

Fig. 6.4. UV-vis spectra of the SnO_x films deposited by microwave plasma CVD at 250 °C.
Partial pressure of O_2 : 0.20 Torr
Partial pressure of TMT :
(a) 0.005 Torr, (b) 0.01 Torr,
(c) 0.03 Torr, (d) 0.05 Torr,
(e) 0.10 Torr.
Deposition time : 1h

References

[1] I. Kato, S. Wakana, S. Hara and H. Kezuka, *Jpn. J. Appl. Phys.*, **21**, L470 (1982).

[2] C. G. Borman and R. G. Gordon, *J. Electrochem. Soc.*, **136**, 3820 (1989).

[3] S. Chang, *IEEE Trans. Electron Devices*, **ED-26**, 1875 (1979).

[4] M. Arai, S. Hamada and Y. Nishiyama, *Bull. Chem. Soc. Jpn.*, **65**, 1141 (1992).

[5] S. Reich, H. Suhr and B. Waimer, *Thin Solid Films*, **189**, 293 (1990).

Chapter 7

NO_X Sensing Properties of SnO_X Thin Films

Response of SnO_X thin films prepared by the microwave plasma CVD method against NO_X is investigated. The resistance of the film increases on exposure to NO_2, with a reversible response at above 250°C. The optimum operating temperature is around 300°C, considering sensitivity and response speed. The resistance is 10 times higher in 20 ppm NO_2 than in air. The response time is about 60 s. The sensitivity to NO_2 is 5 times higher than to NO. The response to inflammable gases, such as hydrogen, carbon monoxide and hydrocarbons, is very low. As a result, the SnO_X film is concluded to be a promising sensing material for NO_2, because of its high sensitivity and selectivity.

7.1 Introduction

The amount of NO_X produced by industrial combustion equipment has increased, and it has become a serious environmental problem. NO_X are known to cause acid rain, and in these years low pH acid rain is observed in Japan as has been observed in Europe and America.

Simple methods for measuring NO_X concentration is required to reduce the NO_X discharge, for the controlling systems of combustion equipment. The most widely used current technique to detect NO_X is the chemical luminescence method, which needs a sampling system and troublesome maintenance. Hence, this method is used only in restricted application, such as environmental NO_X measurements in the ppb order range. Semiconductor gas sensors are stable, simple and can be used for continuous monitoring [1]. Among the semiconductors, sintered tin oxide (SnO_2) material has been used most commonly as gas sensors for detection of flammable gases [2–4]. However, it has problems as NO_X sensors, particularly because of its low selectivity and stability [5]. Thin films of tin oxide have different properties from the sintered materials, and it is expected that the thin film sensors will exhibit high selectivity and fast response speed, because of its large surface area [6]. Chang *et al.* prepared tin oxide thin films by using reactive RF sputtering from a tin target and suggested that the thin films can be used as NO_X sensors [7–9].

It is found that SnO_X thin films can be prepared from tetramethyltin by the microwave plasma CVD method, as described in Chapter 6. In this chapter, the gas responding property of the SnO_X thin films against NO_X was investigated, and optimum sensor operation conditions were determined. The influences of flammable gases, such as carbon monoxide, hydrogen and hydrocarbons, all contained in exhaust gases, were also investigated.

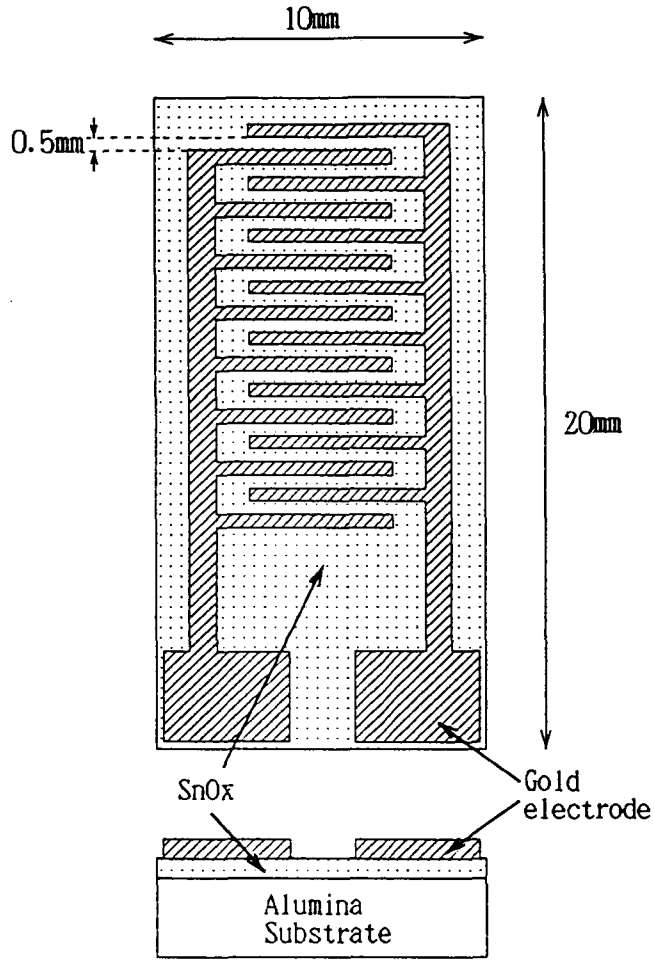

Fig. 7.1. Schematic diagram of SnO_x sensor layout.

7.2 Experimental

7.2.1 Sensor preparation

Aluminum plates (10 mm × 20 mm, 0.5 mm thick) were used as substrates. Figure 7.1 shows details of the sensor layout. The sensing material, a semiconductor SnO_X thin film, was deposited on the substrate using the microwave plasma CVD method; the apparatus for which was described in Chapter 6. The partial pressures of tetramethyltin (TMT), oxygen and argon, were 0.01 Torr, 0.20 Torr and 0.40 Torr, respectively. The temperature of these substrates was kept at 250° C, and microwave power (2.45 GHz) was supplied into the plasma chamber at 100 W for 1 h. After CVD, the two gold electrodes were vacuum-deposited on the substrates, which form interdigitated pattern. The thickness of the SnO_X film thus prepared is about 35 nm. The deposited SnO_X film was heat-treated at 300-400° C in air for about 1 h to stabilize the film resistance.

7.2.2 Gas response measurements

The responses of the SnO_X films to hydrogen, carbon monoxide, methane, propane, *iso*-butane and NO were measured using the gas testing chamber (5400 cm^2), as shown in Fig. 7.2, which was purged with dry synthetic air (nitrogen 79%, oxygen 21%). The sensor was mounted on the heater. The temperature was kept constant at the operating temperature with ventilation by a fan. The sample gas was injected into the chamber with a gas syringe after the sensor resistance stabilized. The sensor resistance was measured using a Hewlett-Packard 3478A digital multimeter.

The response of the SnO_X films to NO_2 was measured at the concentration of 15 ppm, which is the usual NO_2 concentration in auto exhausts. The experiments were carried out using the flow system, described in the experimental section of Chapter 1. Dry synthetic air was used as a

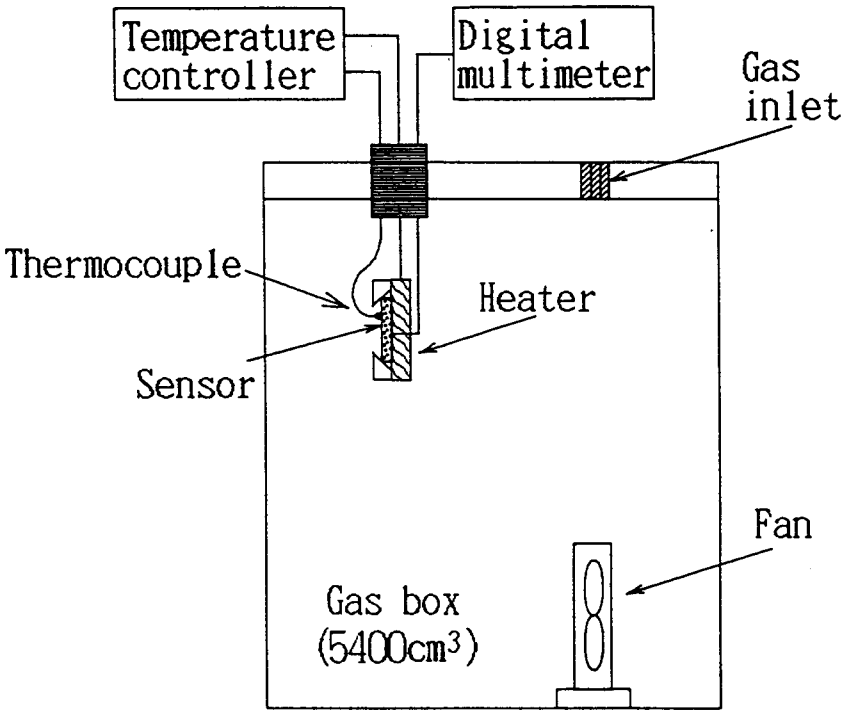

Fig. 7.2. Schematic diagram of a gas testing chamber.

carrier gas, and a P-9-H permeation tube (Gastec) for NO_2 source. The sensor was mounted on the heater, which can control the temperature of the sensor in the range from 50 to 400° C. The resistance between the two gold electrodes was measured using the digital multimeter.

7.3 Results and discussion

7.3.1 Response to NO_2

Figure 7.3 shows the dependence of the response to 15 ppm NO_2 on the operating temperature. It is apparent that the resistance of SnO_X increased on exposure to NO_2. However it did not return to the initial pre-exposure value in the low temperature range, below 200° C, when the sensor was exposed to dry air again. Figure 7.4 shows the typical response of a SnO_X film to 15 ppm NO_2 at 300 ° C. At this temperature, the resistance of the film returned to the initial value in air, and a reversible response was obtained.

Figure 7.5 shows the dependence of sensitivity to 15 ppm NO_2 at operating temperatures from 250 to 350° C. Sensitivity to NO_2 is defined as the resistance ratio R_g/R_a, where R_g is the resistance before exposure to NO_2, and R_a is the resistance reached to steady state in an NO_2 atmosphere. In this range of temperatures, a reversible resistance change, such as shown in Fig. 7.4, was obtained. The sensitivity was highest at 250° C, R_g/R_a = 26, and decreased with increase in temperature. The sensitivity (R_g/R_a) at 350° C was 4. The SnO_X film had no response at over 400° C.

Figure 7.6 shows the dependence of response time on operating temperature. The response time was defined as the time required for the resistance to reach 90% of its steady state value when the test gas was changed from air to NO_2. It takes a long time to reach the steady state at under 300° C, because of the large adsorption of NO_2 molecules and the low

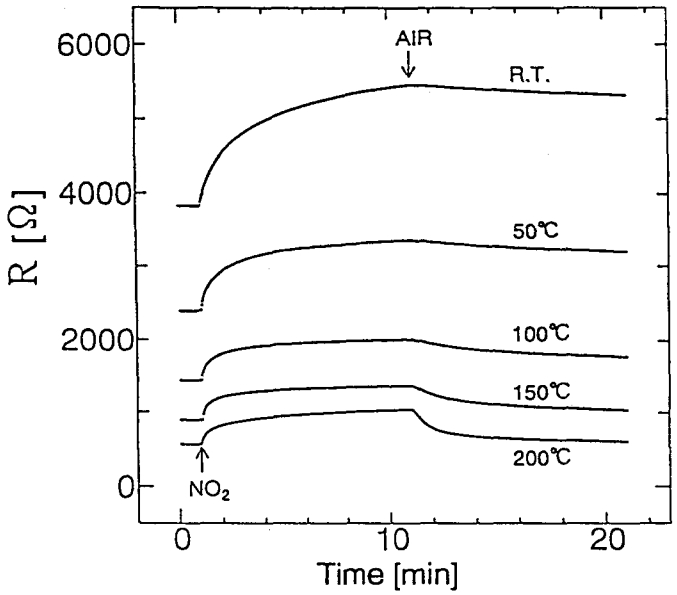

Fig. 7.3. Effect of operating temperature on response to 15 ppm NO_2.

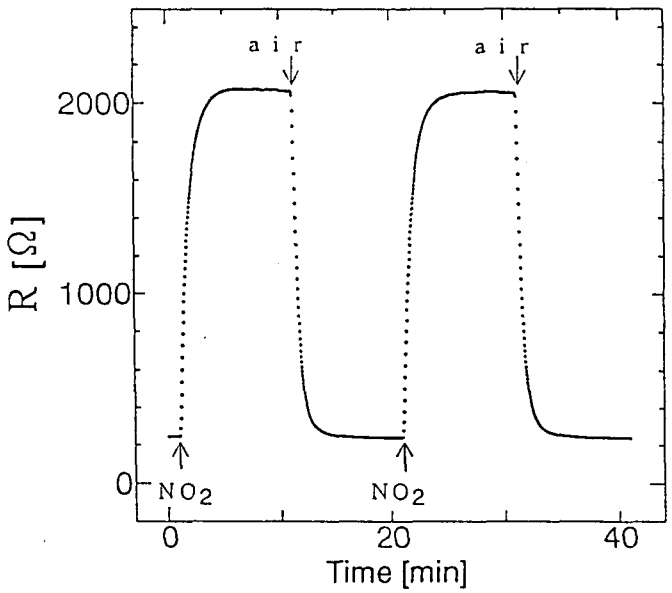

Fig. 7.4. Typical response of SnO_X film to 15 ppm NO_2, 300° C.

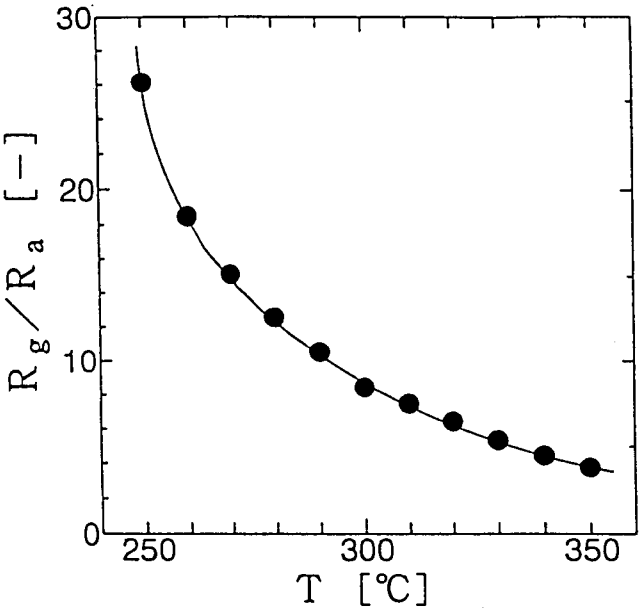

Fig. 7.5. Dependence of sensitivity to 15 ppm NO_2 on operating temperatures from 250 to 350° C.

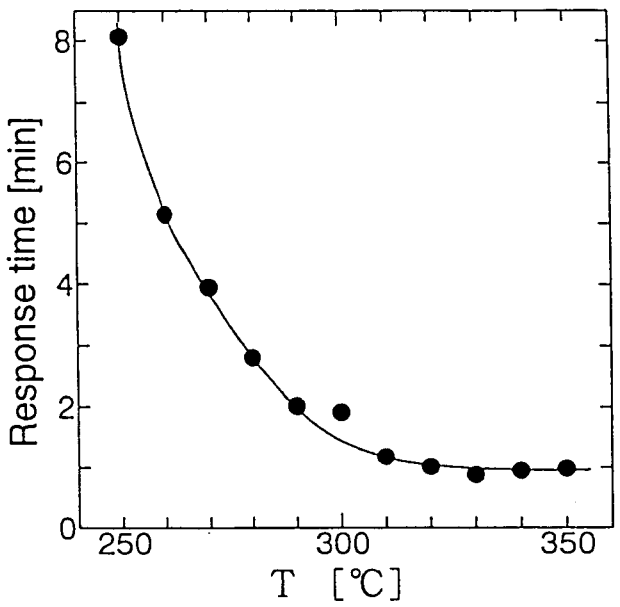

Fig. 7.6. Dependence of response time to 15 ppm NO_2 on operating temperatures from 250 to 350° C.

adsorption speed at low temperatures. The response time at above 300° C was constant at about 1 min. The response at above 300° C is actually very fast, because it takes about 1 min to fill the sensor chamber with the test gas. It is considered from these results that the optimum operation temperature is around 300° C.

Figure 7.7 shows the dependence of the sensitivity (R_g/R_a) on concentration of NO and NO_2 in the range 2.5 to 75 ppm at 300 °C. The sensitivity at 2.5 ppm NO_2 is about 3, and it is possible to detect the low concentrations of NO_2. On exposure to NO, the resistance increased. The sensitivity, R_g/R_a, is appreciably lower than for NO_2. However, the sensor can detect NO in concentrations in the order of ppm.

The relationship between response to NO_2 and operating temperature will next be considered in some detail. At under 200° C, NO_2 adsorbs irreversibly onto the SnO_X surface, and does not desorb completely even in the air. As the adsorption of NO_2 on tin oxide is exothermic, the amount of adsorbed NO_2 decreases with increased temperature. Hence the sensitivity is high at low temperature, and decreases with an increase in temperature. The no response at over 400° C is due to the absence of adsorbed NO_2 on the SnO_X surface. Tamaki *et al.* performed experiments with temperature programmed desorption from SnO_2 powder [10], and reported that NO_2 adsorbed onto the reduced tin oxide surface dissociated to NO, and that desorption of NO commenced at about 250° C, reached a maximum at 330° C, and desorbed completely at 400° C. The same phenomenon is considered to occur on surface of the SnO_X.

7.3.2 Response to inflammable gases

The response to H_2, CO, CH_4, C_3H_8 and $(CH_3)_3CH$ was measured at 300° C to investigate the gas selectivity. These are all gases which may exist in exhaust gas. The response to methanol was measured at 300 °C using the apparatus described in Chapter 1. The sensitivity is defined as R_a/R_g, because

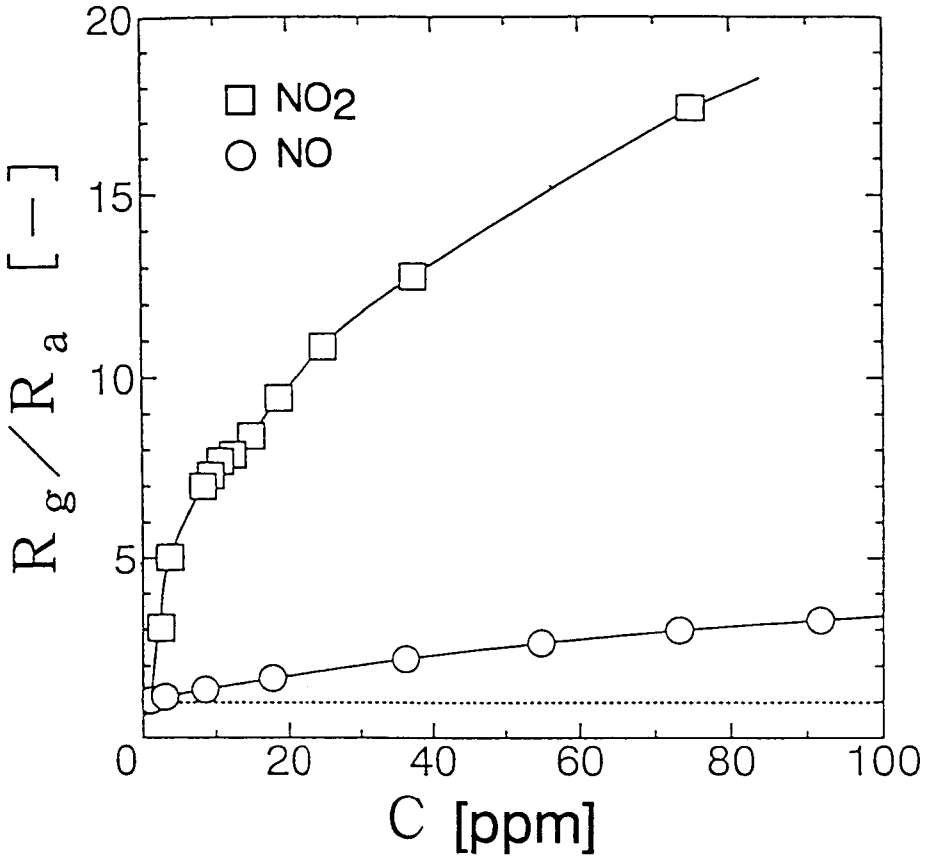

Fig. 7.7. Dependence of sensitivity (R_g/R_a) on concentration of NO and NO_2 in the range 2.5 to 75 ppm at 300° C.

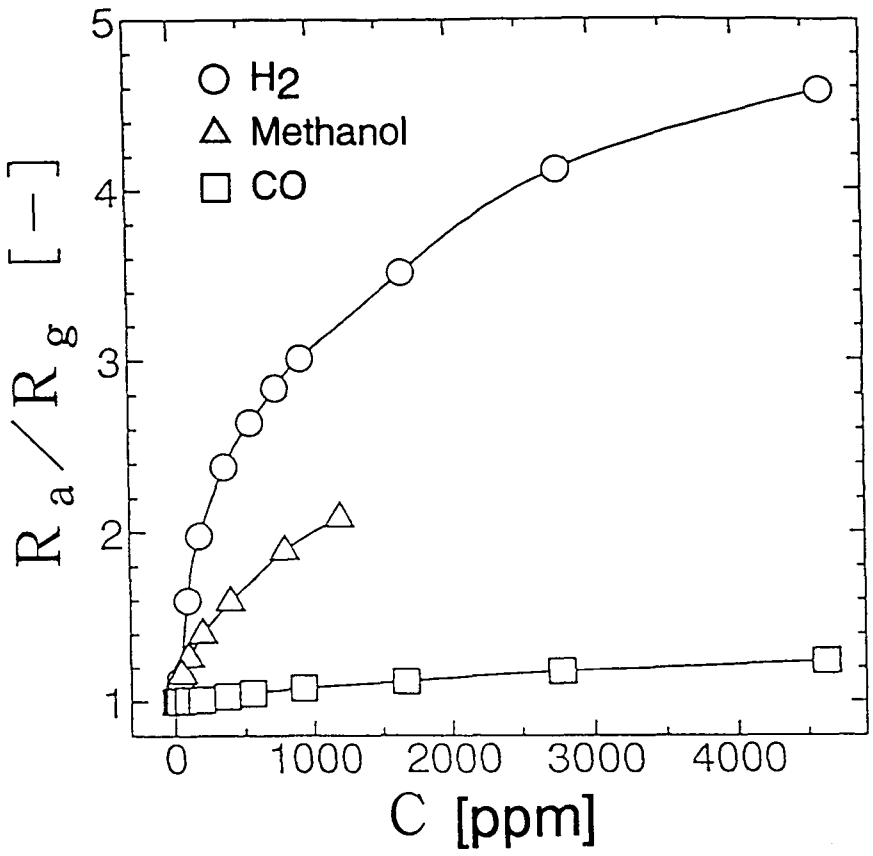

Fig. 7.8. Dependence of sensitivity (R_a/R_g) on concentration of H_2, CO and methanol at 300° C.

R_g is smaller than R_a for these inflammable gas.

Figure 7.8 shows the dependence of the sensitivity (R_a/R_g) on the concentration of H_2, CO and methanol. The resistance of the SnO_X film decreased on exposure to these three gas. The sensor has a sensitivity to H_2 and methanol in high concentrations, and shows low sensitivity to low concentration (under 100 ppm). However, it has very low sensitivity to CO even in high concentrations. It exhibits no sensitivity to CH_4, C_3H_8 and $(CH_3)_3CH$ at 300° C.

Figure 7.9 shows the influence of H_2 and CO on the detection of NO_2. The SnO_X film was exposed first to NO_2. H_2 and methanol were then successively injected into the gas testing chamber. No change of resistance was observed, in spite of the presence of flammable gas.

From these results, it is concluded that SnO_X thin films prepared by microwave plasma CVD methods have high sensitivity to and selectivity for NO_2.

7.3.3 Gas response mechanism for NO_2

The mechanism of response to electronegative gas molecules such as oxygen or NO_X (NO and NO_2) can be explained by the model shown in Fig.7.10. If an electronegative molecule approaches to the semiconductor surface and its electron affinity A is larger than the semiconductor work function W, the molecule will tend to pick up an electron from the semiconductor conduction band and become chemisorbed with negative surface charge. The net result of chemisorption of acceptor-type gas such as oxygen or NO_2 on n-type semiconductors is a decrease in electron concentration in the conduction band near the semiconductor surface, and hence a decrease in conduction band parallel to the surface. The chemisorption of NO_X leads to band bending. The amount of adsorbant increases until the energy level of the surface becomes equal to the potential of adsorbant. The adsorption of NO_2 on the SnO_X film,

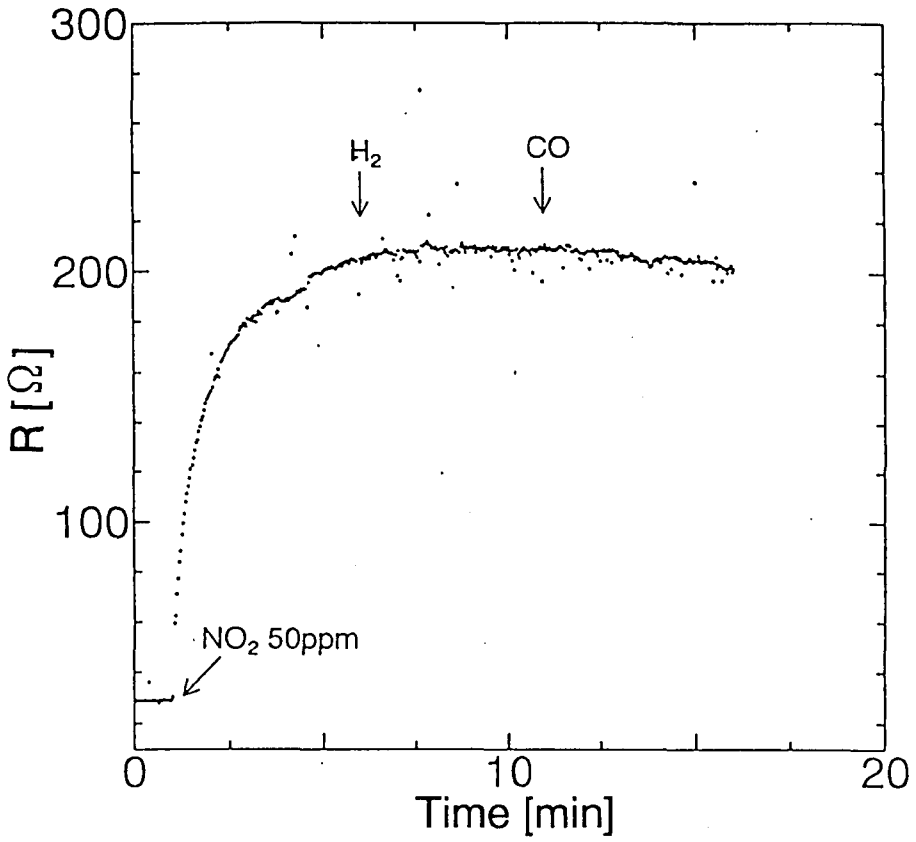

Fig. 7.9. Influence of H_2 and CO on the detection of NO_2.

which is stoichiometrically lacking in oxygen ($x<2$), is compared to that of SnO_2, whose composition is stoichiometric. For SnO_2, equilibrium, as shown in Fig. 7.10 (b), is established for low amounts of adsorbed NO_2, and the resulting resistance change is small, because the density of conducting electrons at the surface is low. On the other hand, the amounts of adsorbed NO_2 on the SnO_X surface is larger than that on SnO_2 when equilibrium is established, as the number of oxygen vacancies, i.e. electron density at the SnO_X surface, is large. Hence, the sensitivity to NO_2 is high, in the case of SnO_X.

The sensitivity of SnO_X films prepared by our methods to flammable gases is low. Generally, oxygen plays a very important role in the detection of flammable gases [11]. Oxygen molecules adsorb on the semiconductor surface with a negative charge, as shown in Fig. 7.10 (b), and make the surface of the semiconductor highly resistive. There are a small numbers of conducting electrons on the SnO_2 surface, and the resistance is very high because the electrons are trapped by the adsorbed oxygen. Conversely, the resistance of SnO_X remains low in spite of electron trapping by the adsorbed oxygen, because the electron density of SnO_X is high, compared with that of SnO_2. When a molecule of a flammable gas approaches to the semiconductor surface, the adsorbed oxygen reacts with it and is consumed, and the electron trapped by the oxygen returns to the semiconductor conduction band. Consequently, the resistance decreases. For SnO_2, the resistance change is very large because the resistance decreases from an initially high value. The resistance of SnO_X changes only a little by consumption of the adsorbed oxygen, because of its low resistivity in air. Therefore, SnO_x thin films are considered to have low sensitivity to flammable gases.

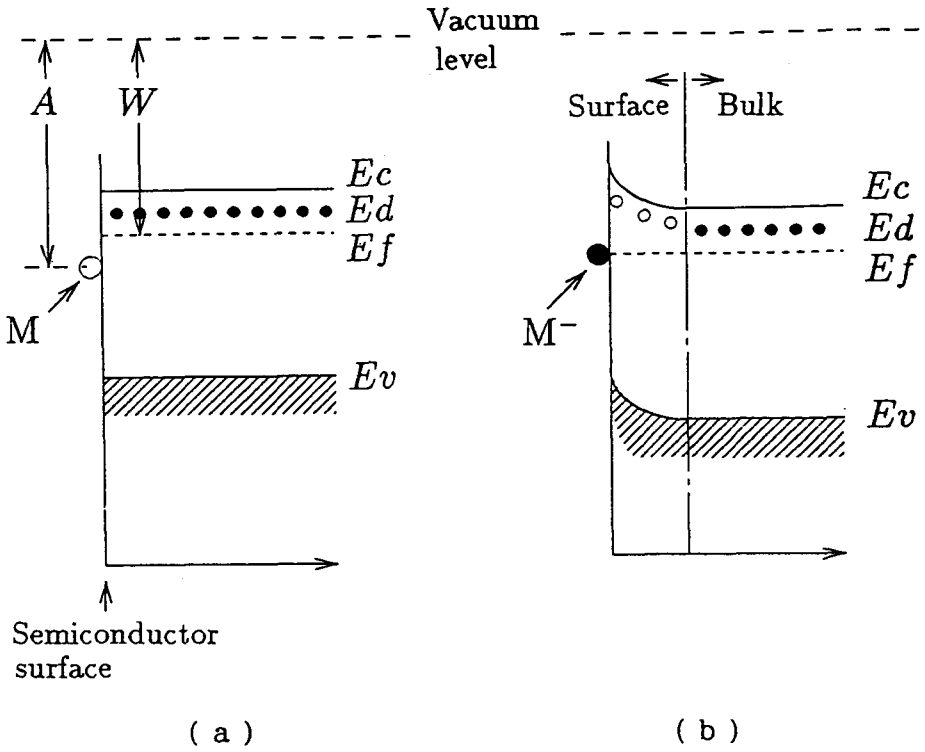

Fig. 7.10. Effects of electronegative molecules chemisorbed on n-type semiconductor surface.
(a) Before chemisorption. (b) After chemisorption,
A : electron affinity of molecule
W : work function of semiconductor
E_c : energy level of conduction band
E_v : energy level of valence band
E_d : donor level
E_f : Fermi level

7.4 Conclusion

The resistance of SnO_X thin films prepared by the microwave plasma CVD method increases in an atmosphere containing NO or NO_2. The film has an especially high sensitivity to NO_2; the resistance of the film becomes three times as large as its initial value at an NO_2 concentration of 2.5 ppm. The sensitivity to NO is one fifth that to NO_2. The optimum operation temperature in view of sensitivity and response speed is around 300° C. Sensitivity to hydrogen, carbon monoxide and hydrocarbons is low enough at this temperature. From these results, the SnO_X thin films prepared by the microwave plasma CVD method is evaluated to have good sensitivity to and selectivity for NO_2. The films are considered to be promising for developing sensors for detecting NO_2 in exhaust gas.

References

[1] K. Satake, A. Kobayashi, T. Inoue, T. Nakahara and T. Takeuchi, *Proc. 3rd Intern. Meeting on Chemical Sensors*, U.S.A., Cleveland, pp.334–337 (1990).

[2] T. Seiyama, A. Kato, K. Fuchiishi and M. Nagatani, *Anal. Chem.*, **34**, 1502 (1962).

[3] G. Heiland and D. Kohl, *Sensors and Actuators*, **8**, 227 (1985).

[4] J. F. McAleer, P. T. Moseley, J. O. W. Norris and D. E. Williams, *J. Chem. Soc., Faraday Trans. 1*, **83**, 1346 (1987).

[5] J. Tamaki, M. Akiyama, T. Jo, N. Miura and N. Yamazoe, *Preprints of the 24th Autumn Meeting of Chem. Engrs.*, Japan, Nagoya, No.1, p. 153 (1991).

[6] H. Pink, L. Tretinger and L. Vite, *Jpn. J. Apply. Phys.*, **19**, 513 (1980).

[7] S. C. Chang, *IEEE Trans. Electron Devices*, **ED–26**, 1875 (1979).

[8] S. C. Chang, *Society of Automotive Engineers, Technical Paper Series*, **1980**, 107.

[9] T. W. Capehart and S. C. Chang, *J. Vac. Sci. Technol.*, **18**, 393 (1981).

[10] J. Tamaki, M. Nagaishi, Y. Teraoka, N. Miura, N. Yamazoe, K. Moriya and Y. Nakamura, *Surface Sci.*, **221**, 183 (1989).

[11] H. Windischmann and P. Mark, *J. Electrochem. Soc.*, **126**, 627 (1979).

List of Publications

1. "Effect of Doping Anions in Polypyrrole Gas Sensors"
   Hiroyasu Nagase, Hiroyuki Abe and Toshinobu Imanaka,
   Sensors and Actuators B, **13-14**, 596-597 (1993).

2. "Response Mechanisms of Polypyrrole Films to Methanol"
   Hiroyasu Nagase, Hiroyuki Abe and Toshinobu Imanaka,
   Proc. of the Symposium on Chemical Sensors II, Honolulu, pp. 317-324 (1993).

3. "Organic Vapor Sensing Characteristics of Polypyrrole Thin Films"
   Hiroyasu Nagase, Hiroyuki Abe, Michio Matsumura and Toshinobu Imanaka, *Proc. of the East Asia Conference on Chemical Sensors*, Fukuoka, pp. 57-60 (1993).

4. "Application of SnO_X Thin Films Prepared by Microwave plasma CVD to a NO_X Sensor"
   Hiroyasu Nagase, Tetsuo Hirono, Yasuaki Okamoto and Toshinobu Imanaka, *Kagaku Kogaku Ronbunshu*, **19**, 856-862 (1993).